UNIVERSITÉ DE MONTRÉAL

MULTIDISCIPLINARY DESIGN OPTIMIZATION (MDO) OF TRANSONIC FAN BLADE

SAIMA NAZ

DÉPARTEMENT DE GÉNIE MÉCANIQUE

ÉCOLE POLYTECHNIQUE DE MONTRÉAL

THÈSE PRÉSENTÉE EN VUE DE L'OBTENTION

DU DIPLÔME DE PHILOSOPHIAE DOCTOR

(GÉNIE MÉCANIQUE)

DÉCEMBRE 2014

UNIVERSITÉ DE MONTRÉAL

ÉCOLE POLYTECHNIQUE DE MONTRÉAL

Cette thèse intitulée :

MULTIDISCIPLINARY DESIGN OPTIMIZATION (MDO) OF TRANSONIC FAN BLADE

présentée par : NAZ Saima

en vue de l'obtention du diplôme de : Philosophiæ Doctor

a été dûment accepté par le jury d'examen constitué de :

M. LAURENDEAU Éric, Ph. D., président

M. TRÉPANIER Jean-Yves, Ph. D., membre et directeur de recherche

M. TRIBES Christophe, Ph. D., membre et codirecteur de recherche

M. GUIBAULT François, Ph. D., membre

M. KOKKOLARAS Michaël, Ph. D., membre

DEDICATION

To my parents . . .

ACKNOWLEDGEMENTS

RÉSUMÉ

La conception de pales d'un rotor est une tâche complexe et difficile en raison de l'écoulement transsonique, du large espace de design et de l'implication de plusieurs disciplines de l'ingénierie dans le but d'augmenter les performances de métriques multidisciplinaire tels que l'efficacité, le rapport de pression, le stress. Pour faire face à tous ces défis, une comparaison d'approches pour les optimisations aérodynamiques et multidisciplinaires automatisés (MDO) des pales de soufflante transsonique est présentée. Le processus de conception proposé intègre une méthode de paramétrisation géométrique des pales, une modélisation CAO et des outils d'analyse haute-fidélité pour l'aérodynamique, la structure et la dynamique. Une méthode de paramétrisation de pales à multi-niveau a été utilisée pour modifier efficacement la géométrie de la pale avec un faible nombre de variables de conception. Le modèle CAO a été construit dans CATIA afin d'utiliser un modèle commun pour les analyses de structure et dynamiques. Le modèle des équations de Navier-Stokes (RANS) tridimensionnelles moyennées intégré au logiciel commercial CFD ANSYS CFX, a été utilisé pour l'analyse aérodynamique du rotor transsonique tandis qu'un modèle éléments finis (EF) implémenté sur ANSYS a été utilisé pour réaliser les analyses de structure et dynamique. Des algorithmes d'optimisation heuristiques et hybrides sont utilisés pour résoudre le problème d'optimisation de la forme des pales. La vérification des codes et des méthodes a été effectuée en comparant les résultats calculés à des données expérimentales disponibles dans la littérature pour le NASA Rotor 67, un cas test représentatif d'écoulement complexes en trois dimensions.

Afin de vérifier la faisabilité du processus automatisé intégré dans l'optimisation, une optimisation aérodynamique visant à maximiser l'efficacité du point de conception tout en maintenant le débit massique et le rapport de pression constant, est élaboré et exécuté pour redessiner le cas de test Rotor 67. En outre, ce cas a aidé à sélectionner l'algorithme d'optimisation adapté à la résolution du problème et explorer l'espace de conception. Cependant, la conception de pale de soufflante transsonique est inévitablement un processus pluridisciplinaire qui nécessite la participation de nombreuses disciplines telles que l'aérodynamique, la structure, la dynamique, etc., au cours des différentes étapes du processus de conception. En outre, les procédures de conception actuelles impliquent une optimisation de la structure et de la dynamique après l'optimisation aérodynamique. Il s'agit d'une optimisation

séquentielle. Le principal inconvénient de cette procédure est qu'une bonne conception aérodynamique pourrait ne pas satisfaire aux exigences de conception de la structure et la dynamique, ce qui fait de cette procédure de conception un processus itératif. Dans ce cas, la méthode de conception d'optimisation multidisciplinaire (MDO) est utile afin d'améliorer la performance globale du problème multidisciplinaire.

Ce travail a conçu, mis en œuvre et comparé trois formulations d'optimisation multidisciplinaire dont une formulation à un seul niveau Multi Design faisabilité (MDF) et une formulation ATC multi-niveaux (Analytical Target Cascading). ATC est sélectionné en raison de la proximité de l'anatomie du problème de conception. Une stratégie de filtrage modifiée à partir de MDF est aussi proposée. Cette approche de filtrage tire avantage du fait que l'analyse aérodynamique est informatiquement coûteuse par rapport à l'analyse de la structure et la dynamique. Le processus de solution ATC, y compris la méthode d'initialisation du problème et la manipulation des cibles au niveau du système et au niveau de la discipline, est présenté. Une description de chaque formulation MDO et une description du problème de performance associée à chaque formulation MDO sont fournies en détails. La méthodologie décrite a ensuite été mise en œuvre pour reconcevoir le cas test Rotor 67 aux conditions du point de design pour améliorer l'aérodynamique, la performance structurelle et les vibrations en optimisant les angles de la pale, l'épaisseur, l'empilage, comme les variables de conception géométriques.

L'optimisation aérodynamique a améliorée de 0,99 points d'efficacité au point de design tout en maintenant le rapport de pression et le débit massique à 0,25% du Rotor 67 et en utilisant un total de 500 évaluations (ou 150 heures). Les approches MDF, filtrage et ATC ont amélioré la performance aérodynamique respectivement de 0,19, 0,66 et 0,70 points d'efficacité au point de conception. Le temps du processus d'optimisation de MDF et de filtrage étaient de 180 heures et 132 heures respectivement. Une analyse approfondie des écoulements et des flux, des contraintes et de la dynamique a été réalisée pour les pales optimisées pour analyser le choc, l'interaction du choc avec la couche limite, l'écoulement secondaire, la contrainte et les fréquences de vibrations. La méthodologie proposée a été prouvée très efficace et pratique avec une augmentation significative de l'efficacité, une réduction de la contrainte maximale de Von-Mises et a pu éviter les modes propres de vibrations du moteur.

ABSTRACT

The design of current transonic fan blades is a complex and challenging task due to multifaceted transonic flow field, large design space and involvement of many engineering specialists to increase performance on multidisciplinary metrics such as efficiency, pressure ratio, stress. To tackle all these challenges, a comparison of approaches for the automated aerodynamic and multidisciplinary optimizations (MDO) transonic fan blades is developed. The developed design process integrates the fan blades geometrical parameterization method, CAD modeling and high-fidelity analysis tools for aerodynamics, structure and dynamics disciplines. A multi-level parameterization method of fan blade was utilized to efficiently modify the blade geometry with a low number of design variables. The CAD model was built in CATIA, to use a common model for structure and dynamic analyses. The three-dimensional Reynolds-Averaged Navier-Stokes (RANS) equations based commercial software ANSYS CFX was used for aerodynamic analysis of transonic rotor; whereas Finite Element (FE) analysis based commercial software ANSYS Mechanical was used to conduct the structure and dynamic analyses. Heuristic and hybrid optimization algorithms are employed to solve the fan design optimization problem. The capability of the codes and methodologies was validated by comparing the computed results to experimental data available in the open literature for NASA Rotor 67, a test case representative of complex three-dimensional flow structures in transonic blade design problems.

In order to verify the feasibility of automated integrated optimization working flow, an aerodynamic optimization aiming to maximize the design point efficiency while maintaining the mass flow rate and pressure ratio, is formulated and executed to redesign a test case. It further helped to select the suitable optimization algorithm and explore the design space. However, transonic fan blade design is inevitably a multidisciplinary process which requires involvement of many disciplines such as aerodynamics, structure, dynamics, etc., during different stages of design process. In addition, the current design procedures involved the structure and dynamic disciplines optimization after aerodynamic discipline i.e. a sequential discipline optimization. The main drawback of this procedure is that a good aerodynamic design might not satisfy the structural and dynamic design requirements which make this design procedure an iterative

process. In that case, the coupled multidisciplinary optimization (MDO) design technique is required in order to improve overall performance.

This work has proposed, implemented and compared three MDO formulations including a single-level formulation Multi Design Feasibility (MDF) and a multi-level formulation Analytical Target Cascading (ATC). A filtering approach modified from MDF strategy is also proposed. This filtering approach takes advantage of the structure of design problem in which aerodynamic analysis is computationally costly as compared to structure and dynamics analyses. ATC was selected due to its closeness to the anatomy of the design problem. The ATC solution process, including the specific way of initializing the problem and handling system level and discipline level targets, is presented. A description of each MDO formulation and description of problem performance associated to each MDO formulation is given in details. The described methodology was then implemented to re-design a test case at design point conditions to improve the aerodynamic, structural and vibration performance by optimizing the blade angles, thicknesses and stacking geometrical design variables.

The optimal rotor configurations, which correspond to the aero-optimized and MDO-optimized designs, are obtained and compared to the original Rotor 67 design. The aerodynamic optimization improved +0.99 points of design point efficiency while maintaining the design point pressure ratio and mass flow rate both within 0.25% of the Rotor 67 blade using a total of 500 evaluations (or 150 hours). MDF, Filtering approach and ATC MDO optimized blade designs were improved +0.19, +0.66 and +0.70 points in design point efficiency, respectively. The design point pressure ratio and mass flow rate were within 0.5% and 0.4% of Rotor 67 blade. The optimization process time for MDF and filtering approach were 180 hours and 132 hours respectively. The detailed investigation of flow, stress and dynamics analyses were performed for the optimized blade shapes to analyze the shock, shock boundary layer interaction, secondary flow, stress, frequency modes, etc. The proposed methodology was proved quite successful and practical as it increased the efficiency, reduced the maximum von-Mises stress and prevented the natural frequency modes from engine crossings.

TABLE OF CONTENTS

LIST OF TABLES

LIST OF FIGURES

LIST OF APPENDICES

NOMENCLATURE

Symbols

σ_{max}	Von-Mises Stress
x_{geo}	Geometrical design variable
η	Isentropic efficiency
$\dot{m}_c$	Corrected mass flow
P_{01}	Total pressure at inlet
T_{01}	Total temperature at inlet
H_{01}	Isentropic total enthalpy at inlet
F_1	First dynamic frequency mode
F_2	Second dynamic frequency mode
F_3	Third dynamic frequency mode

Acronyms

PR	Pressure ratio
RPM	Revolution per minute
ASA	Adaptive Simulated Annealing
SA	Simulated Annealing
NOMAD	Nonlinear Optimization by Mesh Adaptive Direct Search
MIGA	Multi-Island Genetic Algorithm
GA	Genetic Algorithm
SND	Structure and dynamics
MDO	Multidisciplinary design optimization
MDA	Multidisciplinary analysis
AAO	All-at-Once

IDF	Individual Discipline Feasible
MDF	Multidisciplinary Feasible Design
ATC	Analytical Target Cascading
CO	Collaborative Optimization
CSSO	Concurrent Subspace Optimization
BLISS	Bi-Level Integrated System Synthesis
RSA	Response Surface Approximation
EA	Evolutionary Algorithm
PS	Pressure side
SS	Suction side
TE	Trailing edge
LE	Leading edge
SST	Shear Stress Transport
CFD	Computational Fluid Dynamics
RANS	Reynolds-Averaged Navier-Stokes
FE	Finite element
APDL	ANSYS Parametric Design Language
CAD	Computer Aided Design

CHAPTER 1   INTRODUCTION

1.1   Background

Transonic fans are extensively used as the first stage of large civil and military aero-engines. They experience high tip velocity in the range of 380–490m/s and as a result the inlet relative Mach number is high, up to 1.7. Nowadays, an efficient transonic fan has total pressure ratio in the range of 1.5-2.2. The modern transonic fan designs have reached a high level of performance, making further improvements a challenging task. Nevertheless, a small increment could lead to significant savings in the fuel cost and reduced environmental impact, which are one of the prime intentions of the aero-engine manufacturing industry [1-3].

Modern transonic fan design requirements are evolving towards an increase in fan diameter and a higher bypass ratio to improve the efficiency and reduce the noise emission. This results in more multifaceted geometries, consequently extremely complex detrimental flow structures including shock, shock-boundary layer interaction, secondary flows, etc. Furthermore, the transonic fan blade aerodynamic design is also affected by the mechanical requirements such as maximum stress, vibration modes, etc.

1.2   Human driven fan design process

The fan design process is explained here in its most basic form as per information available in the literature and communication with engineers from our industrial partner.

The transonic fan blade design is inherently a multidisciplinary process which requires the involvement of several disciplines including aerodynamics, structures and vibration. Each discipline is responsible for different performance parameters of fan blade design. Moreover, disciplines exchange information with each other at different stages of the design process which increases the complexity of the process. Furthermore, a traditional three-dimensional fan blade design technique is based on the personal expertise. In most situations, designers have to perform manual modifications to the blade shape based on their judgment and analysis. Basically, the designers use a "trial-and-error" approach, where blade geometry is set up, analyzed and then modified repeatedly towards the optimal design.

The design process starts with the aerodynamics discipline as non-linear transonic flows are very sensitive to the fan blade shape. The aerodynamics discipline primarily focuses to improve the efficiency or to reduce the losses. The high performance aerodynamic fan design geometry is transferred to the structural and vibration disciplines in order to check the mechanical integrity in terms of the maximum allowable stress level, safety margin and excitation frequencies that should be avoided in the engine running range. If the mechanical requirements are not met then the geometry is sent back to the aerodynamics discipline. This often results into several back and forth iterations between the aerodynamics and the mechanical analyses in order to achieve a satisfactory compromise in the fan blade design. So, the classical fan design is intrinsically a sequential iterative process which is also expensive in terms of the computational resources and design cycle time.

Usually, a fan blade geometry definition roughly includes 15-20 two-dimensional sections and 20-25 geometrical design parameters per section, which together give a total of 200-500 parameters. Moreover, every discipline is using different commercial and in-house softwares to perform relevant analyses. This large number of design variables and the variety of analyses performed with the intensive computational tools increase the complexity of handling the fan design process. Consequently, in relation with the increased fan shape complexity, the fan design iterative process has become more and more difficult to converge, and requires more iterations and more compromises between disciplines.

1.3 Need of multidisciplinary design optimization (MDO) methodology

In recent years, the turbomachinery industries have integrated high fidelity computational tools such as Computer Aided Design (CAD), Computational Fluid Dynamics (CFD) and Finite Element Analysis (FEA) solvers in order to understand the complex flow structures and intricate mechanical characteristics in relation with the performance of the components.

Despite these modern solvers and the availability of efficient optimization algorithms, fan blade shape optimization is not applied intensively in the industry due to a number of factors. First, the performance of a transonic fan blade is very sensitive to the shape changes so the geometry must be parameterized with a suitable number of parameters. Moreover, the characteristic functions of a fan design problem are often multimodal and nonlinear because the flow field is governed by the nonlinear Reynolds-Averaged Navier-Stokes partial differential equations. Furthermore,

several constraints from multiple disciplines, such as mass flow rate, maximum stress, and others make the optimization a difficult task.

In addition, the fan blade design involves multidisciplinary optimizations conducted sequentially with "performance" compromises in search of an overall optimal, or at least a good design. In addition, a blade that is optimized or traded at one discipline might not satisfy the requirements of the other disciplines. Mostly, improvement in one design requirement results in performance degradation of the other requirements. In general, the blade design process consisting of defining a geometry that meets many rigorous requirements is a challenging task.

Thus, there is an essential need of a methodology that can address all above design requirements and designers' needs by providing a computational framework for the interaction of multi-disciplines. It is believed that multidisciplinary design optimization (MDO) technologies can help to solve the complex fan design problem. In essence, the MDO methodology aims to subdivide a complex design problem into optimization sub-problems each with respect to the design variables that are relevant to a discipline specialist and to manage to the strong interactions between several disciplines involving a multitude of constraints, design variables and objectives. This further leads to task parallelization to efficiently utilize the available computational resources.

MDO methodology has been successfully implemented in numerous engineering domains such as aircraft design, wing design, automobile, etc. However, applying MDO in transonic fan blade design problem is still a challenging task due to many reasons. First, MDO is computationally more expensive in comparison to the sum of the single discipline optimizations. For example, it might be practically difficult to handle the analysis of all the disciplines and their coupling under a single optimizer while using a variety of intensive computational software with diverse analyses times and a large number of design variables. Furthermore, a single discipline optimization may have only one objective function whereas MDO based design optimization can involves several multi-objective optimizations. Secondly, the organizational complexity is also a challenge for MDO implementation in fan design problem, especially when large numbers of design variables are involved. For example, different computationally intensive analyses can run on multiple machines at various physical locations. For this reason, an accurate representation of the multidiscipline interactions and the real engineering team work must be understood [4, 5].

Finally, although several MDO frameworks are available in the literature to express a design optimization problem, the MDO implementation is entirely problem dependent, which requires not only comprehension of the problem particulars, but also involves a deep understanding of the underlying complexity of MDO frameworks and the specificities of optimization algorithms.

1.4 Motivation and objectives

The global objective of the present work is to develop, exploit and propose various approaches for the multidisciplinary design and optimization of the transonic fan blades.

The specific objectives can be defined as:

- Develop an automatic integrated analysis process based on CAD-CFD-FEA for transonic fan blade multidisciplinary analyses. The CAD model will be parameterized and all the analyses modules will seamlessly link with the CAD model to perform the design evaluations.

- Exploit the integrated analysis system to understand its characteristics and identify the possible avenues for the problem decomposition.

- Propose, implement and compare MDO based design approaches that are tailored to the transonic fan design process, to optimize aerodynamic design while respecting stress and vibration constraints.

1.5 Outline of the thesis

This thesis contains five chapters. Following the above introductory section, chapter 2 provides a literature review of the available MDO formulations, their comparisons and MDO implementations in aeronautics and propulsion domain. This chapter also covers the recent progress in transonic fan design optimization. In chapter 3, the discipline analyses modules used for the present research are presented, followed by the MDO methodology in chapter 4. Chapter 5 gives the results and discussion followed by the conclusions and future work.

CHAPTER 2   LITERATURE REVIEW

This literature review covers the advanced techniques used for the design and optimization of transonic compressor blades. This chapter is divided into three sections. The first section provides a general description of multidisciplinary design optimization (MDO) formulations developed in the past decades along with the comparison of the formulations available in literature and their implementation in aeronautics and propulsion industries. The second section describes the blade design optimization which covers the blade geometry parameterization, performance evaluation, optimization algorithms, and highlights of adopted fan blade design methodologies in literature. A brief overview of recent progresses on axial transonic fan and compressor blade optimization is also included in this section. The final section provides a brief summary of literature review, which directly links the conclusive steps to the methodology adopted in this thesis.

2.1   Multidisciplinary design and optimization (MDO)

Multidisciplinary design optimization (MDO) problems typically involve a large number of design constraints, variables and objectives from different disciplines. For MDO problems, the most important task is the seamless linkage of various system models and optimization algorithms. Furthermore, the design requirements must be defined and then formulated mathematically, as objective and constraints functions.

MDO provides an opportunity to find the optimal solution of a system by establishing the interaction between the various disciplines. However the solution is not likely the best solution for a single discipline.

The selection of an appropriate MDO formulation has a huge importance to come up with an efficient solution of the design problem. In the following subsection, we introduce MDO formulations with respect to problem decomposition and architecture. After that, published comparative studies of existing MDO formulations are analyzed.

2.1.1 Problem decomposition and architecture

A large system is described by a large number of design variables and is usually computationally too expensive to be optimized for all the variables at the same time. One way to deal with this

kind of problem is to decompose the system into subsystems, which can be optimized in parallel. There can be «natural» decompositions of a system into subsystems using *hierarchical*, *non-hierarchical* and *hybrid* approaches. The hierarchical approach allows communication between below and above disciplines. The non-hierarchical approach allows communication among any disciplines and the hybrid approach is the combination of hierarchical and non-hierarchical approaches.

The MDO formulations can be classified on the basis of the disciplines interactions as 'single-level' or 'multi-level.' The single-level formulations such as All-at-Once (AAO) [6], Individual Discipline Feasible (IDF) [6-8], Multidisciplinary Feasible Design (MDF) [6, 7, 9] involve a single optimizer.

The multi-level formulations require an optimization framework with several interacting optimizers. Among multi-level formulations we can cite Collaborative Optimization (CO) [10], Concurrent Subspace Optimization (CSSO) [11, 12], Bi-Level Integrated System Synthesis (BLISS) [13] and Analytical Target Cascading (ATC) [14, 15]. A brief description of the work presented in all above cited references is listed in Table A-1(Appendix-A).

While defining an optimization problem, the first step is to specify the objective function(s), and the design variables with bounds and constraints. Then the optimization formulations can be stated. Before discussing the details of the MDO formulations employed in this work, a general form of problem formulation such as AAO (in the notation given by Martins and Lambe [16]), is taken as a baseline:

$$\text{maximize} \quad f_0\,(x,y) + \sum_{i=1}^{N} f_i(x_0, x_i, y_i) \tag{1}$$

$$with\ respect\ to \quad x, \hat{y}, y, \bar{y}$$

$$subject\ to \quad c_0(x,y) \geq 0$$

$$c_i(x_0, x_i, y_i) \geq 0 \qquad \text{for } i= 1,\dots, N$$

$$c_i{}^c = \hat{y}_i - y_i = 0 \qquad \text{for } i= 1,\dots, N$$

$$R_i\big(x_0, x_i, \hat{y}_{j\neq i}, \bar{y}_i, y_i\big) = 0 \quad \text{for } i= 1,\dots, N$$

where, x is a vector of design variables. y is a vector of coupling variables or output from discipline analysis. f is an objective function, c is a vector of design constraints. c^c is a vector of consistency constraints. R is a set of governing equations of a discipline analysis in residual form or discipline analysis constraints. $\bar{y}$ is a vector of state variables or variables used inside only one-discipline analysis. N is the number of disciplines. The subscript 0 represents those functions or variables that are shared by more than one discipline. The subscript i represents functions or variables that apply only to discipline i. The cap symbol "^" represents independent copies of variables distributed to discipline.

The formulation given in Eq.(1) includes all the coupling variables, copy of the coupling variables, constraints, consistency constraints, state variables and residual of governing equations. AAO solves MDO problem in a straightforward way by giving control to a system-level optimizer. Some authors state AAO as Simultaneous Analysis and Design (SAND) [9, 17]. Figure 2-1 represents the AAO problem framework [16].

In Figure 2-1, a type of flowchart is used to describe the AAO framework. The components (in this case discipline analyses) are placed in diagonal. The special rounded rectangular component or driver controls the iterations. The component is used to process the data. The data flow is displayed in *thick gray line*. The component takes the data input from the *vertical line* and output data in the *horizontal line*. Therefore, the connections flow above the diagonal flow from left to right and top to bottom, and the connections below the diagonal flow from right to left and bottom to top. An off-diagonal node in the shape of a *parallelogram* is used to label the data. The external inputs and outputs are placed on the top row and the leftmost column respectively. The *thin black lines* represent the process flow. The superscript * represents the function or variables at their optimal value. Any block referring to discipline i denote a repetitive pattern for every discipline. A numbering system is used to show the order in which components are executed.

The AAO formulation given in Eq.(1) is used to derive the selected formulations for this work. Due to its nature, several simplifications can be made to the general formulation when stating the transonic fan design optimization problem; this is presented in the following chapter.
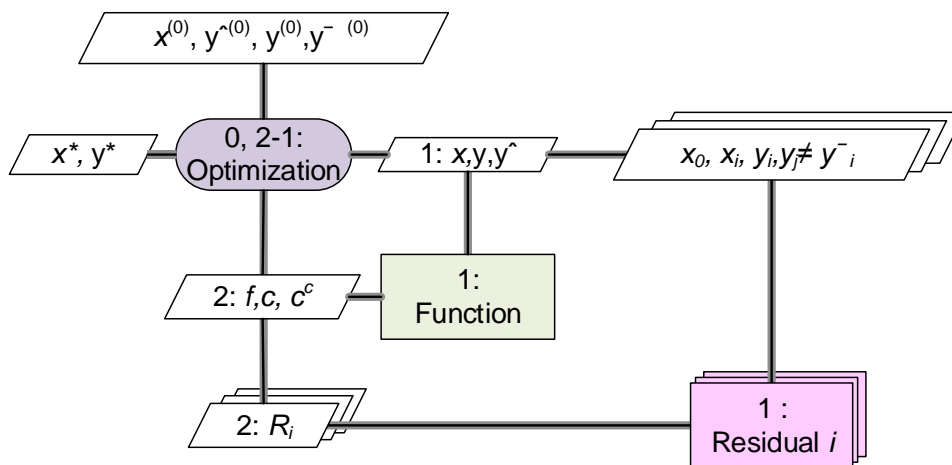
Figure 2-1: AAO framework using the flowchart from Martins and Lambe [16]

2.1.2 Comparison of MDO formulations

The purpose of this section is to review and analyze the published comparative studies on the existing MDO formulations which will further help to select suitable MDO formulations for the transonic fan blade design problem.

A number of comparative studies have been reported in the literature to evaluate the capabilities and effectiveness of each proposed MDO formulation, as well as their limitations for a given design problem. The evaluation of different MDO formulations can take into consideration the optimization and formulation aspects [18-24].

Hulme and Bloebaum [20] compared various MDO formulations including the MDF, IDF and AAO on five analytical examples of varying size and complexity. Metrics such as the number of iteration cycles, design variables and the accuracy are the basis of this evaluation. Based on these metrics they concluded that MDF is the "best" solution for all the test problems with the smallest number of executions The same metrics are used by Chen, Zhang et al. [19] to evaluate CO, CSSO, and BLISS on two application examples. They recommended CO for systems with little interaction between disciplines, BLISS for highly coupled system and CSSO formulation only for small-scale systems.

Another comparative study was carried out by Perez, Liu et al. [23] with a set of metrics (see Table 2-1), for both formulation considerations and optimization performance criteria. They determined the characteristics of each formulation (MDF, IDF, CO, CSSO, and BLISS) by

analyzing two test cases based on the proposed metrics. A summary of this work is presented in Table 2-1.

MDF is found to be the most accurate formulation as it performs the full disciplinary system analysis, but its efficiency suffers with increase in complexity. IDF offers an alternative to MDF when portability analysis is not an issue. The BLISS formulation accuracy is similar to centralized formulations but computationally more expensive. Its main advantage lies in the portability for distributed analyses. CO shows best choice for conceptual design process due to the high probability to fit in the existing system and its simplicity makes it easy for modification. However, CSSO is found efficient for small scale problems or analytical formulations since system approximation increases the complexity of implementation. Moreover, BLISS provides certain amount of portability and suitable for the problem where highly coupled systems analysis is available.

Table 2-1: MDO formulations comparative summary (Perez, Liu et al. [23])

	Accuracy	Efficiency	Transparency	Simplicity	Portability
Best	MDF	IDF	MDF	MDF	CO
	IDF	BLISS	IDF	IDF	CSSO
	BLISS	CSSO	CO	CO	BLISS
	CO	CO	CSSO	CSSO	IDF
Worst	CSSO	MDF	BLISS	BLISS	MDF

The comparison of ATC with other MDO formulations is not often available in literature yet. However, ATC and other multi-level frameworks such as CSSO, CO and BLISS are compared by De Wit and van Keulen [24]. These frameworks are studied on the same design optimization problem with a gradient-based optimizer and are compared to AIO solution in terms of the number of function calls and discipline evaluations. This study shows that CO and ATC performed equally well in terms of number of function calls. It is also found that, ATC with other multi-level frameworks are not competitive with single-level framework in terms of function calls and discipline evaluations.

In general, it is difficult to draw a definitive conclusion between the existing MDO formulations using the current literature available in the references (see Refs. [18-23]) due to the reason that if one MDO framework is suitable for one system, it is not necessarily a good choice for other systems because all systems have different attributes such as different objectives to achieve with different number of design variables, limits of constraints and sequences of disciplines, which cause differences in the level of success.

2.1.3 MDO implementation in aeronautics and propulsion

The application of MDO formulation within the aeronautics and propulsion fields involves several subsystems/disciplines: for example aerodynamics, structure and dynamics, and potentially many other disciplines. In literature, the most commonly found applications of MDO are about design of aircraft [25-27], rotorcraft [28-30], wind turbines [31], spacecraft [32, 33] and propeller [34].

A Boeing 747-400 aircraft was redesigned by Allison, Walsh et al. [35] by employing AIO and ATC product development formulations. The objective was to minimize the gross take-off weight (GTOW) with satisfactory performance constraints for takeoff, cruise and climb mission conditions. ATC performed well in the system oriented design environment and improved the objective function by 17% as compared to AIO. The authors concluded that for some cases ATC requires more computation time but it offers a flexible design space exploration that helps to find the global optimum.

Several researchers conducted the aerodynamics and structural optimization to redesign a helicopter rotor blade (see Refs. [30, 36-38]). Lee and Hajela [38] used a Genetic Algorithm (GA) in a decomposition-based approach for the design of a helicopter rotor blade to minimize the vibration at the rotor hub. They found that the decomposition-based approach is more effective as compared to the AIO formulation.

Tribes, Dubé et al. [39] executed a simple wing design MDO optimization problem based on simplified aerodynamics and structure analyses by using two single-level MDO formulations Distributed Analysis Optimization (DAO), Fully Integrated Optimization (FIO) and two bi-level MDO formulations including Inexact Penalty Decomposition (IPD) and a new proposed formulation called Distributed Optimizations (DO). The design problem involves the

aerostructral coupling as well. The authors concluded that for this wing design problem DO performs well but DAO is found to be more efficient as compared to FIO, IPD and DO. A requirement to study the influence of the number of design variables on the performance of different MDO formulations is highlighted.

A multi-layer optimization of disk and blade, was performed by Wang, Jia et al. [40]. Multilevel MDO formulations were implemented in three ways, which include BLISS 2000 two layers and two subsystems (aerodynamics and structure), BLISS 2000 two layers and triple-subsystems (aerodynamics, blade and disk structure) and BLISS 2000-CO formulations for three layers (structure optimization further subdivided into blade and disk optimization). A total of 13 geometrical design variables, 8 stress reliability constraints and 1 radial elongation constraint were considered. It is observed that the two layer MDO formulations perform better as compared to the three-layer MDO formulations caused by the additional calculation between the second and third layer. Moreover, Allison, Kokkolaras et al. [41] reported that CO could be nested within ATC.

Recently, the similar multi-level MDO frameworks were applied by Yang, Chen et al. [42] for turbine blade design problem to perform aerodynamics and thermal optimization. To maximize the efficiency and minimize the weight, a single weighted objective was considered along with the maximum blade temperature, mass flow rate, maximum stress and blade tip elongation constraints. They concluded that CO performance may be affected by the weighted sum to handle the two objectives. However, BLISS 2000 was found more robust as compared to CO; and a need for other multi-objective approaches is also mentioned.

In summary, MDO frameworks are powerful tools for designing aircraft components, as they allow the consideration of various subsystem requirements during the whole design process. It is also observed that not many studies presented MDO application for turbomachinery high-fidelity design problems especially the transonic fan and compressor design problems.

2.2 Blade design optimization

The turbomachinery automatic blade design optimization process mainly consists of integration of the blade geometry parameterization, performance evaluation (flow, stress and dynamics analyses) and optimization algorithms. In addition, to improve the performance of automatic

design optimization process, various methodologies are adopted by different researchers such as surrogate model, adjoint method, etc., and will be reviewed in the following subsections.

2.2.1 Blade geometry parameterization

Transonic fan blade performance is sensitive to its shape and thereby the appropriate choice of design parameters and the approach to modifying the design parameters are essential and determine by the blade geometry parameterization method. A blade parameterization with minimal parameters is desirable during the design as it allows to efficiently explore a less intricate design space and to obtain directly a smooth blade shape without further geometrical operations. Hence, the blade geometry parameterization plays an important role in turbomachinery blade design optimization.

The most popular turbomachinery blade geometry parameterization techniques are B-spline and Bézier curves. The B-spline parameterization were implemented by Oyama, Liou et al. [43, 44]; Lian and Liou [45] and Pierret, Coelho et al. [46] to parameterize a transonic NASA Rotor 67 fan blade. The Bézier curves were used by Buche, Guidati et al. [47]; Benini [48]; Arens, Rentrop et al. [49] and Lotfi, Teixeira et al. [50] to parameterize a turbomachinery blade. Furthermore, the higher order sets of polynomials were employed by Chen, Zhang et al. [51] to construct a transonic compressor blade. The blade perturbation parameterization approach by using Hicks–Henne polynomial function and its variants was employed by Wang, He et al. [52]. They have used a total of 143-design variables to parameterize a Rotor 67 blade. Thus, either approach takes at least 20 parameters to define a single two-dimensional section. In most situations, more than 100 parameters are needed to generate a complete three-dimensional blade geometry. Recently, blade geometry changes such as the lean (moving the blade section in the circumferential direction) and sweep (moving blade in the axial direction) [53-55], the maximum thickness location along chord [56], the camber distribution [57], the skew (stacking line in the rotational direction) [58] and the solidity [48] have been used with some success in order to reduce the number of design variables [51, 59-66].

Recently, Lupien [67] has presented a three-dimensional parameterization approach (see details in Section 3.2) to represent and optimize a transonic fan blade with fewer design variables which is favorable for optimization. The parameterization software also ties the geometry to computer-

aided design software (CATIA), in order to share a common model for structure and dynamic analyses. This parametrization has been adopted in this thesis work.

2.2.2 Performance evaluation

In the design process, the performance of turbomachinery blade is evaluated at different levels of fidelity to achieve the full engine design. For an entirely new style engine, the first step is to employ the empirical relations in order to establish the compressor configuration. However, for a variant of an existing engine design, an accurate computational solver is required to evaluate the detailed performance of a modified geometry [3]. For the current thesis work, the following performance evaluation analyses have been considered.

2.2.2.1 Flow field analysis

The optimization of transonic fan and compressor blade consists of modifying the blade to achieve the targets such as mass flow rate and pressure ratio while minimizing the undesirable flow features such as high incidences, high shock losses, large blade passage flow separations, etc. Thus, fully three-dimensional CFD methods are needed to evaluate these effects.

Various commercial and in-house softwares were developed for flow analysis of turbomachinery blade. In this regard, TRAF3D [68, 69], a three-dimensional Navier-Stokes based code (see Refs. [5, 44, 46, 70-74]) and ANSYS commercial software (see Refs. [48, 75-77] are used by many research groups for transonic fan and compressor design optimization. Due to its wide range of features, ANSYS has become a popular choice for transonic fan and compressor manufacturer and is also utilized in the current thesis work.

2.2.2.2 Stress and dynamic analyses

The high rotational speed of the fan or the compressor rotor adds the complexity by means of static stress and vibration, into the blade design optimization problem. Therefore, finite element (FE) method is used to evaluate the mechanical requirements. The FE analysis commercial software ANSYS was used in many aero-mechanical optimization of turbomachinery blades (see Refs. [5, 65, 75, 78, 79]).

2.2.3 Optimization algorithms

A number of optimization techniques for efficiently solving engineering design problems are available in some of the classical text books like Fletcher [80], Gill et al. [81], Rao [82], Moré, Wright et al. [83]. In general, the optimization algorithms are classified into gradient-based and non-gradient based methods and an overview of this subdivision is presented in the following section.

2.2.3.1 Gradient-based methods

The optimization process using *Gradient-based methods* requires derivative information for the objective and constraint functions to obtain a direction of search. The performance of a gradient-based method strongly depends on the initially supplied values for the design variables. These methods are well suited for continuous design space but may not be appropriate for searching the global optimum of a multi-modal problem [84].

Gradient-based methods have demonstrated their ability to solve engineering design optimization problems such as wing design [85], aircraft configurations [86] and turbomachinery blade design [52, 87-89]. Burguburu, Toussaint et al. [89] used gradient-based methods to improve the efficiency of a transonic compressor while maintaining the pressure ratio. The three-curvature control points on suction side were taken as design variables.

Although, the gradient-based methods are rapid optimization methods and require a small number of evaluations as compared to non-gradient based methods, but they can easily be trapped by local minimum. Due to this reason, these methods are also recognized as local optimizers [90].

2.2.3.2 Non-gradient methods

The *Non-gradient methods* do not require any derivatives of the objective function in order to search for an optimum. One of the advantages of these methods is that they are more likely to find global optimum and not be trapped by a local optimum. These methods are well suited for nonlinear, multimodal problems and discontinuous design space. However, non-gradient-based methods require a large number of evaluations and result into relatively high computational cost.

A number of methods exist in this group such as the evolutionary algorithm, particle swarm, simulated annealing, etc. Among them, the evolutionary algorithms are the most common choice

to solve the design optimization of transonic compressor blade problem (see Refs. [5, 43, 48, 73, 75, 78, 91-95]).

In addition, each optimization algorithm has its own strengths and weaknesses. A commonly reported opinion is that "no-single optimization algorithm is suitable for all problems." For this reason, in a preliminary study, it is valuable to compare several optimizers.

2.2.4 Blade design methodologies

A number of studies are published to redesign transonic fan and compressor blade by using surrogate models, adjoint method and inverse design approach. The detail of all these investigations is discussed below.

2.2.4.1 Adjoint method

An *adjoint method* computes accurate gradient for the governing equations and provides sensitivities of the objective and constraint functions with respect to the design variables. It can be coupled with gradient-based optimizers and has been adopted by many researchers in turbomachinery design (see Refs. [52, 88, 96-99]).

Recently, Luo, Zhou et al. [88] implemented an adjoint method on RANS equations by using the SST turbulence model to perform single (at design point) and multipoint (at the design point, near choke and near stall) design optimizations to improve the adiabatic efficiency of NASA Rotor 67 while having the mass flow rate and total pressure ratio under constraints. The single objective optimization has improved adiabatic efficiency by 1.10% but reduced the total pressure ratio. The multipoint optimization gives higher adiabatic efficiency with no reduction in the total pressure ratio. However the improvement in the adiabatic efficiency is slightly smaller than the single objective gain.

However, the development cost of adjoint codes to solve the system of equations for the complex, three-dimensional flow with many unknowns, might be the main shortcoming [90]. Moreover, at the present time, adjoint methods are not readily available in commercial softwares such as CFX or Fluent.

2.2.4.2 Surrogate models

A *surrogate model* is often used in MDO system to get relatively good high-fidelity model information throughout the optimization without computational expenses associated to a high-fidelity analysis. The surrogate models or Meta-models are analytical equations that approximate outputs of the intricate systems that are built by providing a limited set of computational expensive simulations. Surrogate-based optimization approaches have been implemented and tested by various researchers on computationally expensive problems such as turbomachinery design problems due to their inherent advantages.

Surrogate models applications include Design of Experiments (DoE) with Response Surface Approximation model (RSA) by Myers and Montgomery [100], Artificial Neural Networks (ANN) by Turban and Frenzel [101], Kriging Meta-model (KRG) by Martin and Simpson [102], Radial Basis Neural Network (RBNN) by Orr [103] and weighted average surrogate model based on RSA, KRG and RBNN by Goel, Haftka et al. [104]. Goel, Haftka et al. [104] concluded that the weighted average surrogate model is robust and better as compared to the other best individual surrogate models for both low and high dimensional problems regardless the number of points used in the model response.

Numerous researchers ([5, 46, 60, 75, 105, 106]) have optimized the transonic fan and compressor blade in a multidisciplinary context by using several different surrogate models. One of the possible reasons of surrogate models selection is that the surrogate models might be simple and could help the optimizer to optimize the design problem with less computational time. However, the surrogate models might not be able to capture the information for a large design space and unable to predict the optimum design with accuracy as compared to the high-fidelity solutions.

2.2.4.3 Inverse design method

The turbomachinery blade design performance improves during an optimization in terms of efficiency, pressure ratio, stress, vibration, etc., by varying geometrical design parameters or blade geometrical dimensions. Conversely, in the *inverse design methods*, the blade is redesigned by aiming prescribed flow characteristics such as blade pressure distribution, circulation, velocity and varying local geometrical parameters.

In the last two decades a number of papers were published on the inverse design approach on the transonic axial compressor (see Refs. [57, 107-114]). In this context, Tiow, Yiu et al. [115] redesigned NASA Rotor 67 by improving the incidence near the hub and shock formation near the tip with change of static pressure loading. Moreover, Geng, Chen et al. [95] applied a simple method of redesigning the pressure (or Mach number) distribution on the suction side of NASA Rotor 37 by controlling the shock to enhance the adiabatic efficiency. This method was able to reduce the shock strength level and decrease the boundary layer separation loss to increase the efficiency.

However, inverse design method is struggling in establishing criteria for the optimal loading distribution and mechanical constraints implementation due to the presence of secondary flow. A lot of vision is required to modify the mechanical and geometrical parameters for the velocity variations [90].

2.2.5 Recent progress

Fan design shares many similarities with the design of a single stage axial compressor. So, in this section, the recently published studies on transonic compressor or transonic fan blade design problems are presented. The section is subdivided into three subsections to discuss aerodynamics optimization, aerodynamics-structure optimization and aerodynamics-structure-dynamic optimization. An overview of this recent progress is tabulated in Table A-2 and Table A-3 (Appendix-A).

2.2.5.1 Aerodynamics optimization

In recent years, several studies have focused on the aerodynamics design optimization of transonic fan and compressor blade. The optimization problem is most commonly targeted to improve the efficiency or reduce the losses subject to some required constraints, such as mass flow rate, pressure ratio and others (see Refs. [43, 44, 59, 62, 71, 87, 88, 116]). Lee and Kim [87] optimized a compressor blade by using a gradient-based optimization method. Their objective was to minimize the aerodynamics losses/maximize the efficiency by taking a stack line as a variable. Another single objective optimization to improve efficiency of NASA Rotor 37 is executed by Jang, Samad et al. [62] by taking sweep, lean and skew design variables. A

conclusion has been made that among these design variables skew is the most effective for efficiency enhancement.

In the past, the turbomachinery design and optimization were limited to fewer design variables due to computationally expensive three-dimensional flow analyses. In recent years, analyses tools, optimization software and blade parameterization have improved to produce impressive results such those from Oyama et al. [43] to redesign NASA Rotor 67 with 56-design parameters. They successfully developed a high-fidelity numerical aerodynamics optimization tool for transonic compressor blade design by using three-dimensional Navier-Stokes solver (TRAF3D). In this tool, an evolutionary algorithm named real-coded adaptive range genetic algorithms (ARGA) was adopted. The entropy production was reduced by 19%, which further led to a significant gain in efficiency of 2% as compared to baseline design.

After that, Oyama, Fujii et al. [44] added an additional thickness constraint but did not get a significant reduction in entropy due to tight constraints. They recommended considering a multi-objective and multidisciplinary (aerodynamics, stress and dynamic) design optimization in order to achieve a better blade design.

In all of above cited works, the blade aerodynamics is optimized on a single objective, i.e. either aerodynamics loss or efficiency at design point. However, a compressor has to satisfy design requirements not only at the design point but also at the off-design points, as an aircraft engine operates over a large range of operational regimes. Thus, a transonic fan and compressor aerodynamics design optimization problem involves multiple measures of performance or multi-objective such as design point efficiency, stall margin, choke margin, total pressure ratio, etc., in order to get the trade-off solutions between the contradicting design goals. The multi-objective optimizations provide insight to the engineering design problem that further helps to achieve many Pareto-optimal solutions (a set of compromise solutions) and more information to the designers. A number of investigations dealt with the multi-objective aerodynamics transonic fan and compressor design optimization (see Refs. [48, 70, 71, 93, 94, 117-119]). A multi-objective optimization was performed by Benini [48] to maximize the efficiency and pressure ratio of NASA Rotor 37 while keeping mass flow rate under constraint. A higher-pressure ratio helps to reduce the number of stages which further leads to reduce the engine weight. An evolutionary algorithm [120] was used for optimization. The overall efficiency was improved by 1.5% without

changing the pressure ratio. However, another optimal blade was obtained with a 5.5% pressure ratio rise and a 0.8% efficiency drop.

More recently, the enhancement of the design performance (peak efficiency) and off-design performance (stall margin) of NASA Rotor 67 were considered by Okui, Verstraete et al. [71]. In this optimization the choked mass flow was constrained. The optimization was conducted in two stages: first a meta-model coupled with artificial neural network (ANN) and then with a differential evolution (DE) method. A 0.6% efficiency improvement was obtained with backward sweep together with S-shaped camber line and chord length movement. Stall margin is slightly improved.

Another way to handle the multi-objective optimization problem is to reformulate the multiple objectives into a single objective function mostly by weighted sum method (see Refs. [46, 88]). However, it is difficult to set appropriate weights for different objectives as it requires insight information of the inner relations.

2.2.5.2   Aerodynamics and structure optimization

Aerodynamics optimization in turbomachinery blade design problem is often performed with structural constraints or objectives such as maximum stress, weight, safety factor, etc. (see Refs. [5, 73, 77, 105]).

An aero-structural optimization that focuses on maximizing the pressure ratio and minimizing the weight was conducted by Lian and Liou [5]. This optimization included a stress safety factor (ratio material yield stress to the equivalent stress) and a mass flow rate constraint. The high fidelity analysis tools, the genetic algorithms and response surface approximation were used. As compare to the baseline Rotor 67 the optimized design had 1.88% rise in the pressure ratio and 5.36% reduction in the weight while stratifying the aero-structural constraints. In addition, the maximum von-Mises stress was located at the root of the blade.

The enhancement of safety factor along with the efficiency improvement was studied by Kang, Park et al. [105] on a single-stage transonic axial compressor. Both objectives were reformulated into a single objective function by giving certain weights. The genetic algorithm (GA) was applied to explore the Pareto front and to find the maximum value of the objective function. After that gradient-based optimization was implemented on the final design to improve the accuracy of

the optimization. They were able to improve 3.69% efficiency with 2.3% safety margin from the baseline while limiting the pressure ratio and mass flow rate. The authors reported that the optimized design had good agreement with the compressor test results.

Recently, a similar work was carried out by Joly, Verstraete et al. [73], where both the aerodynamics and the aero-structural optimizations were executed on a highly loaded and compact contra-rotating fan blade to improve the design efficiency and to reduce the maximum von-Mises stress with imposed mass flow rate and pressure ratio constraints. A differential evolution (DE) method was integrated with NSGA-II for optimization. The Calculix [121] solver was used to calculate the von-Mises stress. The blade was optimized at the design point condition, so, it was assumed that the blade deformation is small due to the pressure as Lian and Liou [5] mentioned. The deformation was calculated one time by considering the aerodynamic pressure loading during the structural analysis and it was subtracted from the optimized design to get the actual shape of blade to be manufactured. The multidisciplinary strategy was found very effective when the aerodynamics and the aero-structural optimization were compared. A 65% attenuation of the stress was obtained as compared to only the aerodynamics optimization. Though, it was achieved at cost of 1% and 0.47% reduction in the aerodynamics efficiency and the pressure ratio respectively.

2.2.5.3 Aerodynamics, structure and dynamic multidisciplinary optimization

As mentioned earlier, an aircraft experiences different operating conditions such as takeoff, cruise, etc., so, the compressor blade suffers time-varying repeated loading at the takeoff and especially at the cruise condition as there is reduced load due to the turbulence or the vibration. Thus, the aerodynamics design of turbomachinery blade is unavoidably affected by the vibration characteristics, which results into vibration modes required to calculate, tune and have proper safety margin to avoid resonance. The Campbell diagram is used to determine the frequency safety margin or tuning and to display the resonant crossings. The frequency tuning is usually based on past experience and vary with intend to use, operating conditions, engine-to-engine and design philosophy. The frequency safety margins were mostly applied as constraints during design optimization process (see Refs. [46, 65, 74, 75, 78, 92, 122]). Some of the researchers have imposed this type of constraint by limiting the percentage difference of design speed frequency modes, such as three forbidden dynamic mode ranges of ±12%, ±7% and ±5% are

imposed on 1st to 3rd frequency modes, and some of them are imposed based on the rotational speed such as no mode arise within 95% to 105% of running speed. It is observed that, the wider margin of frequency constraints makes the optimization problem stiffer.

A ±2.5% forbidden range was applied on the first two vibration frequency modes by Pierret, Coelho et al. [46] with maximum stress (structural), mass flow rate and pressure ratio (aerodynamics) constraints during a design optimization to rise the performance of the NASA Rotor 67 at design and off-design conditions. In this work the objective was to improve the efficiency at three different operating conditions including the design point, choked mass flow and near stall point while imposing the lower limit of pressure ratio at all three-operating points and the mass flow rate at design point. All three objectives and constraints were combined in a single objective function through a penalty function method. They employed an optimization methodology with a combination of GA and Meta-model (Radial Basis Function: RBF) to accelerate the optimization process. A Finite Element Structural Mechanics Software (SAMCEF) was used to calculate the stress analysis and modal frequencies. The authors mentioned that an accurate frequency modes prediction would require a volume FE grid and a blade modeled with disk. However, the presented work did not include both aspects. A 0.5% improvement in adiabatic efficiency was achieved. It was observed that the thickness along the mid-section and trailing edges is very small near blade tip. Also, the obtained performance plot of the optimized design has short operating range as compared to the aerodynamics optimized Rotor 67 baseline.

Similar aerodynamics and dynamic constraints were implemented in the work done by Luo, Song et al. [78], such as limiting the mass flow rate, pressure ratio and the five forbidden dynamic mode ranges, ±12%, ±7%, ±5%, ±4% and ±3%, were imposed on 1st to 5th frequency modes. They redesigned the NASA Rotor 37 by maximizing the efficiency and minimizing the maximum stress. The differential evolution algorithm was implemented for optimization. Unlike the previous study they modeled a blade with disk and considered volume grid. Fluid pressure was imposed during the mechanical simulations. The optimization process was performed with 10 CPUs (3.0 GHz). Each FEM solution required 6 minutes and aerodynamics solution was obtained in an hour. It took seventeen days to solve the MDO problem. The maximum efficiency design has improvement in the efficiency, pressure ratio and mass flow rate by 1.52%, 1.35%, and 1.49% respectively and has reduction in maximum stress by 17.8%. In addition, the lower

stress blade design has reduced maximum stress by 37% and improved efficiency, pressure ratio and mass flow rate by 1.35%, 1.54%, and 1.41% respectively.

In the work carried out by Deng, Guo et al. [75], frequency constraints were implemented within the rotational speed varying from 95% to 105% that means within this speed no mode were allowed in the engine running range. In this work, multi-objective including enhancement in efficiency at design point and the slope of adiabatic efficiency, at the point 95% of the design mass flow rate to redesign a transonic fan blade were considered. A total of nine (9) constraints were considered: one constraint for choke margin, one for mass flow rate, one for pressure ratio, two for von-Mises stress and three for dynamic frequency modes. Stress analysis was carried out at the red line speed (engine maximum speed). The commercial software Isight was used for the optimization. The optimization process was based on first DoE database construction from high-fidelity computations (CFD/FEA) to initialize a Kriging surrogate model. After that Non-dominated Sorting Genetic Algorithm (NSGA II) was used to obtain Pareto front. The design optimization achieved a 0.2% efficiency gain at design point and a 0.67% efficiency improvement at 95% of the cruise mass flow rate condition.

Recently, Astrua, Piola et al. [74] worked with multi-objective optimization on an axial compressor transonic blade to reduce rotor loss while achieving the proper stall margin, choke margin, sufficient structural safety margin and initial three dynamic mode margins. The ANN and random walk search algorithm were implemented to determine the multi-objective Pareto front. For mechanical analyses, the blade is considered to be clamped at hub and the disc effect was not considered. In addition, only one time aerodynamics pressure loading was extracted at design point and stored in database, so, no pressure loading was implemented during the optimization for stress and dynamic analyses. Dynamic frequency modes were calculated at three different speeds (including the design point) in order to respect the engine running order but the rotating speed limit is not mentioned in the paper. Moreover, a dynamic analysis was performed on off-design speed with coarse grid and fine at nominal speed in order to reduce the computational time. No hot-to-cold conversion was considered. A design with peak efficiency +0.25%, choke margin +0.25%, and near stall mass flow +2% with appropriate mechanical requirements was achieved.

2.3 Summary

These investigations show that numerical optimization techniques have been widely used to enhance transonic fan and compressor blade performance and provide the following steps which can be used in this research:

- A number of studies were carried out to improve the performance of transonic and compressor blade by considering either single aerodynamics optimization or multi-objective multidisciplinary design optimization. However, MDO application with disciplines decomposition is rarely presented in transonic fan blade design problem. Therefore, there is a need to investigate the suitable MDO formulations for transonic fan blade design in order to solve the real industrial fan design problem in a computationally efficient manner, which also ensures that the design process is properly aligned with the disciplines relationships.

- These studies show that aerodynamics, structure and dynamics are the most influential disciplines in order to effectively improve transonic fan blade performance. Thus, aerodynamics, structural and dynamic analysis methodologies are required to develop and verify an MDO methodology.

- The transonic NASA Rotor 67 axial-fan blade was frequently used in transonic fan blade design optimization studies. This test case will be used for the validation of our approach and present in Chapter 3.

- As mentioned earlier, different design softwares are involved to perform aerodynamics, structure and dynamics discipline analyses within the design process. It is essential to map the designers' actions onto a flexible and transparent platform. Therefore, the commercial process integration and optimization software Isight is used in the present work to integrate the aerodynamics, structural, dynamic discipline analyses and parameterization software in order to perform MDO formulation for transonic fan blades.

- A fan design problem involves several design parameters, many design objectives and large number of constraints. Therefore, fan design formulation is required to identify prior to the optimization, which involves grounds for the selection of design parameters,

constraints and objectives for chosen disciplines. This will be discussed at the beginning of Chapter 4.

- It is observed that an aerodynamic optimization is often performed at the beginning of the design process. This is not only to ensure the robustness of the design process but also explores the design variables and obtains a comparative optimized design for MDO study. This will be present in Section 4.2.

- MDF, a single-level, most popular and straight forward MDO formulation, was employed in many industrial test cases due to its ease of implementation where an optimizer controls the complete multidisciplinary analysis and maintains system feasibility at each iteration cycle. In addition, a multi-level MDO based promising approach, ATC is employed due to its inherent nature close to the industrial design process. These MDO formulations will be discussed in detail in Section 4.3.

- It is also observed that non-gradient algorithms are well suited for solving the fan design problems with nonlinear and multimodal objectives and discontinuous design space. Moreover, it is difficult to find a single optimization algorithm which is suitable for all the design optimization problems, therefore a number of non-gradient based optimization algorithms are considered in the present work in order to explore suitable optimization algorithm for current fan design problem.

CHAPTER 3   PARAMETERIZATION AND ANALYSES
METHODOLOGIES

This chapter covers a selection of test case, fan blade parameterization, aerodynamic, stress and dynamic analyses, which further integrate during the transonic fan blade optimization process.

3.1   Selection of a test case

Transonic NASA Rotor 67 has been chosen for the presentation of methodology and validation purpose. It has been experimentally studied by the NASA Lewis Research Centre (Strazisar, Wood et al. [123]).

NASA Rotor 67 is a well-known and widely used test case for the three-dimensional transonic fans because detailed experimental results are available in literature. The rotor has 22 blades, with a tip clearance of 0.1016 cm (1.1% blade tip chord and 0.7% blade span), a tip speed of 428.9 m/s, an inlet tip relative Mach number of 1.38 and a 16043 RPM rotational speed at design speed. The rotor design point pressure ratio is 1.63 with a mass flow rate of 33.25 kg/s. Figure 3-1 represents the Rotor 67 test geometry.
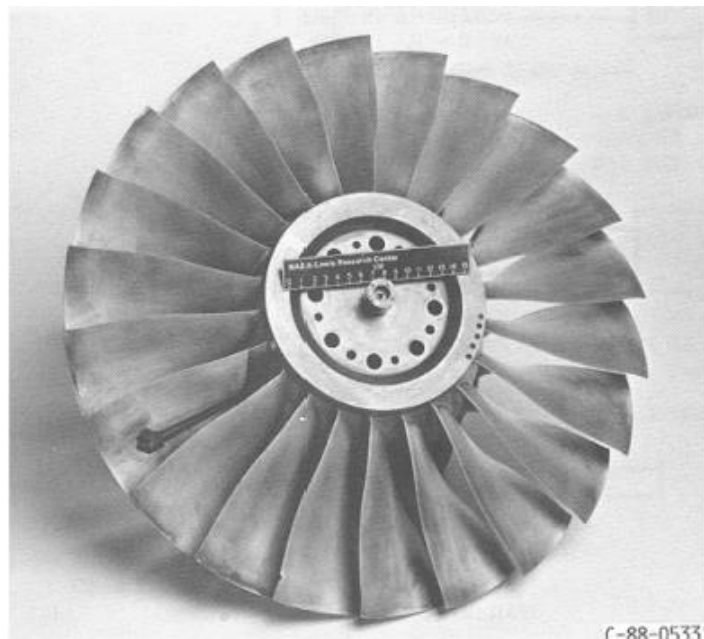
Figure 3-1: Test rotor (Lian and Liou [5])

Detailed computation of internal flow through Rotor 67 has been performed by Hah and Reid [124] and Chima [125]. The tip clearance effect was examined by Jennions and Turner [126] and Adamczyk, Celestina et al. [127]. Arima, Tamura et al. [128] and Arnone [68] have described the complex flow nature of Transonic Rotor 67 in detail. Furthermore, it has become a popular test case for design optimization study (Oyama, Liou et al. [43]; Pierret, Coelho et al. [46]; Wang, He et al. [52]; Lian, Oyama et al. [45]; Lian and Liou [5] and Li, He et al. [65]). However, not many researchers have investigated Rotor 67 for stress and dynamic features. One of the reasons is that the structural configurations are not available for that blade.

Practically, a fan blade is attached to a disk. The disk data and material properties for Rotor 67 are not available in literature as this blade is an aerodynamic test case. However, in the current research work targeting the realistic stress and dynamic analyses, a disk is obtained by offsetting a streamline at the bottom of the blade. A fillet radius is defined as 3% height of the blade (roughly scaled from other designs). Thus, a fillet radius of 0.00381 m (0.15 inch) has been taken for a 0.127 m (5 inch) tall blade. The blade with attached disk is depicted in Figure 3-2.
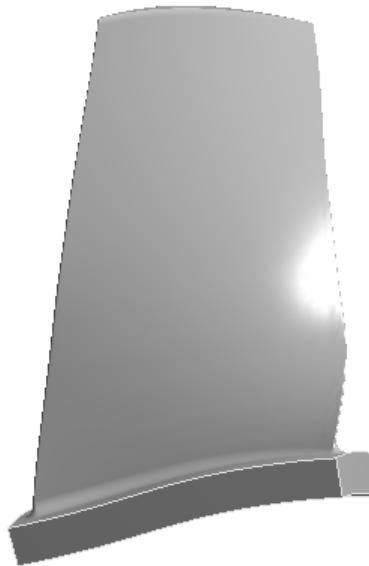
Figure 3-2: NASA Rotor 67 with simple disk

3.2 Blade shape parameterization

The turbomachinery blade shape parameterization is an important step in the automated multidisciplinary design optimization process to seamlessly link it with the design analysis process. As mentioned in literature review, many researchers have been using various parameterizations. In some papers, the parameterization has been considered as a separate research domain (see Refs. [129] -[130]).

A key requirement for fan blade designer is to have a natural link between the design parameters and the design requirements, while keeping the blade shape smooth. For example, an aerodynamic engineer wants to modify the blade angles and a structure/dynamic engineer usually adjusts the blade thickness and position according to their needs.

As mentioned earlier, various approaches have been reported for the blade geometry parameterization but most of them result into a large number of design variables to generate a transonic fan blade. Therefore, the best way of parameterizing a turbomachinery blade is still uncertain. However, Samareh [131] has surveyed blade shape parameterization techniques for high fidelity multidisciplinary optimization and summarized that an ideal shape parameterization approach must be automated to be employed easily in an integrated MDO framework without human interaction, have less design parameters, must be able to produce smooth shape with small or large modification, be able to couple with existing CAD system, have easy local control so that engineers can modify geometry according to their needs and be able to reduce computational resources which further leads to reduction of design cycle time [131].

Lupien [67] has adopted these ideal shape parameterization requirements to develop a fan blade parameterization. He improved the classical fan blade parameterization by adding control points in the spanwise direction which brings the continuity in the distribution of parameters. The present thesis work is using this three-dimensional fan blade multi-level parameterization, which proceeds in two major steps: (1) Sections parameterization (2) Multilevel module and its main characteristics are summarized in the following subsections. The parameterization includes the design variables listed in Table 3-1.

Table 3-1: Geometrical design variables for section parameterization

AX	Parameter that define the length and position of the meridional chord in the meridional direction
pcm	Position of the control points for the β-angles distribution
β	Beta-angles distribution (angle between the tangent of the curve and the meridional direction)
$d\beta/ds$	Beta curvatures: derivative with respect to s of the β-angle distribution
ps	Position of the control points for the thickness distribution
Tb	Thicknesses value
dTb/ds	Derivative with respect to s of the thickness distribution
θ	Stacking, section shift in the θ-direction from the position of its centroid
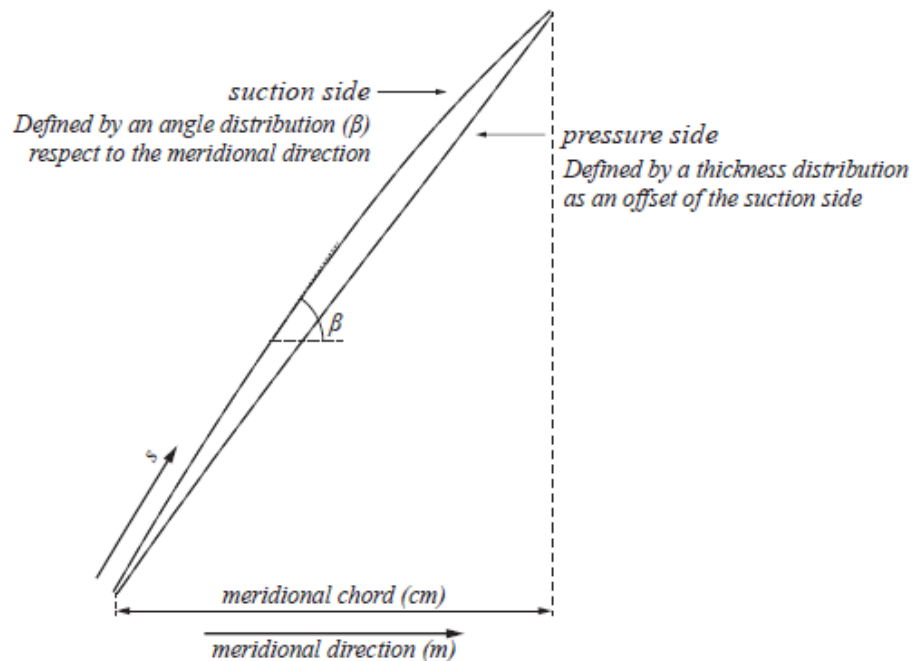
Figure 3-3: Definition of the suction side and the pressure side of each section [67]

Figure 3-3 illustrates the β-angle distribution (angle between the tangent of the curve and the meridional direction) to generate the suction side of the blade and a thickness distribution as an offset of the suction side to generate the pressure side [67].

In order to have designer's direct control on parameterization, the engineering parameters such as β-angles, β-curvature and maximum thickness have been used. As they can be intuitively linked by human designers to the flow characteristics in turbomachinery.

3.2.1 Section parameterization

This parameterization is based on a classical axial blade parameterization approach of multiple two-dimensional sections radially stacked.

In this parameterization, each section of blade is composed of four parts: suction side, pressure side, leading edge and trailing edge. The suction side is generated with β-angles and β-curvature distributions. Practically, angle distribution has more influence on suction side compare to pressure side. The thickness distribution is taken perpendicular to the mean camber line to generate the pressure side. Third order B-spline curves define these distributions and the number of splines are based on the number of points available in axial direction.

Figure 3-4 (a-b), present the β-angles and thickness distributions along spanwise and axial directions. Both are defined by a set of points (typically three to five) and the curve between those points is generated by considering the derivative distribution also defined as a set of points.

Furthermore, the suction side and the pressure side of the section are closed by circular arcs that create the leading edge and the trailing edge of the section, while the tangent continuity condition is maintained at the junction.

At last, the two-dimensional sections are positioned in the tangential direction (θ-parameter) position. The sections are stacked at centroid along the spanwise direction. Thus, the achieved two-dimensional blade sections are directly laid on the streamline surface (see Figure 3-4(c-d)). In addition, the continuity of parameters distribution in the spanwise direction is accomplished due to the spanwise control of parameters in this parameterization.
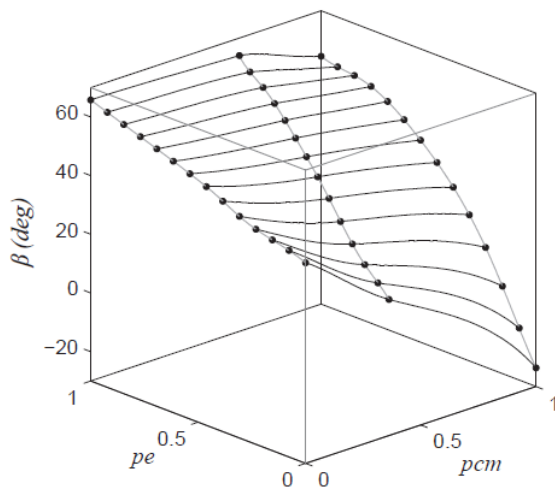
(a) β-angles distribution
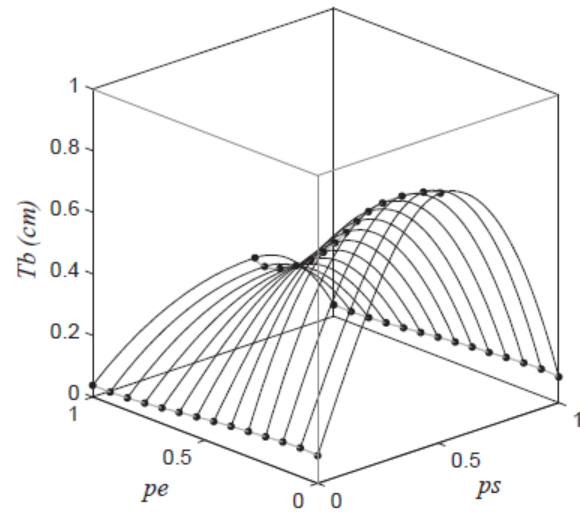
(b) Thickness distribution
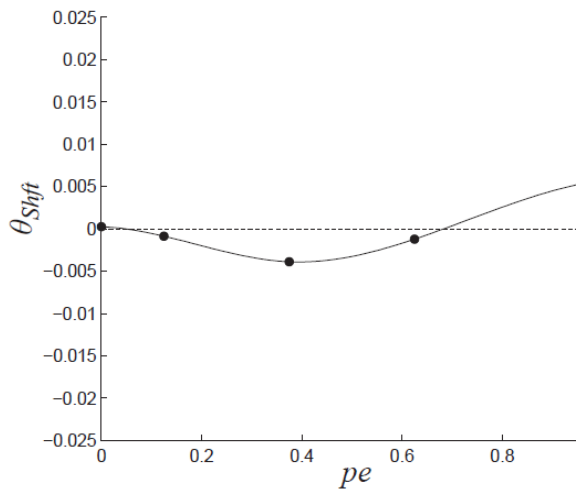
(c) Staking
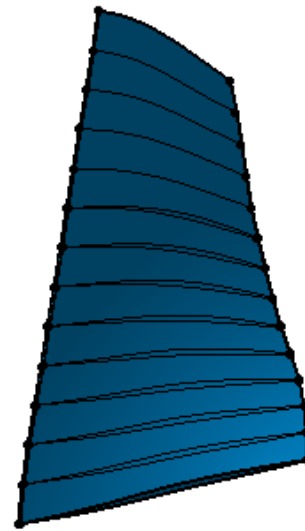
(d) NASA Rotor 67 fan Blade

Figure 3-4: 3D parameter distributions and a fan blade [67]

3.2.2 Multilevel module

This parameterization also provides a reduced set of parameters to smoothly modify the geometry more globally or locally by a multilevel module. The multilevel module is based on Gaussian curve given by:

$$Infl(Pe) = e^{-(pe-\mu)^2/2\sigma^2} \tag{2}$$

where, μ is the mean of the function and σ is the standard deviation. The μ is taken as the position in the spanwise direction of the requirement and σ (deviation) is taken as the range over which the modification will affect a control point. This deviation (σ) could be adjusted locally or globally to change the blade parameter distribution. It modifies five control points smoothly along the spanwise direction. This modification may be employed at different spanwise locations and for multiple design parameters. In the current work, the summation of modification distribution curves is taken as final spanwise distribution of the parameter. This approach also helps to reduce the number of design variables during the optimization process. An example of thickness modification by 0.01 cm at 30% span is presented in Figure 3-5. It shows that the modification is smoothly applied along the span.

Thus, Lupien [67] proposed parameterization requires a total of 128 parameters to accurately match NASA Rotor 67 fan blade (see Figure 3-4 (d)), but much less 10 to 22 parameters are used for optimization. In this research work twenty-two (22) geometrical design parameters have been selected for MDO.
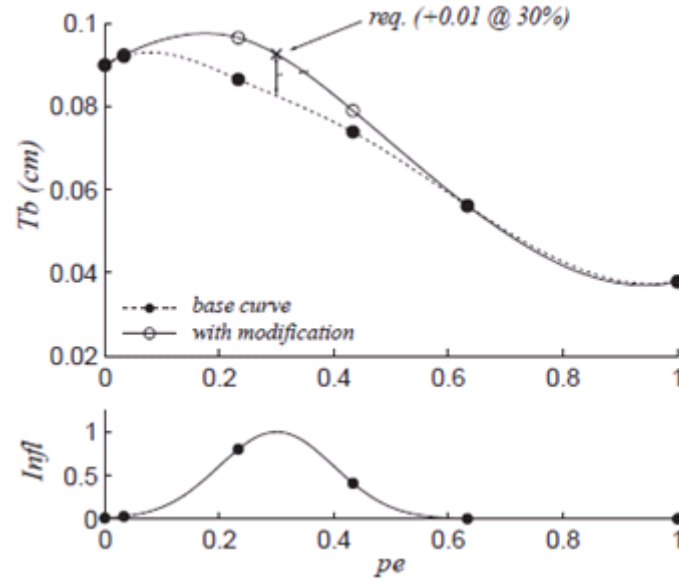
Figure 3-5: Modification of thickness distribution near leading edge at 30% span [67]

3.3 Aerodynamic analysis

This section provides the preliminary steps to build up the process for the blade aerodynamic performance prediction. It includes the computational tool selection, turbulence modeling, grid generation, boundary conditions and final validation of computational tool with the selected test case.

3.3.1 Computational tool

In this thesis work, widely used commercial Computational Fluid Dynamics (CFD) software ANSYS CFX is chosen to predict the performance of transonic fan blades, i.e. efficiency and pressure ratio. ANSYS has become extensively used for turbomachinery analyses due to its wide-range CFD analysis capabilities.

ANSYS CFX is a three-dimensional, viscous solver implementing cell-vertex finite volume, coupled implicit, pressure based scheme to solve the Reynolds-averaged Navier-Stokes (RANS) equations. The RANS simulation method is utilized as it is the most commonly used in the industry. The other method such as Large Eddy Simulation (LES) and Direct Numerical Simulation (DNS) are computationally too expensive. So it is out of scope of this research work.

3.3.2 Turbulence model

Turbulence is a highly complex phenomenon and even today it's modeling demands much more research to successfully predict the flow structure in a large range of situations. For practical application such as turbomachinery, the selection of a turbulence model depends upon the desired accuracy and the associated computational cost.

ANSYS CFX can use implementations of the classical two-equation turbulence models $k - \varepsilon$, $k - \omega$ and Shear Stress Transport (SST). The SST model combines $k - \omega$ model in near wall boundary and $k - \varepsilon$ model away from the boundary to get the benefit of both models. To get continuity between both layers, the SST model is using a special blending function. Furthermore, the SST model is recommended for high accuracy and robust boundary layer simulation by ANSYS. Therefore, the SST model has been used to predict the turbulent eddy viscosity in the flow.

3.3.3 Boundary conditions

The flow domain and meridional view of NASA Rotor 67 for simulation is shown in Figure 3-6. The inlet and outlet of the flow domain are defined at least 1-chord away from the blade leading edge and trailing edge to ensure that it does not affect the flow field.
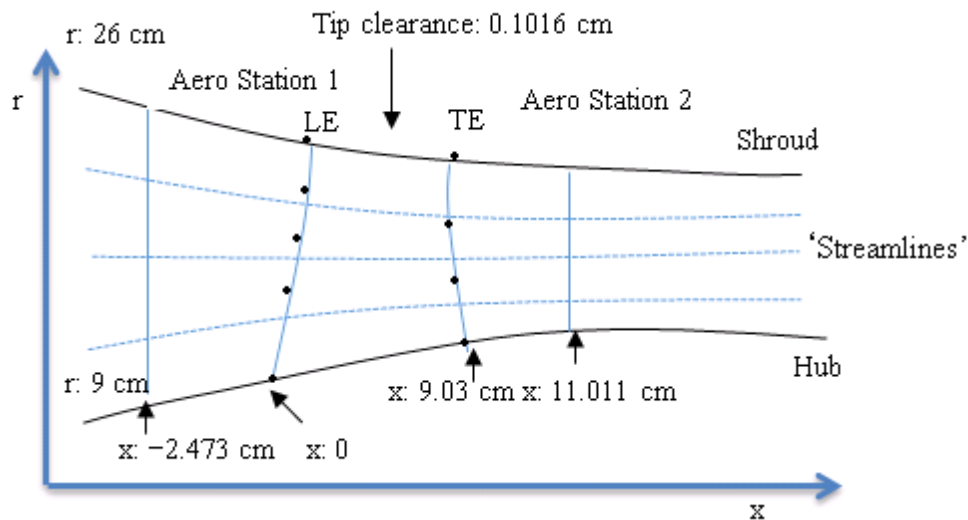
Figure 3-6: Meridional view of NASA Rotor 67

In order to simulate the flow for a single blade passage, following boundary conditions are specified:

- Periodic boundary condition is applied on the circumferential boundaries.
- The total pressure (P_{01}) and total temperature (T_{01}) are assigned at the inlet of the computational domain.
- An exit corrected mass flow is specified at exit domain.

The exit corrected mass flow rate boundary condition is useful as the fan needs to maintain mass flow. This means that the running line or operating points of the gas turbine is fixed to a constant corrected exit mass flow rate. As ANSYS CFX does not have a direct way to impose this boundary condition, an outlet mass flow boundary condition as an function of a constant exit corrected mass flow and varying total stagnation outlet pressure and temperature (see Eq.(3)) is specified. The CFX solver accommodates the temperature and pressure to obtain the prescribed exit corrected mass flow.

No slip and adiabatic wall conditions are taken on all wall boundaries. To resolve tip clearance flow explicitly, a counter rotating wall model is used in the frame of reference of the rotor shroud. In order to capture temperature change accurately for a high speed flow, the total energy equation is solved. The air is treated as an ideal gas.

3.3.4 Study parameters

In the present optimization study, the performance parameters including the isentropic efficiency, mass flow rate, total temperature ratio and total pressure ratio are computed.

The post processing analysis is performed in CFX Post and mathematical expressions are defined for the required parameters. These computations are executed at inlet (Aero station 1) and outlet (Aero station 2) as shown in Figure 3-6 of the computational domain where stagnation properties are mass averaged and static properties are area averaged.

The exit corrected mass flow is defined as:

$$\dot{m} = \frac{\dot{m}_c \left(P_{02} / P_{std} \right)}{\sqrt{T_{02} / T_{std}}} \tag{3}$$

where, P_{02} and T_{02} are the total pressure and total temperature in the stationary frame at Aero station 2 and P_{std} and T_{std} are the standard pressure (101325 Pa) and standard temperature (288.18 K) at the sea level.

The total to total pressure ratio is defined as:

$$PR = \frac{P_{02}}{P_{01}} \tag{4}$$

where, P_{02} is the total pressure in the stationary frame at Aero station 2.

The total to total isentropic efficiency is useful for the devices where work is either performed on the fluid (example a compressor or a pump) or extracted from the fluid (example a turbine). It is defined as the ratio of required isentropic work to the actual required work and the mathematical expression is given below:

$$\eta = \frac{H'_{02} - H_{01}}{H_{02} - H_{01}} \tag{5}$$

where, H_{01} and H_{02} are calculated in the stationary frame at Aero station 1 and Aero station 2 respectively. H'_{02} is isentropic total enthalpy at Aero station 2.

3.3.5 Grid generation

ANSYS CFX TurboGrid is selected for fan blade grid generation. A structured grid is used for this research work.

A mesh should resolve the flow of physics specific to the blade. Therefore, a grid convergence study is essential. A finer grid is computationally expensive whereas the quality of grid suffers by reducing the number of nodes. In addition, a selected grid will re-run thousands of times during the optimization process. So, it is not easy to build a computationally reasonable grid with high

quality and satisfactory level of refinement. Thus, grid sensitivity is performed to attain a good compromise between accuracy and computational latency for optimization process.

To generate grid the following recommendations are considered:

- Use at least 10-nodes in the boundary layer for accurate results with the SST turbulence model [132]. A similar recommendation has been specified by Van Zante et al. [133] to capture the tip clearance phenomena at least 12-nodes are suggested for a tip clearance of 1% span.
- In order to follow the no slip approach, $Y+ \approx 1$ near walls (blade hub casing) regions the grid density must be kept high around these regions.

Figure 3-7 shows the comparison between number of grid nodes, efficiency and solution time. It is observed that a 1,000,000-node fine grid is suitable for accurate high quality results as the efficiency is close to the experimental result but the solution time is almost 5 hours. On the other hand, a 150,000-node coarse grid requires around 18 min to get the result. However it has some deviation with the experimental result. It should be noted that, all the calculations were performed on a desktop machine with the following specifications: Intel Core i7 (16 GB RAM) Six-core processor.
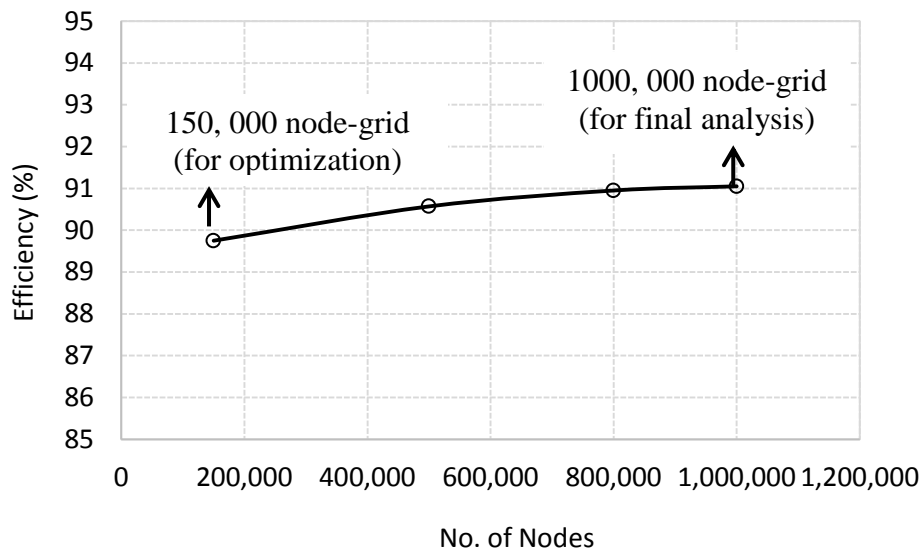
Figure 3-7: Grid sensitivity between number of nodes and efficiency

Ideally, a 1% of deviation with the experimental results is considered to be "good" but the experiment also has uncertainty that cannot be ignored. In a purely academic exercise of driving code, not only matching the test data is important, but also all the details of the flow solution should be captured. Optimization has a slightly different focus in which the geometry can change progressively to try and achieve a better result where the difference from design to design has more importance then to get the actual absolute answer. If a grid is chosen with per solution times greater than 2 hours then only 12 cases per day will be studied. The gradient evaluation for a system with a very small design space of 12 variables will take one day and then the line search could take another day. So, there is a need to find a grid that can return a solution within less than 30 minutes. Therefore, a grid with 150,000-nodes is found to be adequate to start the optimization workflow with a solution time of 18 minutes. It will facilitate much quicker optimization runs.

Figure 3-8 and Figure 3-9 show the view of computational grid for Rotor 67 with 1,000,000-node and 150,000-node grids. The computational domain with O-type grid near the blade surface and J/H/C/L-type grid in the other regions are chosen to get benefit the meshing feature for upstream and downstream end of passages with J-type grid on leading edge and H-type grid on trailing edge. The grid size at boundary layer is controlled by Y+ method, by specifying the Y+ height to 1 and Reynolds number 10^6. The grid resolution for a single blade passage is taken 1,000,000-nodes including the total 20-nodes in spanwise direction to define the tip clearance (0.1016 cm is equivalent to 1.1% blade tip chord or 0.7% blade span) between the rotor blade and the casing. In the tip clearance, grid size expends from Y+ $<<$ 1 at the hub to Y+ $\approx$ 5 at the blade tip.

For the 150,000-node grid, Y+ varies from Y+$\approx$ 1 at hub and around Y+ $\approx$13 near tip, which is not in the viscous sub-layer (y+ $<$ 5). But the SST turbulence model is capable to solve flow near the wall accurately with high Y+ value as long as 10 nodes exist in the boundary layer by switching between no slip boundary condition to wall-functions automatically [132].

As per CFD best practices, not only a root mean square (RMS) convergence criterion to achieve 10^{-5} on all the primitive variables, but also the convergence of mass flow rate, pressure ratio and efficiency to the 10^{-3} or 10^{-3} decimal place are considered. The interested readers are referred to Figure B-1 to Figure B-3 (Appendix-B), for the last 200 iterations convergence history plots of pressure ratio, efficiency and mass flow rate change for a 150,000-node grid. It shows that the maximum difference between two iterations is in order of 10^{-6}.
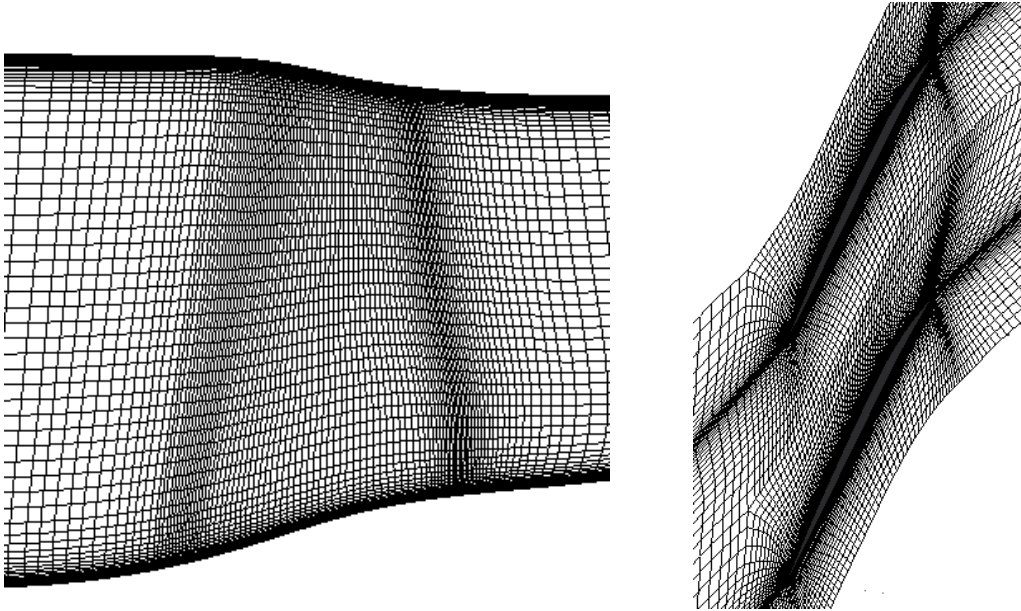
Figure 3-8: Meridional and blade to blade view of computational grid for Rotor 67

(1,000, 000-node grid)
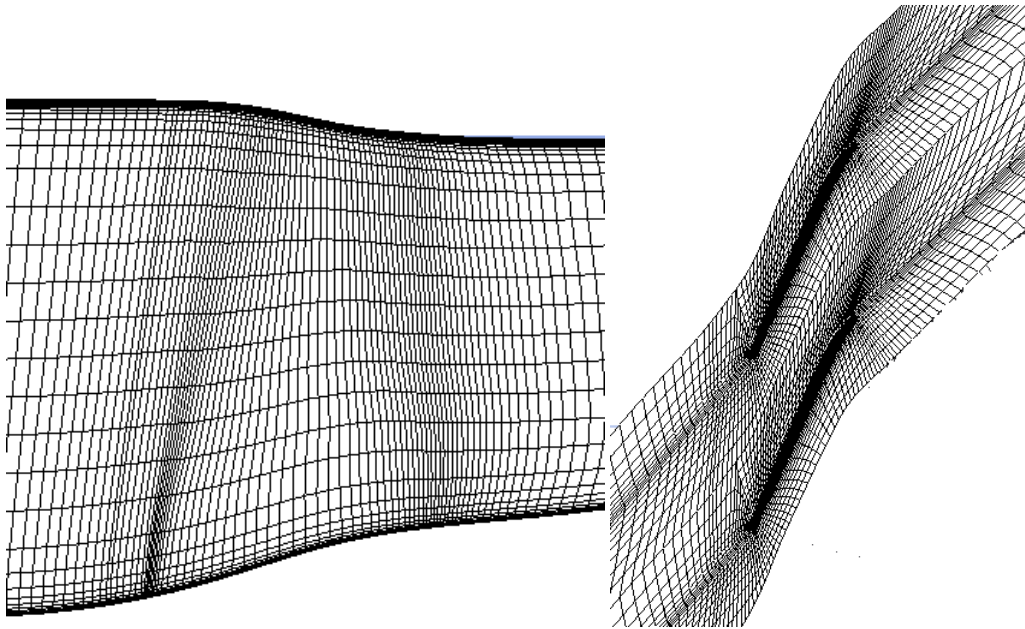
Figure 3-9: Meridional and blade to blade view of computational grid for Rotor 67

(150,000-node grid)

3.3.6   Computational tool validation

The validation of CFX solver tool is performed prior to executing the optimization. To computationally validate the tool and show the capability of the flow solver to capture the performance, a detailed comparison between experimental laser anemometer (Strazisar, Wood et al. [123]) and simulated from CFX solver Mach contour for design point at 30%, 70% and 90% spanwise locations are presented in Figure 3-10. Note that the contours are plotted at constant percent radius surface not on constant radius surface.

At 90% span, a shock starts from the leading edge and crosses the passage inside the blade row; a normal passage shock might also exist near trailing edge on the suction side. These findings are similar to the previous studies (Refs. [68, 125, 128]). At 70% span, the shock is moved forward. The other computations (Refs. [124, 126]) and current numerical study also observed the shock-boundary layer interaction and resulted thickening of boundary layer at 70% and 90% span. However, this shock-boundary layer interaction is not clearly illustrated in the experimental Mach number contour. At 30% span, the Mach number is subsonic with supersonic bubble existence near the leading edge on the suction surface. This observation is consistent with Chima [125] and a shock is mentioned might be the cause of bubble termination. It is also noted that the other computations and current numerical study observed the flow separated region at 30% span near the trailing edge.

Moreover, the comparison of numerically obtained performance plot of NASA Rotor 67 along with experimentally measured data is shown in Figure 3-11. A total of 7 and 12 different operating conditions are calculated to assess the overall accuracy in the numerical prediction of performance for 1,000,000-node and 150,000-node grids. The mass flow is normalized with choking mass flow. The choke mass flow is found 1.45% (with 1,000,000-node grid) under prediction then experimentally observed value. The same under prediction of choke mass flow was reported by Arnone [68]; Chima [125]; Jennions and Turner [126] and Hah and Reid [124]. The computed pressure ratio agrees very well with the experimental result. The computation is also under predicting the efficiency. The same trend was observed by Arnone [68]. The overall predicted performance of Rotor 67 has good agreement with experiment.

In general, CFX numerical studies resemble with the experimentally measured flow field [123] and reported by other researchers. Therefore, it is concluded that the CFX solver has an adequate qualitative agreement with experimental results.

In summary, the 150,000-node grid might not be sufficient to capture the fully detailed resolution of all local flow effects. However, the aim of this research work is to analyze the primary performance and stability of optimization process with adequate computational time. In addition, the trend is important for the current optimization research study. The discrepancies between both grid results have not much effect on the conclusion. Moreover, all the optimized design solutions will be analyzed with 1,000,000-node grid to confirm the results.
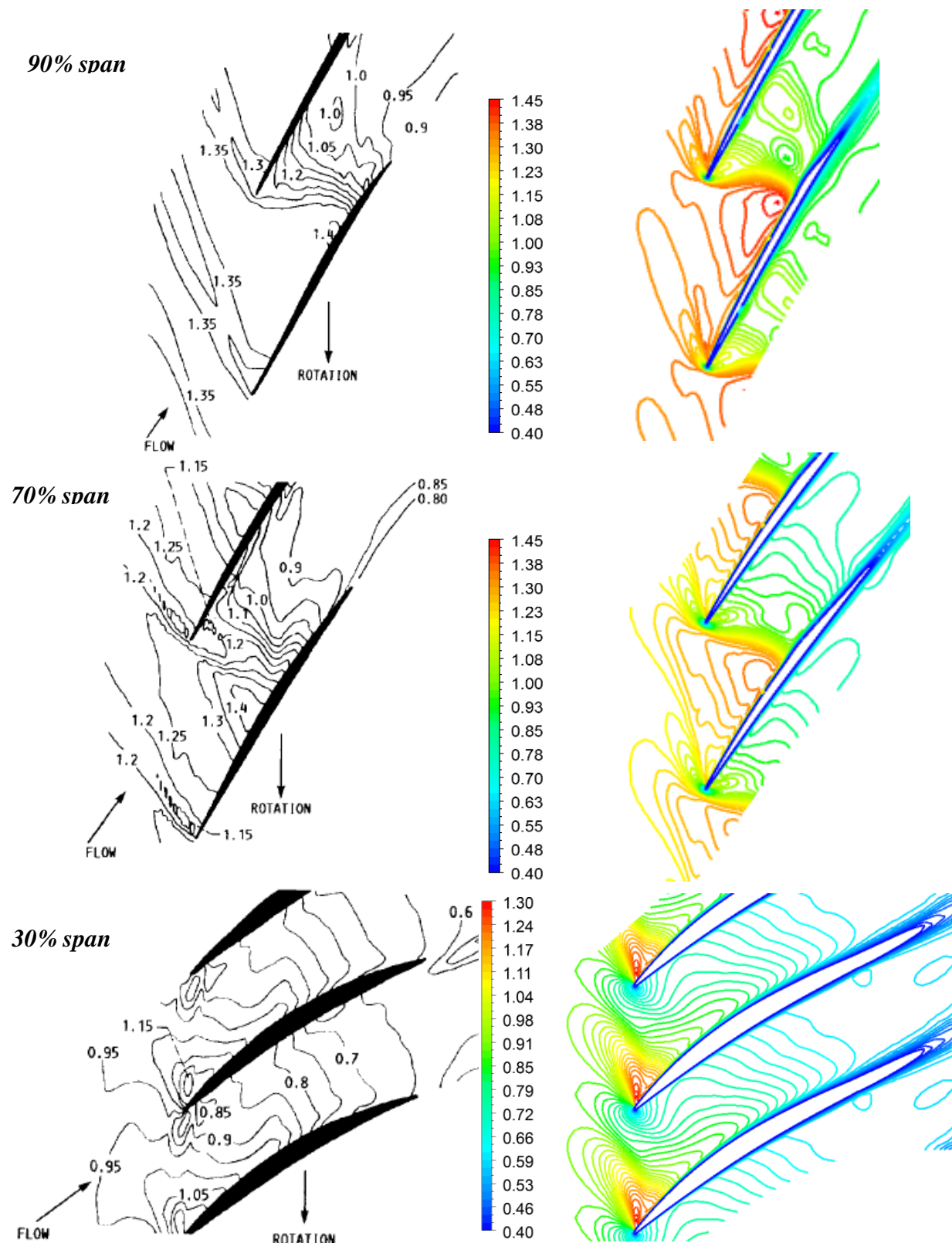
Figure 3-10: The comparison of Mach contour of Rotor 67 between (a) Experimental (Strazisar, Wood et al. [123])) (b) Current numerical study (1,000,000-node grid)
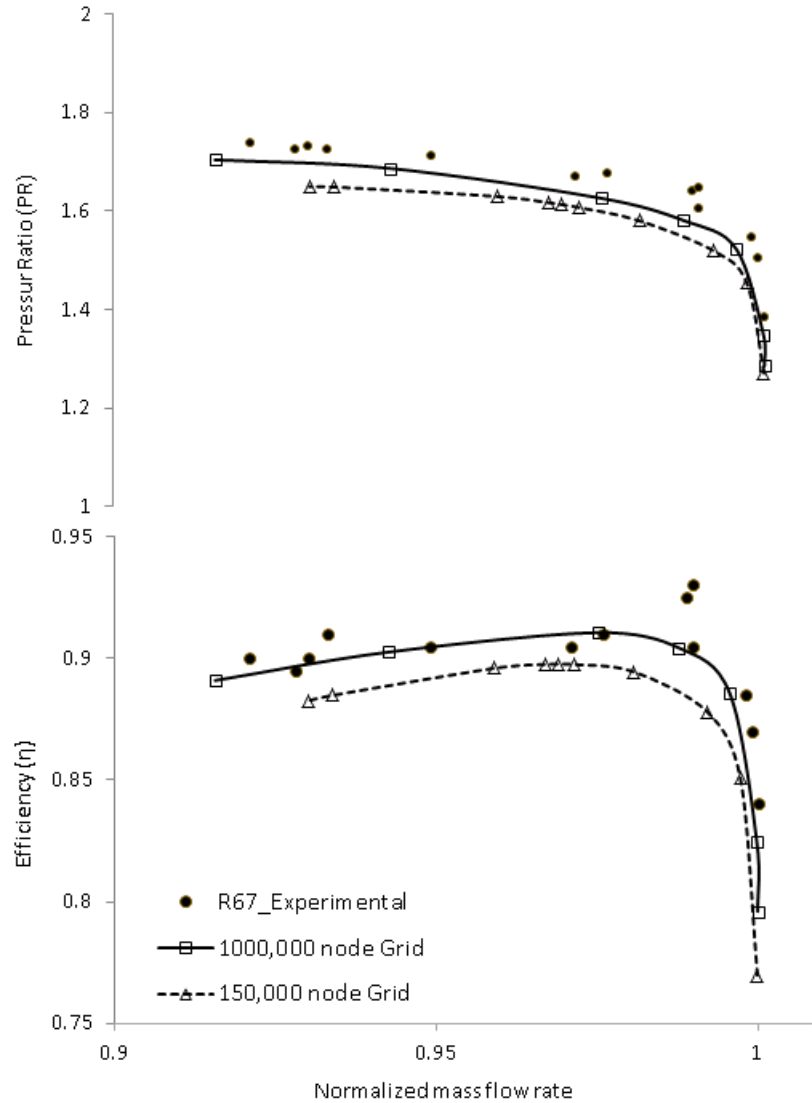
Figure 3-11: The performance comparison of Rotor 67 at design point between experimental (Strazisar, Wood et al. [123]) and current numerical study (1,000,000-node and 150,000 node grids)

3.4 Stress and dynamic analyses

The requirements for the structural blade design processes are obtained from literature, which are based on the material selection, accurate positioning of material, compromise between natural frequencies, blade thickness, number of blades, geometrical tolerance, etc. However, in the current thesis work, maximum stress and first three natural frequencies have been considered. The information of maximum stress can aid to identify the location where fracture is more likely

to occur. Whereas, the understanding of frequencies helps to identify and eliminate the excessive excitation such as distortion and strut/van passing which further leads to fatigue.

3.4.1 Computational tool

The stress and dynamic analyses are carried out in widely used Finite Element Analysis (FEA) commercial software ANSYS mechanical. ANSYS Parametric Design Language (APDL) has been adopted due to the fact that it is easy to be scripted for the optimization design process. A blade CAD model is imported from CATIAV5 to ANSYS mechanical APDL in order to perform both analyses.

3.4.2 Boundary conditions

For this research work, the following boundary conditions are employed:

- No displacement is allowed at the blade disk root.
- Only centrifugal force has been considered by implementing blade rotational speed.
- Pressure loading is not considered when performing the stress and dynamic analyses.

At the operational condition or design point, von-Mises stress is largely caused by the centrifugal force rather than by the aerodynamic pressure force [5]. This is also verified for the existing problem by calculating Rotor 67 von-Mises stress with and without pressure loading and no significant difference (<1.8 %) at the design point is observed.

The "large deformation" option is not taken into consideration although it is recommended by ANSYS 14.5 for an accurate result as it is taking into account the stiffness changes resulting from changes in element shape and orientation due to large deflection, rotation, and strain (ANSYS help). This option increases the analysis time from 5 minutes to 27 minutes while a (<9.7%) difference is found in maximum von-Mises stress.

As the dynamic analysis with pre-stressed option would provide more realistic values for natural frequencies, the modal analysis is performed by taking a pre-stress modal by turning on the centrifugal stiffening option. *ANSYS* model analysis "Block Lanczos" mode extraction method has been chosen.

3.4.3 Material

The material properties for Rotor 67 are not available in literature. Typically aluminum alloy, titanium alloy, steel or stainless steel materials are used for fan blade construction. The turbofan engine original equipment manufacturer (OEM) are mostly used titanium based material [134]. However, for this thesis work a fictitious material (solid titanium alloy with change modulus of elasticity) used by Doi and Alonso [135] has been chosen. The Young's modules is E = 1.422E+11 Pa, Poisson's ratio, $\upsilon = 0.3$, and density $\rho = 4539.5$ kg/m^3.

3.4.4 Grid generation

A common solid grid in ANSYS is created for both structural and dynamic analyses. A 10-node tetrahedral SOLID187 element, which has three translation degrees of freedom per node, is selected to generate the grid. According to ANSYS user guide, this element is well suited for grid generation of complex geometries.

A grid initially was generated by defining key points on the line of geometry and then by creating an area by joining those key points. It allows obtaining a fine grid near the stress concentration area. But when this grid is placed in optimization workflow, it fails for some geometries due to change in the geometry lines during the optimization by changing the curvature and thickness of sections. So, the number and quantity of lines varies and cannot be predicted. Therefore, a script based on key points and lines may not be well suited for structural optimization workflow. To resolve this issue, another grid is created by initializing nodes on area, as the area does not change during the optimization process. Although, the grid quality is not the same as the first script but, as mentioned earlier in this research work, the trend is more important than an absolute value.

A grid sensitivity study is performed, and the results are shown in Table 3-2. It shows the computed maximum von-Mises stress of the blade in the four different grids. Last three grids show small changes in their calculated maximum stresses, whereas the number of nodes of Grid 4 is about twice as many as of Grid 2. The von-Mises stress difference is extremely small in Grid 3 and Grid 4 (0.12%). In addition, not much difference were found in dynamic frequency modes

for all four grids, however the computational time was increased by increasing the grid size. Therefore, an appropriate 90,000-node grid has been selected for structural analysis.

Table 3-2: NASA Rotor 67 grid sensitivity for structural analysis

	Number of nodes	Maximum von-Mises stress (MPa)
Grid 1	51,586	556
Grid 2	90,000	561
Grid 3	113,065	561.7
Grid 4	217,558	561

Grid selected for optimization process

3.4.5 Finite element (FE) simulations

As only aerodynamic experimental data (Strazisar, Wood et al. [123]) is available for Rotor 67, not many researchers performed stress and modal analyses. These results were also never validated due to material difference, lack of parameters specification such as meshing element, disk information, boundary conditions, etc. However, when analyses were performed without disk and taking similar material, similar results were obtained.

A structured grid is generated in order to compare the difference between both structured and unstructured grid results (see Figure 3-12). These results are provided in Table 3-3. The maximum stress is located at the bottom of the blade (near hub) for both grids (see Figure 3-13). The maximum stress location is validated by taking the node to node difference and found it within 4% difference. The maximum stress location is similar to the published results.

Table 3-3: von Misses stress results

Grid type	Von-Mises stress (MPa)	Total deformation (mm)
Structured grid (423,000-node)	498	2.8
Unstructured grid (90,000-node)	561	4.6

(a) Structured grid
(423,000-node)

(b) Unstructured grid
(90,000-node)
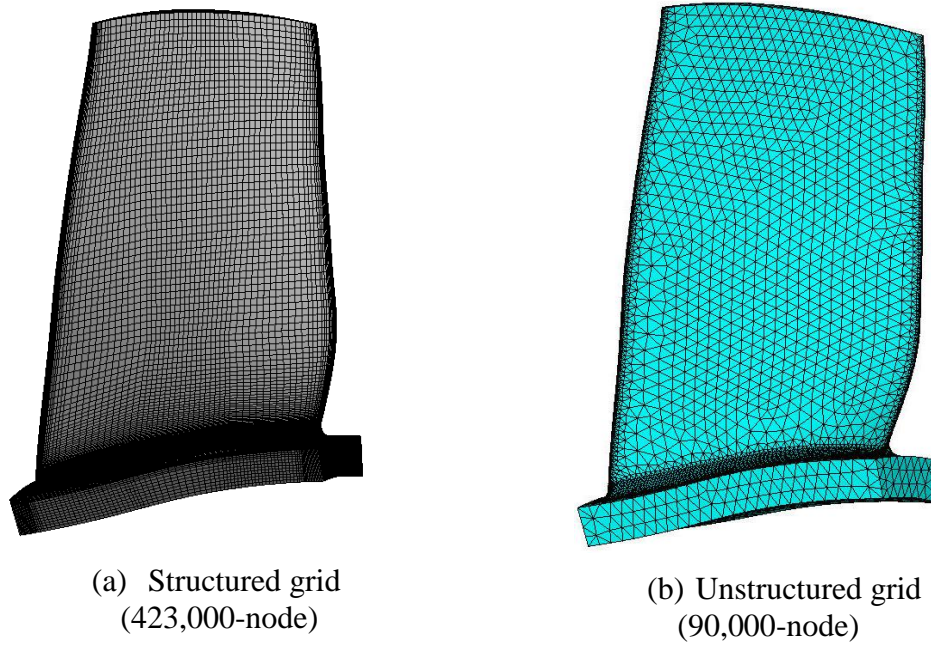
Figure 3-12: Finite element modal of Rotor 67

(a) Structured grid
(423,000-node)

(c) unstructured grid
(90,000-node)
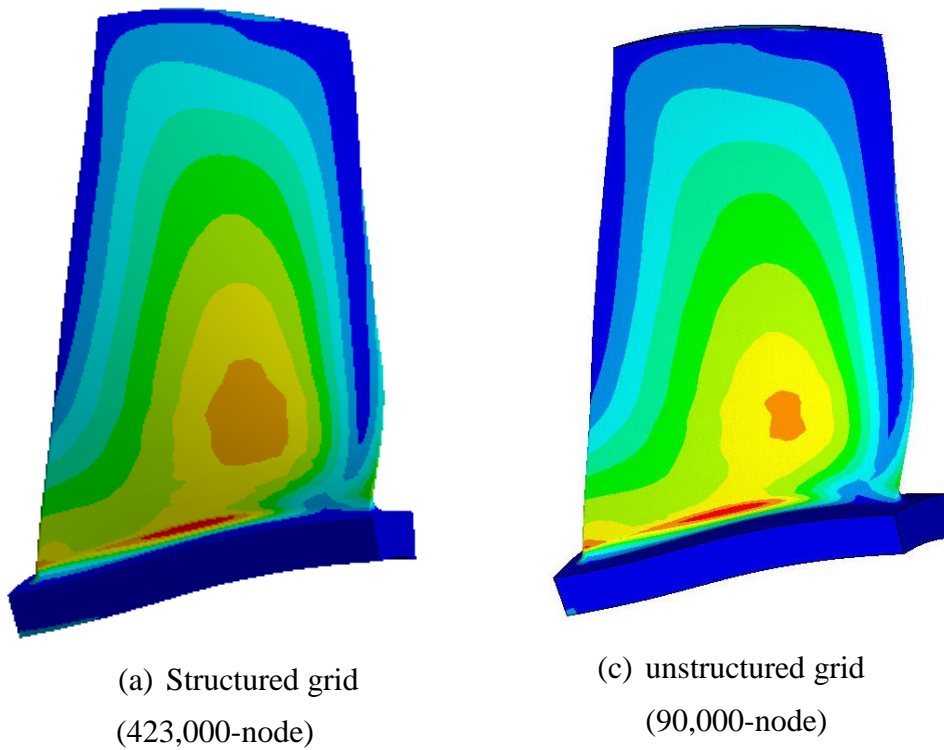
Figure 3-13: von-Mises stress contour of Rotor 67 at design speed

The computed mode shapes and modal frequencies for the Rotor 67 are presented in Figure 3-14 (a-d). The blade is drawn with thinner (hollow) grid lines represent the original blade shapes and the other solid images show the corresponding mode shapes. The torsional motion behavior near the tip of every mode is similar. In addition, more bending motion components near the tip can be seen in the higher frequency modes particularly in the fourth mode.

The Rotor 67 Campbell diagram is presented in Figure 3-15. The x-axis labels engine running speed in revolution per minute (RPM) and y-axis represents the frequency (Hz). The almost horizontal thick lines are the natural frequencies of the Rotor 67 blade for the first 3 modes. The slope lines or diagonal lines are characterized as the sources of excitation or engine orders such as struts/vane (1E to 5E and 8E). If an engine order line crosses the natural frequency line at an operating speed it is said to be "resonant crossing". The natural frequency lines should not arise in the running engine order. The red circles in Figure 3-15 represent that the 1st mode is crossing the 2E, the 2nd mode is crossing the 5E and the 3rd mode is crossing the 8E in engine running range between 90% (engine ground idle) and 110% (engine maximum speed) of the Rotor 67 design speed. This crossing can be avoided by an iterative process called "blade tuning" which is mostly based on past experience.

The blade tuning can be done by balancing the stiffness and the mass properties of the blade depending on the particular frequency mode. The basic guidelines for tuning from Ref. [136] are as follows: to lower a particular natural frequency, the associated region stiffness must be reduced and/or the mass must be increased. The inverse actions are applied to increase the mode frequency. Moreover, it is also mentioned in Ref. [137] that a common way to modify the blade frequency is to tailor the thickness distribution along the span. Furthermore, the design variables such as aspect ratio, taper, solidity, and radius ratio can also affect the blade frequency.
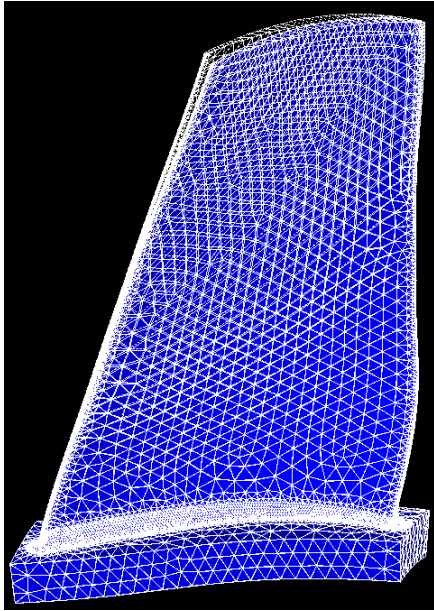
(a) First mode: 559 Hz
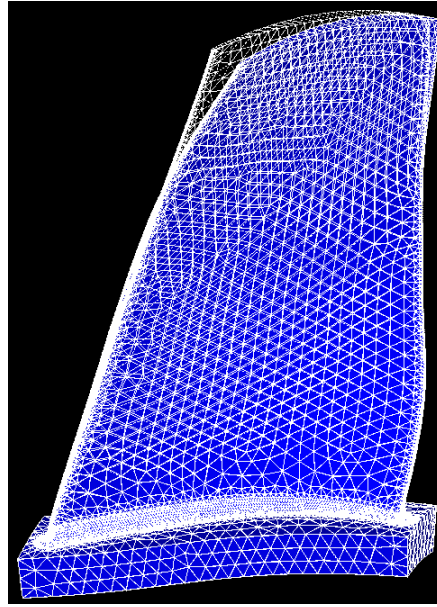
(b) Second mode: 1299 Hz
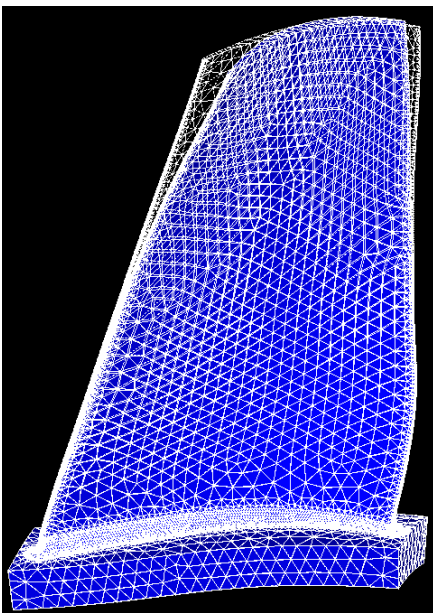
(c) Third mode: 1964 Hz
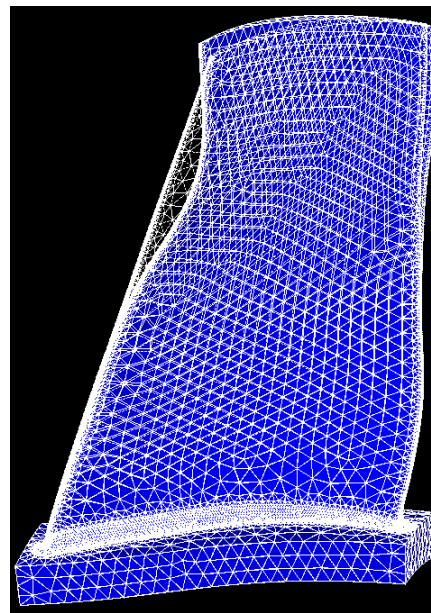
(d) Fourth mode: 2712 Hz

Figure 3-14: Mode shape of Rotor 67 at design speed (90,000-node grid)
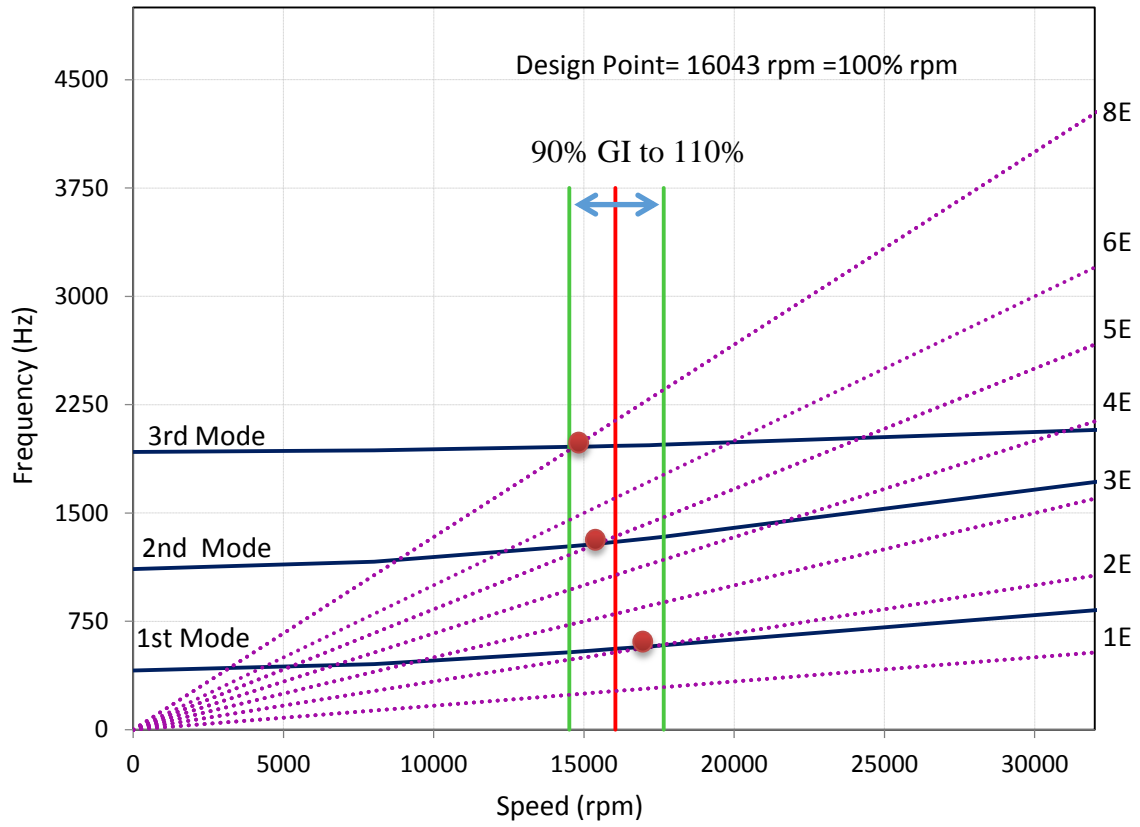
Figure 3-15: Campbell diagram of Rotor 67

CHAPTER 4   MULTIDISCIPLINARY DESIGN OPTIMIZATION (MDO) OF A TRANSONIC FAN BLADE

This chapter contains transonic fan blade design problem statement, which further leads to formulate the aerodynamics optimization and select the suitable MDO formulations. An overview of the selected MDO formulations and their implementation to the transonic fan design problem is also presented.

4.1   Transonic fan blade design problem statement

In this thesis work, the aerodynamics, structure and dynamics disciplines are considered to optimize a transonic blade. Although some other disciplines such as design, acoustics, etc. are always considered in practice during the design process conducted in industry, the three selected disciplines are the most important. Based on the discussions with our industrial partner it was decided to focus only on aerodynamics, structure and dynamics, in order to the potential benefit of using a multidisciplinary design optimization approach on a realistic problem. The formulation of the optimization problem must include the objectives and constraints similar to what discipline specialists must handle.

When a fan blade is modeled for design purposes, a possible objective is to maximize the efficiency. It makes aerodynamics the disciplines responsible for improving the aerodynamic efficiency at design condition (peak efficiency) while ensuring that the blade can operate on the existing engine by imposing constraints such as pressure ratio and mass flow rate. As mentioned in Section 3.3.3, an outlet mass flow that is a function of a constant corrected mass flow and varying outlet stagnation pressure and temperature is imposed. If outlet pressure and/or outlet temperature changes, one gets a change in mass flow, even though the corrected mass flow value did not change. Thus, a constraint is specified on the pressure ratio to control the mass flow with the exit corrected mass flow boundary condition. So, the mas flow constraint is not directly imposed.

The blade is subjected to very high centrifugal forces. Thus, the structural integrity under extreme conditions must be maintained. The structure discipline is responsible to ensure that the new design will be safe during the running condition. As mentioned in the literature review (Section 2.2.5.2), this can be accomplished in different ways such as by imposing safety factor or by

limiting maximum von-Mises stress by the material yield stress. But here it is addressed by limiting the maximum von-Mises stress inside the blade, i.e.$(\sigma_{max\,reference\,blade} - \sigma_{max\,design\,blade}) \geq 0$, where $\sigma_{max\,reference\,blade}$ = Maximum von-Mises stress of Rotor 67 blade and $\sigma_{max\,design\,blade}$ = Maximum von-Mises stress of optimized blade.

For all turbomachine blades, it is essential to tune the blade from a possible resonance and thus avoid fatigue failure. Consequently, the dynamic discipline is accountable to get a resonance-free design. This can be achieved by imposing design constraints on dynamic frequency modes, which can be illustrated on a Campbell diagram (see Section 3.4.5). Frequency tuning is mostly based on past experience to identify the acceptable, marginal and unacceptable crossings. As mentioned earlier in literature review, various designers have used different criteria to set the frequency margin; some authors [46, 78] imposed three forbidden dynamic mode ranges like ±12%, ±7% and ±5% on the first three frequency modes whereas some authors [74, 75, 122] imposed constraint like no frequency mode arising within the 95% to 105% range of the running speed. In this thesis work, following discussion with P&WC experts, we have considered a wider range than the previous work, that is no frequency mode are acceptable in engine running range from 90% (engine ground idle) to 110% (engine maximum speed) of the Rotor 67 design speed (i.e. 14,515 to 17,650 RPM). These criterions are imposed on the first three frequency modes (for details see Section 3.4.5).

As mentioned by Kroo [8], one of the difficult aspects of MDO problems is to manage the coupling between the disciplines when at least one discipline output is an input for another discipline. Disciplines interactions can be very complex with feed backward and feed forward interactions. In the present fan design problem, a single interaction is identified: the output of the stress discipline is the input for the dynamic discipline in the form of the stress matrix (pre-stressed model) in order to obtain more realistic value of the natural frequencies (for detail see Section 3.4). Consequently, in a scenario of direct coupling, structure and dynamic disciplines cannot run in parallel and can be considered as a single discipline called structure and dynamics disciplines (SND).

As mentioned earlier, transonic fan blade design is a large dimensional problem with multiple design requirements, which makes the optimization process not only time consuming but also makes the design space more complex. Thus, it is essential before optimization to assess the

effect of design parameters on design objective function and constraints. However, it is difficult to know the effect of all the design parameters. Based on the transonic fan blade parameterization (see Section 3.2), the list of design variables is listed in Table 4-1.

Table 4-1: Geometrical design variables, x_{geo}

Tb	x_1	Thicknesses
β	x_2	Beta angles
$d\beta/ds$	x_3	Beta curvatures: derivative with respect to s of the β - angle distribution
dTb/ds	x_4	Derivative with respect to s of the thickness distribution
θ	x_5	Stacking, section shift in the θ-direction from the position of its centroid

A parametric or sensitivity study is performed by considering 20-geometrical design variables: 6 define the β-angle at leading edge (LE), midchord and trailing edge (TE), 6 variables for β-curvature ($d\beta/ds$) at midchord and TE, 2 for stacking (θ), 2 for thickness change along the span, dTb/ds at TE and 4 for thickness, Tb at midchord and TE along the span. No interaction within the different design parameters assumes thereby the influence of each one on the objective function is studied separately. The variance of the objective function or constraints is calculated over the entire range of one design parameter while fixing the rest. The measure of importance of each design parameter is obtained by normalizing the associated variance with total variances [138]. It should be noted that in reality cross-coupling effect also exists and each parameter is not fully independent of the others. Moreover, these studies are often difficult due to step size of design parameters as the 1-unit of β-angle is different from 1-unit of Tb-thickness. The usual design practice is to submit a giant design of experiments matrix and visualize the results graphically and this way is often enlightening.

Among all the studied design parameters β, $d\beta/ds$ and Tb were found the most influential parameters for aerodynamics discipline. Moreover, Tb, dTb/ds, and θ were observed to be the most important parameters for structure and dynamics disciplines (see Figure C-1 and Figure C-2

(Appendix-C)). These findings are close to the industrial designer's recommendations and literature investigations, where it was mentioned that the aerodynamics loss is significantly impacted by blade incidence angle [139], surface curvature [2, 3] and thickness and chordwise location of maximum thickness [3, 140], whereas the maximum stress and blade frequency are mostly adjusted by varying the chordwise location of maximum thickness, thickness along span [137] and stacking.

In summary, the coupling variables and constraints of the current transonic fan design problem were kept simple to exploit and demonstrate the suitable MDO frameworks. Moreover, all disciplines use all the geometrical design variables as input. Some of these design variables have primary influence on a single discipline and others are significant for more than one discipline. This can further help to formulate the fan design MDO problem.

4.2 Aerodynamic optimization

In order to verify the feasibility of the optimization framework and identify the suitable optimization techniques with respect to the current transonic fan design problem, an aerodynamic optimization was performed as a preliminary task. The aerodynamic design optimization solution serves as a reference to evaluate the MDO formulations performance.

4.2.1 Problem formulation

The aerodynamic optimization aims to improve the efficiency of the transonic fan blade (NASA Rotor 67) at a design point (peak efficiency).

To keep the operating conditions of the optimized design as close as possible to the baseline blade, pressure ratio aerodynamics constraints and exit corrected mass flow rate as an output boundary condition are implemented for the aerodynamics analysis.

A synthetic-description of the fan design aerodynamic optimization problem is as follows:

$$
\begin{aligned}
&\textit{maximize} && \eta_{DP} \\
&\textit{with respect to} && x_{geo} \\
&\textit{subject to} && \left| \frac{PR_{DP} - PR_{Rotor67}}{PR_{Rotor67}} \right| \leq 0.5\%
\end{aligned}
\tag{6}
$$

where, "η" represents the blade isentropic efficiency and DP corresponds to design point condition, "PR" the inlet/outlet total pressure ratio, "x_{geo}" presents the geometrical design variables. Note that: aerodynamic optimization does not include the thickness (Tb) design variable. Inclusion of this parameter in optimization can result in a thinner blade which may not satisfy the structure and dynamics disciplines' requirements. This optimization can also produce a geometry that is difficult to manufacture and undesirable at industrial scale. However, the chordwise location of maximum thickness (ps) is included because it is cited in literature ([56]) as the most important design parameter affecting the aerodynamics of the transonic blade. All the geometrical design variables (x_{geo}) utilized in aerodynamic optimization are listed in

Table 5-1. The performance parameters (efficiency, pressure ratio and exit corrected mass flow) description is available in Section 3.3.4.

4.3 Multidisciplinary design optimization

A MDO framework well suited for transonic fan blade design optimization must take advantage of the nature of the problem. This can be achieved by decomposing (or not) the fan design problem into sub-problems that can run concurrently.

From the literature review, we have targeted three MDO frameworks that might be efficient for transonic fan design.

4.3.1 Multidisciplinary feasibility (MDF)

The most common way to solve an MDO problem is to combine all disciplines analyses together into a multidisciplinary analysis (MDA) and optimize under a single optimizer by varying all the design variables.

For a given set of input variables, solving the MDA requires to achieve multidisciplinary feasibility, that is solving the coupling between all disciplines analyses. In our case, there is only a forward coupling between the structure and the dynamic disciplines. The multidisciplinary feasibility is achieved by first performing the aerodynamics and structure analyses. Then the dynamic analysis with the stress matrix as an input from the structure analysis is carried out.

The multidisciplinary feasibility (MDF) strategy is a straightforward, single-level and fully integrated formulation. The key feature of MDF is that the optimizer does not handle the discipline analysis constraints and multidisciplinary feasibility constraints, as consistency constraints are not present (i.e. $R_i = 0$ & $c^c = 0$). The MDO problem can be stated as follows:

$$\begin{aligned}
maximize \quad & f_1\big(y_1(x)\big) \quad &&(7)\\
with\ respect\ to \quad & x \\
subject\ to \quad & c_1\big(y_1(x)\big) \le 0 \\
& c_2\big(y_2(x)\big) \le 0 \\
& c_3\big(y_3(x)\big) \le 0
\end{aligned}$$

where, *1, 2* and *3* subscripts represent the aerodynamics, structure and dynamic disciplines respectively. "f_1" is the efficiency which is an output of the aerodynamic discipline, "x" includes all geometrical design variables, "y" is output of every discipline analysis and "$c_i, i = 1,2,3$" are constraints from each discipline.

Figure 4-1 presents the design variable flow in a block diagram. "y_2", contains the stress matrix which shows that a pre-stressed model is required for dynamic analysis. The output data is in the horizontal direction whereas the thin black line represents the process flow. $()^*$ is a symbol of optimal value of functions or variables.

The fan design optimization problem can be written more specifically as:

$$\begin{aligned}
maximize \quad & f_1: \eta_{DP} \quad &&(8)\\
with\ respect\ to \quad & x: x_{geo} \\
subject\ to \quad & c_1: \left|\frac{PR_{DP} - PR_{Rotor67}}{PR_{Rotor67}}\right| \le 0.5\% \\
& c_2: (\sigma_{\max Rotor67} - \sigma_{max}) \ge 0 \\
& c_3: \Delta F_j \ge 0 \qquad for\ j=1,2,3
\end{aligned}$$

where, "η" represents the blade isentropic efficiency and DP corresponds to design point condition, "x_{geo}" presents the geometrical design variables, "PR" the inlet/outlet total pressure ratio, "σ_{max}" is the maximum stress and "ΔF_j" are the constraints associated to the frequencies or dynamic modes. It is important to mention that MDO does not contain the maximum thickness location along the chord (ps) to maintain the simplicity by reducing the number of design variables.

The calculation of aerodynamics, stress and dynamic parameters are provided in Chapter 3. The list of all the implemented geometrical design variables is provided in Table 5-3. With this formulation a single optimizer handles all variables. The objective and constraint functions must be evaluated for each design vector.
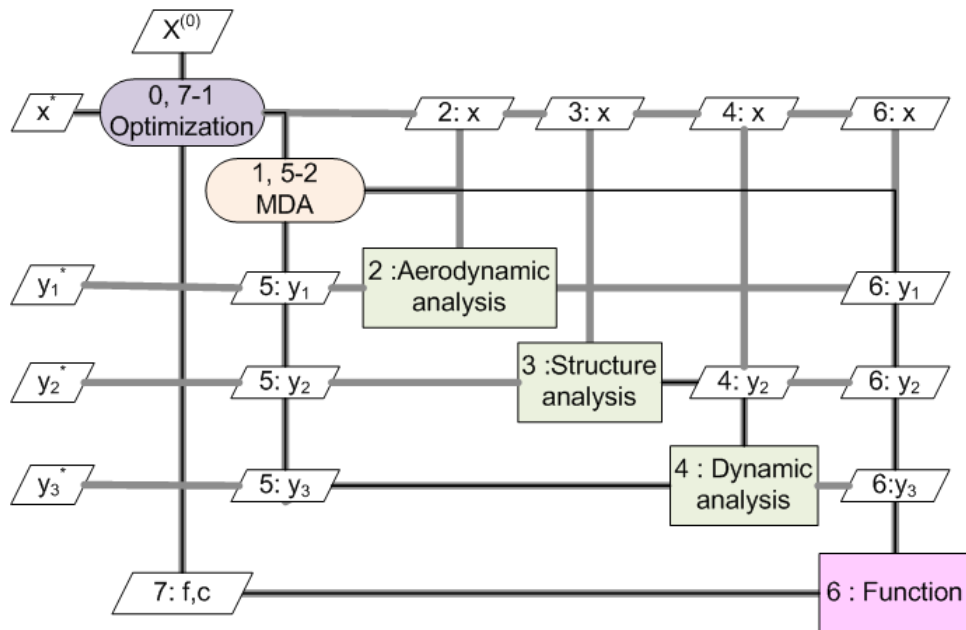
Figure 4-1: Multi Design Feasibility (MDF) framework (using block diagram from Martins and Lambe [16])

4.3.2 Filtering approach

In the existing transonic fan design problem, aerodynamics analysis is taking the longest computational time (≈ 18 min) compared to stress and dynamic analyses (≈ 5 min), the second approach which comes in one's mind is to take the advantage of analyses time.

The Filtering approach consists of a modified MDF approach where the feasibility on the maximum stress and dynamic modes is evaluated first as the structure and dynamic analyses take less time as compared to the aerodynamics analysis. The aerodynamics analysis is performed only if the feasibility on the structure and dynamic disciplines constraints is obtained. Figure 4-2 depicts the design variable flow in a block diagram, where "*s*" represents that the corresponding discipline's analysis attempts only when the above constrains is satisfied.

(s): represents that process will come on this step if it satisfies the upper discipline constraint other wise it will assign a worst value to rest of the discipline output to show that this design is infeasible.
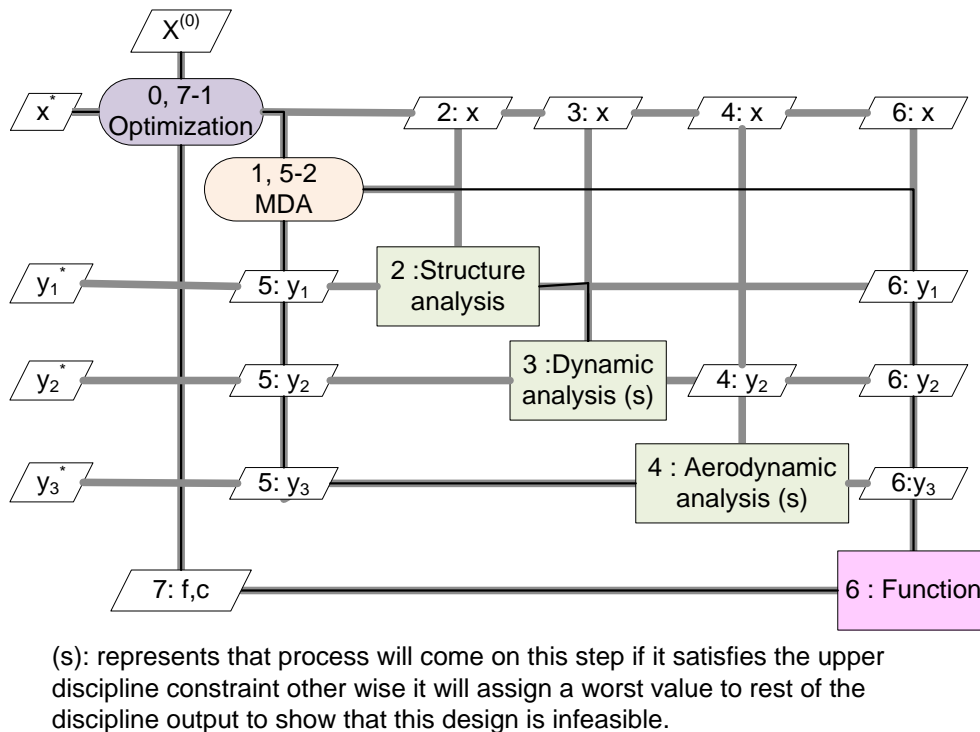
Figure 4-2: Filtering approach or modified MDF framework (using block diagram from Martins and Lambe [16])

4.3.3 Analytical Target Cascading (ATC)

MDF and filtering approaches are single level formulations and have some notable merits which were mentioned in earlier sections. However both also may require a large number of iterations under some conditions and become computationally expensive. Moreover, if a problem has strongly coupled disciplines and analyses, both cannot be run in parallel. As mentioned earlier, the goal of running analysis in parallel or sending the sub-problems to the discipline specialists may be achieved by decomposition of the original problem into a master optimization problem

and several sub-optimization problems. In addition, this problem solving approach is closer to the current industrial design process. A number of decomposition based formulations are available in literature. However, we have targeted the Analytical Target Cascading (ATC) approach in order to exploit the fan design problem decomposition form. As discussed in Chapter 2, ATC was successfully implemented in various engineering design problems including aircraft design, building design and mainly in the automotive industry.

ATC can be applied to a hierarchical as well as non-hierarchical system (Kim [141]; Kim et al. [14]; Tosserams et al. [15]). The generic ATC formulation is given in Kim [141] and Kim et al. [14]. Here a brief introduction and formulation of ATC from Martins and Lambe [16], is presented.

ATC formulations use copies of shared variables in discipline sub-problems together with the corresponding consistency constraints. These consistency constraints are relaxed with penalty functions. System and discipline sub-problems solve their respective relaxed problem independently [16]. Moreover, the penalty weights are increased until the required consistency is achieved. The ATC system level the problem is defined as:

$$
\begin{aligned}
&minimize && f_0(x, \hat{y}) + \sum_{i=i}^{N} \emptyset_i\big(\hat{x}_{oi} - x_0, \hat{y}_i - y_i(x_0, x_i, \hat{y})\big) + && (9) \\
& && \emptyset_0\big(c_o(x, \hat{y})\big) \\
&with\ respect\ to && x_0, \hat{y}
\end{aligned}
$$

At a discipline level:

$$
\begin{aligned}
&minimize && f_0\left(\hat{x}_{oi}, x_i, y_i\big(\hat{x}_{0i}, x_i, \hat{y}_{j\neq i}\big)\right) \\
& && + f_i\left(\hat{x}_{oi}, x_i, y_i\big(\hat{x}_{0i}, x_i, \hat{y}_{j\neq i}\big)\right) + \emptyset_i\left(\hat{y}_i - y_i\big(\hat{x}_{oi}, x_i, y_{j\neq i}\big)\right), \hat{x}_{oi} - x_0) \\
& && + \ \emptyset_0(c_o\big(\hat{x}_{oi}, x_i, y_i\big(\hat{x}_0, x_i, \hat{y}_{j\neq i}\big), \hat{y}_{j\neq i}\big))
\end{aligned}
$$

$$
\begin{aligned}
&with\ respect\ to && \hat{x}_{oi}, x_i \\
&subject\ to && c_i\left(\hat{x}_{oi}, x_i, y_i\big(\hat{x}_{0i}, x_i, \hat{y}_{j\neq i}\big)\right) \geq 0
\end{aligned}
$$

where; $\emptyset_i$: Penalty relaxation of the discipline i consistency constraints, $\emptyset_0$: Penalty relaxation of global design constraints, $i = 1,2,3$, represent the aerodynamics, stress and dynamic disciplines.

The ATC framework is illustrated on Figure 4-3. It shows that two types of optimization levels (in purple) that mean system and disciplines are included. Furthermore, discipline level optimization can run in parallel. Moreover, "v" and "w" correspond to the penalty weights, which are updated at the starting of the system level optimization. The interested reader can find ATC implementation of a geometrical optimization problem in Section C.1 (Appendix-C).
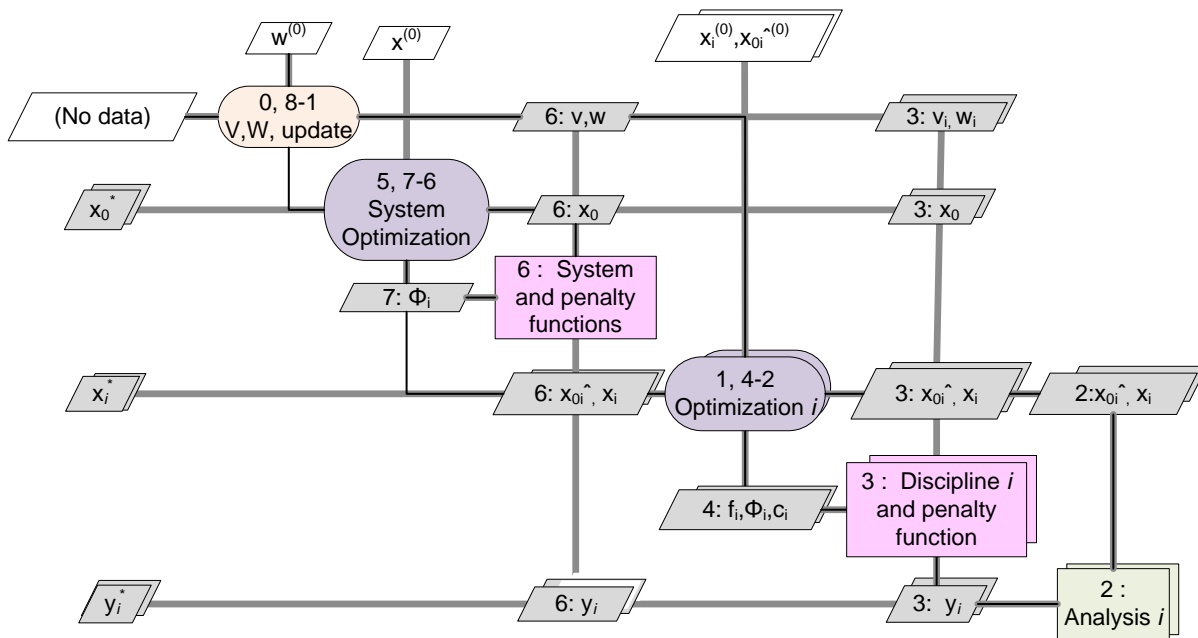
Figure 4-3: Analytical Target Cascading (ATC) framework (using block diagram from Martins and Lambe [16])

4.3.3.1 Augmented Lagrangian relaxation for ATC

Several penalty function choices have been demonstrated for ATC but an augmented Lagrangian penalty function (Bazarra et al. [142]; Bertseka [143]; Tosserams et al.[144]) was selected to relax the consistency and coupling constraints. The augmented Lagrangian penalty function for global design constraint is defined as:

$$\emptyset_0 = v^T c_0 + \|w \ o \ c_0\|_2^2$$

(10)

where, the symbol o represents the Hadamard product, an entry wise multiplication of two vectors such that: $aob = [a_1, \ldots, a_n]^T o [b_1, \ldots, b_n]^T = [a_1 b_1, \ldots, a_n b_n]^T$. v is a vector of Lagrangian multipliers estimate for the consistency constraints and w is vector of penalty weights used in the determination of $\emptyset_i$ and $\emptyset_0$. A similar expression is used to define the $\emptyset_i$ penalty relaxation discipline consistency constraints. These penalty parameters need to be determined by an external mechanism. Tosserams et al. [144] outlined the importance of the weight update mechanism for the success of augmented Lagrangian relaxation.

4.3.3.2 Parameter update schemes

The solution strategy taken from Tosseram et al. [145] is based on inner loop and outer loop. In the inner loop the discipline problem is solved for fixed penalty parameters while in the outer loop the penalty weights are updated based on the solution of the inner loop problem. For outer iteration $k+1$, the penalty parameters v_{k+1} use the update formula:

$$v^{k+1} = v^k + 2w^k w^k c^k \tag{11}$$

where, c^k is the extended consistency constraint at termination of the inner loop problem at k^{th} iteration and

$$w_i^{k+1} = \beta w_i^k \tag{12}$$

with $\beta \geq 1$

4.3.3.3 Outer loop termination

The outer loop termination is based on two conditions:

$$\|c^k - c^{k-1}\|_\infty < \varepsilon_{outer} \tag{13}$$

$$\|c^k\|_\infty < \varepsilon_{outer} \tag{14}$$

The first condition ensures convergence of the sub-problems solution sequence, while the second condition prevents premature termination.

4.3.3.4   Inner loop termination

The inner loop is terminated when the relative change in the system objective function value given by, discipline level (see Eq.(9)), for two consecutive inner loop iterations is smaller than some user-defined termination tolerance ε_{inner}. Let F represents the objective function of the relaxed problem this is condition is written as:

$$\frac{\left|F^{\xi} - F^{\xi-1}\right|}{1 + |F^{\xi}|} < \varepsilon_{inner} \tag{15}$$

where, ξ denotes the inner loop iteration number. $1 + \left|F^{\xi}\right|$ is used for scaling purpose for very large or very small objectives. The termination tolerance of inner loop is smaller than for the outer loop.

We use $\varepsilon_{inner} = \varepsilon_{outer}/100$. The ε can be taken as 10^{-2} or 10^{-3} depending on the precision of the solution. It is noted that this criteria has been implemented in the literature on gradient based optimization technique. However, in the present work, a heuristic optimization has been used. Therefore, the relative change in the system objective function value for two consecutive improved inner loop iterations has been considered for inner loop stopping criteria.

4.3.3.5   ATC implementation on transonic fan blade design problem

The functional dependence table (FDT) is used to formulate the ATC for the transonic fan blade design problem (see Eq. (8)) and presented in Table 4-2.

Similar to Tosserams et al. [15], a checked couple (*i, j*) indicates that the function of row *i* depends on the variables of column *j*. The FDT shows that design variable x_1 (i.e. thickness design variable, Tb) is shared by all three disciplines. However SND (structure and dynamics) sub-problem has 2-local sets of design variables x_4 and x_5, which are the derivative of the thickness distribution with respect to *s* (dTb/ds) and stacking (θ), whereas aerodynamics also has 2 local sets of design variables including x_2 and x_3, which are Beta angles (β) and β-curvatures ($d\beta/ds$). Moreover, in Eq. (8), f_1 and c_1 depend on outputs from aerodynamics discipline while c_2 and c_3 depend on structure and dynamic disciplines respectively.

Table 4-2: FDT for original problem (Eq. (8))

Parameters	x_3	x_2	x_1	x_4	x_5
f_1	■	■	■		
c_1	■	■	■		
c_2			■	■	■
c_3			■	■	■

As mentioned earlier, ATC formulation can be employed to a multi-level hierarchical systems and discipline based Non-hierarchical system. The current fan design problem is divided into one system level and two sublevel problems. One possible partitioning of this two-level problems where at the system-level, objective is only to match the target from discipline-level while having no constraint, i.e. $f_0(x, \hat{y}) = 0$ and $\emptyset_0(c_o(x, \hat{y})) = 0$. In addition, at discipline-level $f_0\left(\hat{x}_{oi}, x_i, y_i(\hat{x}_{0i}, x_i, \hat{y}_{j\neq i})\right) = 0$ and $\emptyset_0(c_o(\hat{x}_{oi}, x_i, y_i(\hat{x}_0, x_i, \hat{y}_{j\neq i}), \hat{y}_{j\neq i})) = 0$. Moreover, the shared variables are the input variables from system-level to sub-level disciplines.

Thus, the current fan design problem can be written as a two-level hierarchical ATC:

At system-level:

$$\begin{aligned} minimize \quad & \sum_{i=i}^{N} \emptyset_i(\hat{x}_{0i} - x_0) \\ with\ respect\ to \quad & x_0 \end{aligned}$$

(16)

At discipline-level:

$$\begin{aligned} minimize \quad & f_i\left(y_i(\hat{x}_{0i}, x_i)\right) + \emptyset_i(\hat{x}_{0i} - x_i) \\ with\ respect\ to \quad & \hat{x}_{0i}, x_i \\ subject\ to \quad & c_i\left(y_i(\hat{x}_{0i}, x_i)\right) \leq 0 \end{aligned}$$

where, $i = 1, 2$ represent the aerodynamics and SND disciplines. Figure 4-4 and Figure 4-5 illustrate that the ATC fan design problem is formulated hierarchically, with the top-level fan design coordinating the SND sub-problem together with the aerodynamics sub-problem.

From fan blade design problem formulation (Section 4.1), it is clear that existing SND disciplines are coupled together. It can also be noticed that the SND disciplines do not contain any discipline objective and has a single objective that expresses the need to meet the consistency constraints. However, the aerodynamics discipline has efficiency ($f_1 = \eta_{DP}$) as a discipline objective together with the matching of consistency constraints. The flow of the response variables is illustrated in Figure 4-4. The feedback targets *"Tb"* at fan design system level with disciplin levels are included in the ATC formulation.

A special attention is taken to address the initial design targets selection. This allows an efficient management of interactions between aerodynamics, structure and dynamics disciplines and updates of penalty weights.

The initial design of Rotor 67 is infeasible for dynamic constraints (for detail see Section 3.4). Therefore, an initial SND discipline optimization has been performed to obtain a feasible design with the additional constraint to be close to Rotor 67. In the next step, an aerodynamics discipline optimization has been performed with Rotor 67 as the target. In the third step, the initial weights are obtained and the target design thicknesses for the next loop are determined by solving the system level optimization. The used initial weights are $v = 0.1$, $w = 1$ and $\beta = 1.25$. The parameter update scheme is presented in Figure 4-5.

The system level optimization has been solved in MATLAB *fmincon* function with default settings. For sublevel or discipline level optimizations "Isight" commercial optimization solver has been used.

$$\text{System-level optimization}$$

$$minimize\ f_{sys}: \emptyset_{SND}(Tb - Tb_{SND}) + \emptyset_{aero}(Tb - Tb_{aero})$$

$$with\ respect\ to\ \ x_{sys}: Tb$$

$$Tb: Tb_{sys} \qquad \qquad Tb_{aero}, Tb_{SND}, \beta, d\beta/ds, dTb/ds, \theta$$

Structure and Dynamic (SND) optimization

$$minimize\quad f_{SND}: \emptyset_{SND}(Tb - Tb_{SND})$$

$$with\ respect\ to\ \ x_{SND}: Tb, dTb/ds, \theta$$

$$subject\ to\ c_{SND}: (\sigma_{\max Rotor67} - \sigma_{max}) \geq 0$$

$$\Delta F_j \geq 0\ \ for\ j = 1,2,3$$

$$dTb/ds, \theta$$

Aerodynamic optimization

$$minimize\quad f_{aero}: \frac{1}{\eta_{DP}} + \emptyset_{aero}(Tb - Tb_{aero})$$

$$with\ respect\ to\ \ x_{aero}: Tb, \beta, d\beta/ds$$

$$subject\ to\ c_{aero}: \left| \frac{PR_{DP} - PR_{Rotor67}}{PR_{Rotor67}} \right| \leq 0.5\%$$

$$Tb_{SND} \qquad \qquad Tb_{aero}$$

Figure 4-4: The ATC framework for the fan design problem
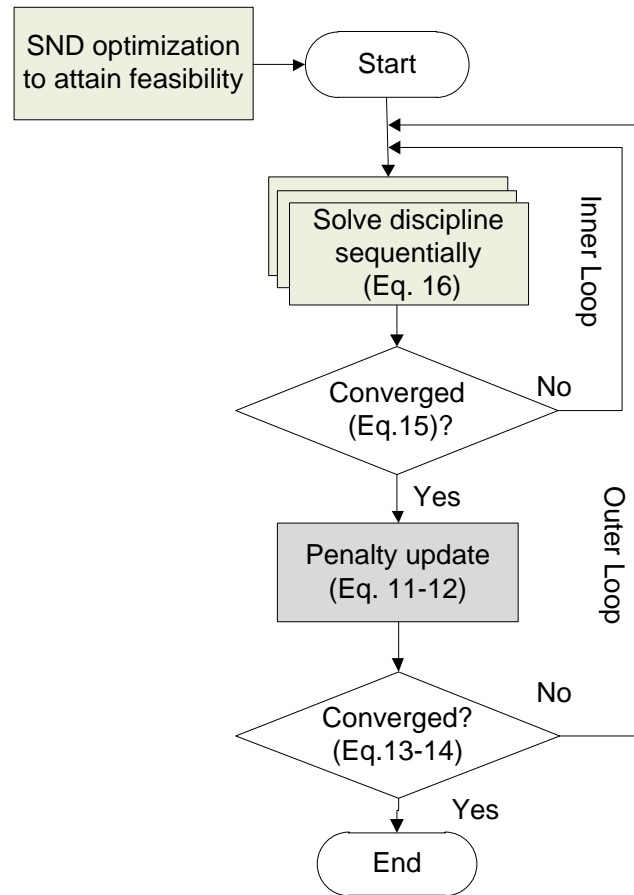
Figure 4-5: Illustration of ATC coordination algorithms for the fan design problem

4.4 Optimization algorithms

A number of optimization techniques exist for solving turbomachinery design optimization problems. However, for the current research work, we utilize the optimization techniques that are available in Isight optimization commercial software.

Several optimization techniques are available in the Isight optimization software. But only a few have been employed with respect to the nature of transonic fan design complex problem. As mentioned earlier in literature review (Section 2.2.3), the gradient based optimization algorithms are not suitable for current non-linear transonic fan design problem due to possibility to fall into

local minimum. Therefore *heuristic and hybrid algorithms* have been selected, including Genetic Algorithms (GA) based MIGA (Multi-Island Genetic Algorithm), Adaptive Simulated Annealing (ASA) and Pointer from *Isight* commercial optimization software. Also a non-commercial application software called Nonlinear Optimization by Mesh Adaptive Direct Search (NOMAD), using MADS (Mesh Adaptive Direct Search) algorithm [146, 147] was used.

4.4.1 Simulated annealing (SA)

SA is a heuristics (rule of thumb/randomization) optimization technique. It was originally proposed by Metropolis, Rosenbluth et al. [148] as a model of the crystallization process. Variants forms of SA exist and were applied to large problems regardless of the conditions of differentiability, continuity, and convexity that are normally required in conventional optimization methods. The name of simulating annealing came from annealing techniques that enhance the material strength by heating and controlled cooling of the material.

SA begins with an initial temperature (higher) and initial design (which is the best known). A new design is randomly produced in the neighborhood of the existing design. The measure of change of temperature between the existing and new design refers to the objective function value. If the new design is better than the existing design, it is taken as new best design and the next iteration starts with a lower temperature. The search is ended with a low temperature which basically corresponds to the probability of accepting worse design is extremely low [149]. The key parameter which controls the algorithm is "temperature". It is very high at the beginning of the optimization and decreases gradually until an optimal solution (minimum temperature level) is found. SA is widely used in the aerospace industry, for example, Tiow, Yiu et al. [115] used it to redesign transonic NASA rotor 67.

ASA (Ingber [150]) is a variant of SA. ASA is recommended for highly non-linear problems. The key of ASA is that it is useful when finding a global optimum is a top priority rather than a quick improvement [151].

4.4.2 Pointer

Pointer (Van der Velden and Kokan [152]) is a hybrid and innovative combination of four optimization algorithms: linear simplex, sequential quadratic programming (SQP), downhill simplex, and genetic algorithms. Pointer is an automatic optimization technique available in

Isight. For smooth problems, it utilizes the NLQPL (Nonlinear Programming by Quadratic Lagrangian) algorithm [153], whereas Downhill-simplex method is used for non-smooth problems. NLQPL and downhill-simplex algorithms determine the best answer based on the previous objective function whereas GA incorporates randomness (function continuity is not required). It is well suited for linear, nonlinear, continuous and discontinuous design space and for long-running simulations.

The control/selection of optimization algorithm and control of internal parameters settings (step sizes, number of restarts, and number of iterations) are automatically determined as the optimization proceeds. Due to this automatic feature it has become a favorite choice in turbomachinery industry. The benchmark studies in Refs. [151] also show that Pointer is the most efficient algorithm among all other chosen single objective algorithms (available in Isight).

4.4.3 MIGA

Genetic Algorithms are computationally expensive as they require many generations and a large number of populations in order to find an optimal design. MIGA (Miki, Hiroyasu et al. [154]) is a single objective optimization technique which divides the population into several subpopulations called « islands ». It performs traditional GA (such as selection, crossover, and mutation) on each subpopulation separately and then individuals are selected periodically from each population to « migrate » in other subpopulations to expand the diversity of search.

In general, a GA with subpopulations (such as MIGA) shows better performance in terms of convergence and fitness value as compare to the case when a single population is used. Furthermore, MIGA searches many locations in design space in order to find an optimal design. Although it is computationally expensive, it has the capability to execute in parallel. It is well suited for discontinuous design space [151]. MIGA was implanted in an axial compressor optimization problem by Keskin and Bestle [93].

4.4.4 NOMAD

NOMAD (Le Digabel and Tribes [146]) is a software based on Mesh Adaptive Direct Search (MADS) algorithm (Audet and Dennis Jr [155]). It is designed for constrained optimization of black box functions. An iteration of MADS contains a "Search" step and a "Poll" step. The Search step serves to identify good points away from the current best solution whereas the Poll

step generates a series of trial points on a mesh in the vicinity of the current best solution. A finer mesh is used if an iteration fails to improve the current best solution.

In general, NOMAD is well suited for functions that are computationally expensive to optimize, where derivative information is not available, in a noisy design space and when failure to provide the result can happen even for feasible points.

CHAPTER 5   RESULTS AND DISCUSSION

This chapter covers the application of the present optimization methodology for improving the efficiency of transonic fans at the design point. This methodology has three phases which include aerodynamic optimization, multidisciplinary design optimization and trade-off study for both aerodynamic and multidisciplinary design optimization results.

Note that, all the calculations were performed on a desktop machine with the following specifications: Intel Core i7 (16 GB RAM) Six-core processor.

5.1   Aerodynamic optimization results

An aerodynamic optimization is performed to optimize the Rotor 67 efficiency by taking 18 geometrical design variables which include β-angles, β-curvature, stacking (θ), and maximum thickness position along the chord (ps) whereas maximum thickness (Tb) on sections are kept the same as Rotor 67. The design space is presented in

Table 5-1.

Several optimization techniques have been employed which include Multi-Island Genetic Algorithm (MIGA), Adaptive Simulated Annealing (ASA) and Pointer from *Isight* commercial optimization software [151]. NOMAD [146] has also been used. The aim is to create a metric to track and compare the different optimization methods to find:

(a) Which method gets highest efficiency while satisfying the constraints?

(b) Which method takes minimum time to achieve the best gain in efficiency while satisfying the constraints?

Optimization algorithms were run with an allocated computational budget of 500 numbers of evaluations (i.e. 150 hours). All optimized designs are further analyzed on a 1-million node grid and results are compared with baseline Rotor 67 design in Table 5-2. It can be seen that the design point efficiency has improved with all optimization techniques while maintaining the pressure ratio and mass flow rate within 0.25% of the baseline blade Rotor 67. The NOMAD optimized blade has maximum stress higher than Rotor 67 while rest of the optimized blades has the maximum stress lower than Rotor 67. The vibration frequencies negative bottom values show that first two vibration frequencies are arising in engine running range for all aero-optimized

blades. Thus, all aero-optimized blades are satisfying the aerodynamic requirements but, as could have been anticipated, are unable to satisfy the stress and dynamic requirements.

Figure 5-1 represents the comparisons between sections obtained from all optimization techniques (dotted sections) and NASA Rotor 67 sections (blue solid sections). It clearly shows that maximum thickness of sections is not changing with respect to Rotor 67 and all design sections are almost similar except the one obtained with NOMAD, which has a positive lean (sections moved towards the suction sides) as compare to the rest. It can also be observed that all optimized blade section trailing edges (TE) at tip (shroud) have a slightly increased camber. This combined with the effect of other design variables changes gives the effect of moving up the section, which can help reducing flow separation. There is also a significant geometry change from original geometry near the hub due to TE thickness change along span wise direction.

The efficiency history plot for the improved feasible solutions is presented in Figure 5-2. It can be used to assess the efficiency of optimization methods very quickly. It is observed that with the assigned computational budget, NOMAD obtains the best gain in efficiency faster than the other optimizers. Furthermore Pointer, ASA, and NOMAD have reached almost the same efficiency when the evaluation budget is completely used. All the methods have been used out-of-the-box without tuning algorithmic parameters. Faster convergence and possibly better results might be obtained with some tuning (please note that this is not a trivial task). It can be anticipated that GA, when used out-of-the-box is not a suitable choice for solving problem with the given budget. Note that GA and ASA solution has stopped after 350 and 400 runs due to license failures, green and cyan lines are used to present that these optimization are restarted (re-optimized) with that design point to complete 500 evaluations.

Table 5-1: List of design variables to optimize Rotor 67

List of design variables	ΔBounds	List of design variables	ΔBounds
β at LE hub	[-3° to 3°]	$d\beta/ds$: 2nd β curvature at mid-chord tip	[-0.05 to 0.05]
β at LE Tip	[-3° to 3°]	$d\beta/ds$: β curvature at TE hub	[-0.05 to 0.05]
β at TE hub	[-3° to 3°]	$d\beta/ds$: β curvature at TE tip	[-0.05 to 0.05]
β at TE Tip	[-3° to 3°]	dT_b/ds at TE	[-0.1 to 0.3]
β at midchord hub	[-3° to 3°]	dT_b/ds Span	[0 to 1] (%)
β at midchord Tip	[-3° to 3°]	Stacking angle, θ	[-1.7° to 1.7°]
$d\beta/ds$: 1st beta curvature at mid-chord hub	[-0.05 to 0.05]	Stacking Span	[0 to 1] (%)
$d\beta/ds$: 1st β -curvature at mid-chord tip	[-0.05 to 0.05]	Meridonal chord for Max. Thickness	[-0.05 to 0.05](%)
$d\beta/ds$: 2nd β curvature at mid-chord hub	[-0.05 to 0.05]	Midchord Span	[0 to 1] (%)

Table 5-2: Comparison between NASA rotor 67 and aerodynamic optimization results for 500-evaluations (1-million node grid)

| Aerodynamics Optimization Results		NOMAD	Pointer	ASA	GA	Rotor 67
Mass flow rate (kg/sec)		1.534 (+0.25%)	1.532 (+0.12 %)	1.532 (+0.12 %)	1.531 (+0.06 %)	1.5301
Pressure Ratio		1.630 (+0.24%)	1.627 (+0.06%)	1.628 (+0.12 %)	1.627 (+0.061%)	1.626
Efficiency (%) Δ(pts)		92.03% (+0.98)	92.01% (+0.96)	92.04% (+0.99)	91.74% (+0.70)	91.05%
Dynamic frequency modes (frequency margin, ΔF_j)	First, F1	545 (-42)	536 (-52)	542 (-46)	561 (-27)	559 (-29)
	Second, F2	1297 (-88)	1278 (-69)	1285 (-76)	1298 (-89)	1299 (-90)
	Third, F3	1758 (120)	1831 (66)	1831 (66)	1886 (49)	1964 (-29)
Maximum von-Mises Stress, σ_{max} (MPa)		567	467	453	447	561
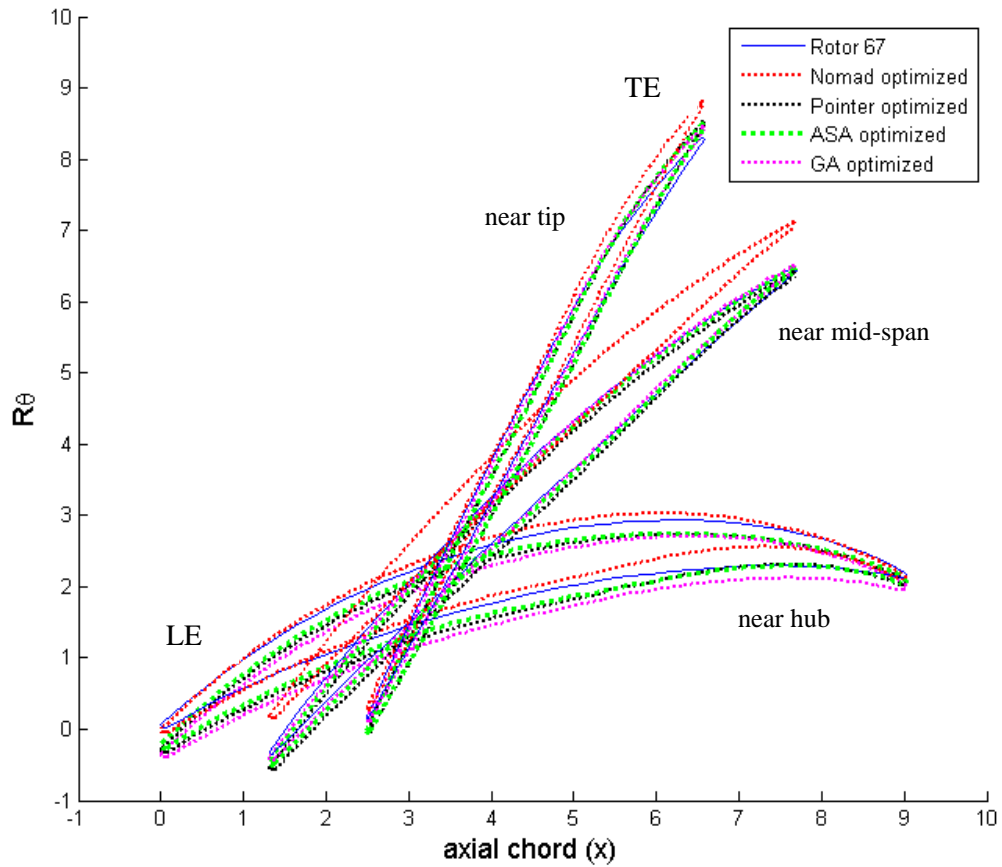
Figure 5-1: Geometry sections obtained by aerodynamic optimization and original Rotor 67
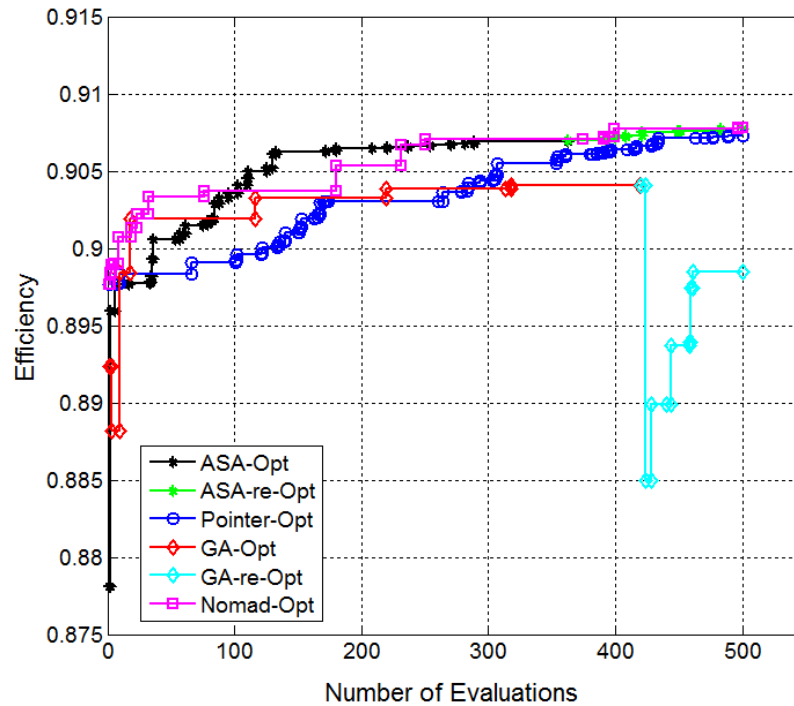

Figure 5-2: Comparison of efficiency history plot (150, 000-node grid)

5.1.1 Flow characteristics of reference and optimum blades

The fan performance characteristic curves for Rotor 67 and aero-optimized design blades are illustrated in Figure 5-3. It shows that, the optimized designs have significantly higher efficiencies and pressure ratios as compared to Rotor 67 fan blade. However, the choke mass flow is reduced and the stall margin is almost the same as Rotor 67 for all aero-optimized blades, except for the NOMAD optimized blade for which stall margin has been increased. This variation is due to the fact that the aero objective function is specifically designed for the design point condition.

Figure 5-4, Figure 5-5 and Figure 5-6 present the spanwise distribution of the circumferentially averaged stagnation pressure ratio, stagnation temperature ratio and spanwise flow angle distribution at rotor exit, respectively. The local stagnation pressure ratio and stagnation temperature ratio are raised in the hub region and lowered in the tip region, shifting the blade loading from the tip region towards the hub region. The exit flow angle of optimized blade is similar to Rotor 67 from 15% span to 60% span, and slightly decreases from blade hub to 15% span, 60% span to 90% span and 95% span to blade tip.

The maximum thickness chordwise location is one of the important design parameter and researchers have investigated the effect of this on the performance of transonic compressor (Wadia & Law [56]; Chen et al., [51]). In the transonic flow, shock usually appears in the blade channel. Thus, better performance is associated with the lower shock loss with enlarging the front flat portion of the blade sections. Figure 5-7 shows that the maximum thickness location for NOMAD and ASA optimized blades has increased for all the sections from 20% span to tip. A similar trend was observed by Chen et al., [51] and they reduced the thermal loss coefficient during transonic Rotor 37 re-designing. However, the maximum thickness location for GA and pointer optimized blades was slightly decreased from hub to 80% span of the blade.
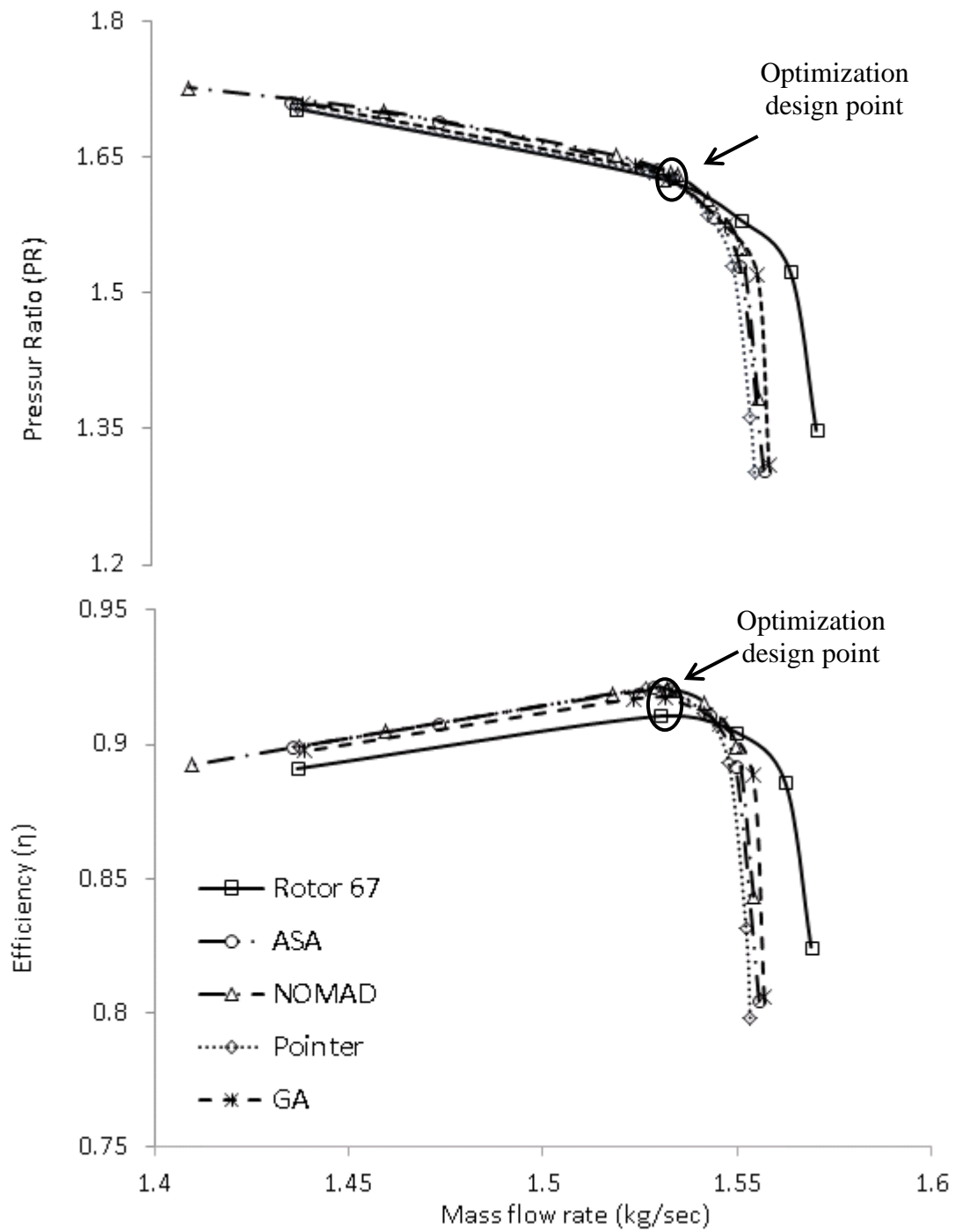
Figure 5-3: Efficiency and pressure ratio versus mass flow rate for aerodynamically optimized

solution (1-million node grid)
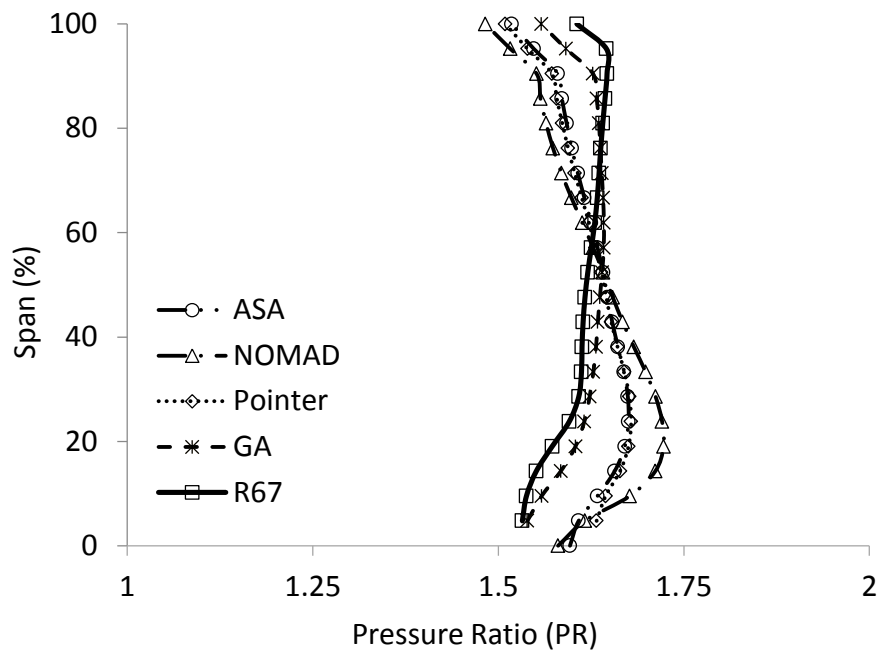
Figure 5-4: Spanwise distributions of the pressure ratio of the Rotor 67 and the optimized blades
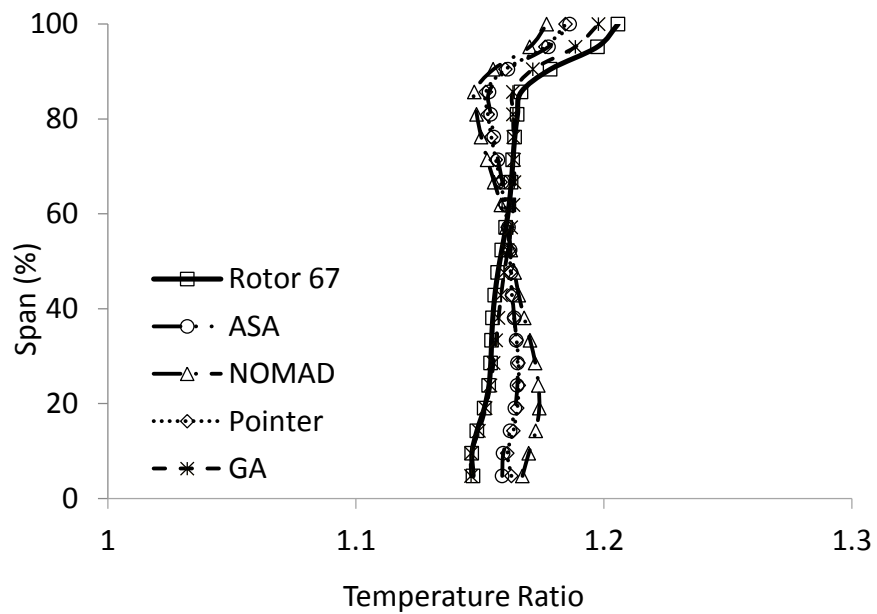
Figure 5-5: Spanwise distributions of the temperature ratio for the Rotor 67 and the optimized blades
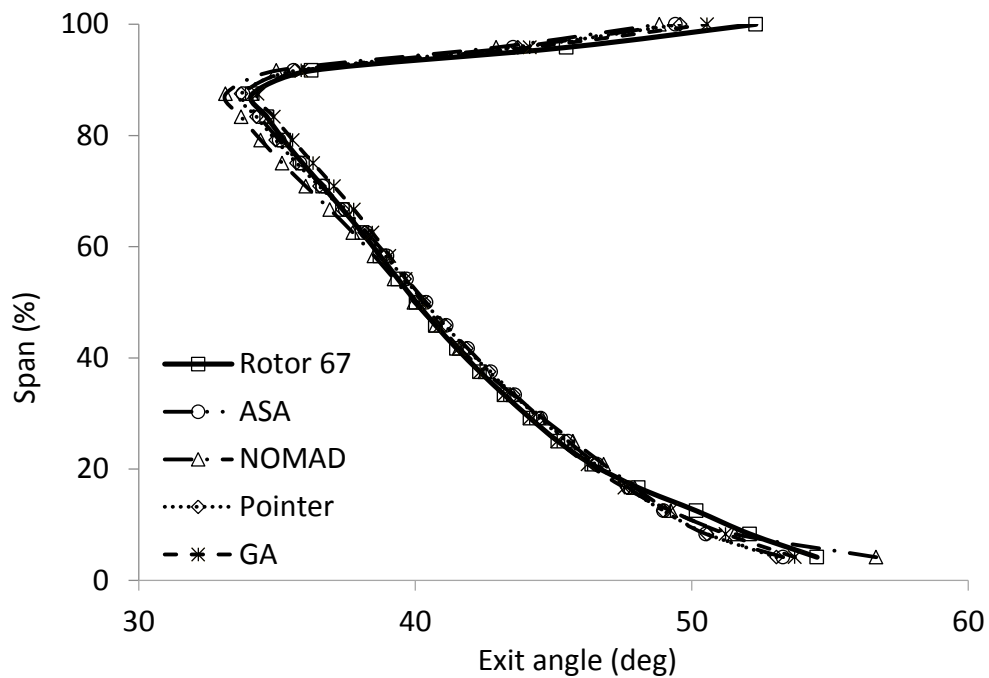
Figure 5-6: Spanwise distributions of the exit flow angle for the Rotor 67 and the optimized blades (downstream the of blade)
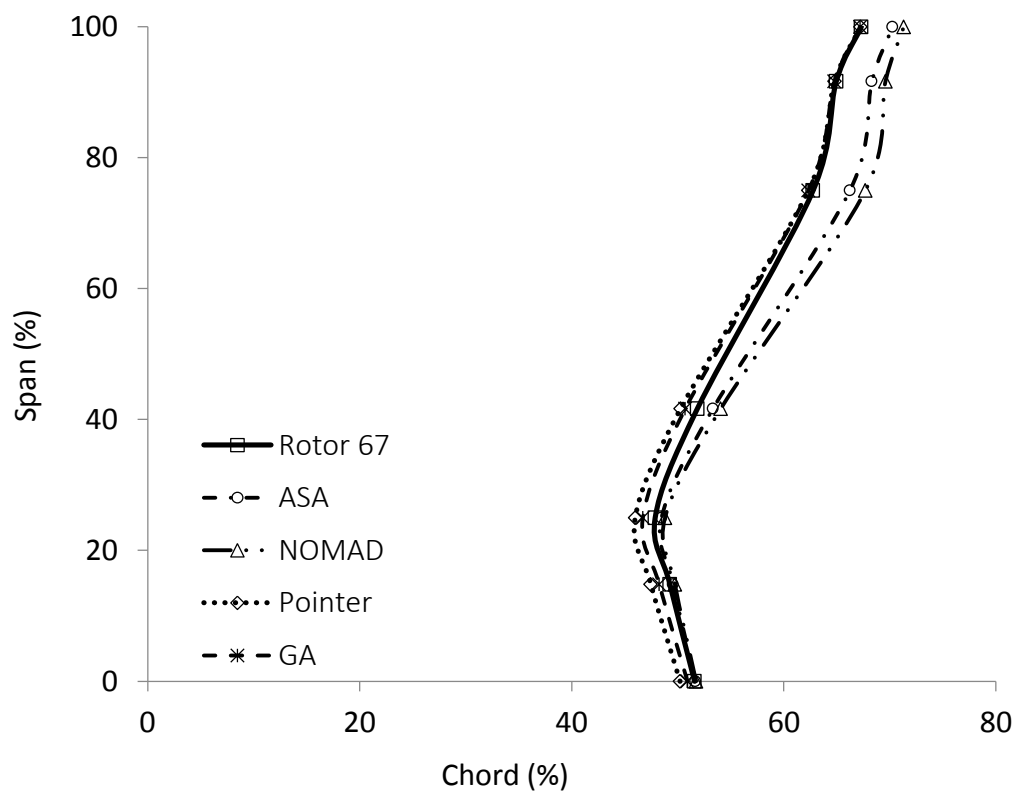
Figure 5-7: Spanwise distribution of maximum thickness location for the Rotor 67 and the optimized blades

The relative isentropic Mach number distribution at 85% and 25% of span section is compared in Figure 5-8 and Figure 5-9, respectively. At 85% span, all the aero-optimized blades have very similar Mach number distributions. At the suction surface Mach number from leading edge to 40% axial distance are almost identical for all optimized blade and Rotor 67. As compared to baseline deign (Rotor 67), Mach number at 62% of chord of suction side (SS) ahead of the shock is considerably decreased for all aero-optimized blades, which may result in the shock strength reduction. This can also be seen in the blade-to-blade Mach contour comparison at 85% span in

. In addition, the shock location of the aero-optimized designs slightly moves toward downstream along the blade as compared to the baseline Rotor 67. Moreover, all optimized blades have more smooth Mach number distribution on pressure side (PS) as compared to Rotor 67 blade. Less loading is observed between 20% to 60% chord, in comparison with the baseline design. At 25% span, less aero loading between the leading edge and 15% chord, is observed for all the aero-optimized designs in comparison with the baseline design Rotor 67.

The Mach number contours comparison at 25% spanwise positions is presented in Figure 5-9. It shows that the supersonic bubble on the suction side near the leading edge is minimized in the flow field of aero-optimized blades. Moreover, in original Rotor 67, flow separation phenomenon is clearly dominant near trailing edge (TE) hub, whereas it is much weaker in aero-optimized blades.
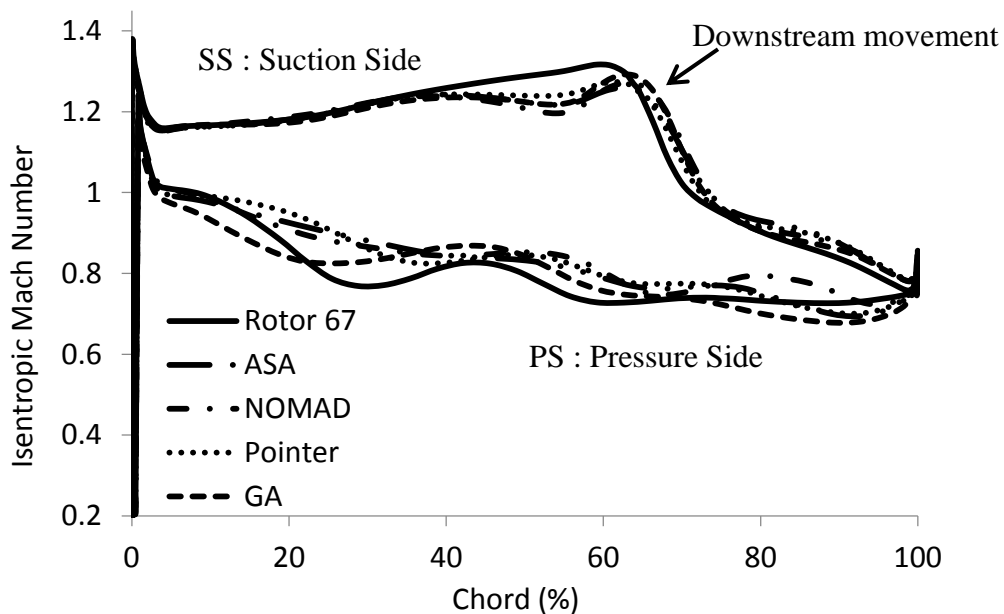
Figure 5-8: Isentropic Mach comparison at 85% span (at design point)
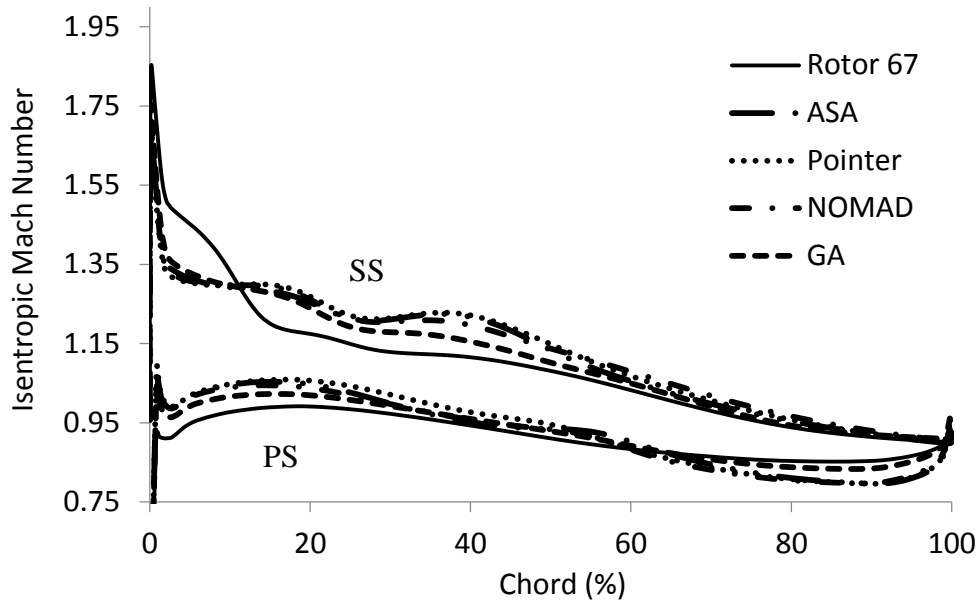
Figure 5-9: Isentropic Mach comparison at 25% span (at design point)

The pressure contour comparison between Rotor 67 and all aero-optimized blades on suction side is illustrated in **Error! Reference source not found.** (a)-(d). A notable change of shock ownstream position is consistent with Figure 5-8. In the central part of optimized blades span, the passage shocks lose their intensity and become weak.

The streamlines of wall shear stress on the suction side of Rotor 67 and aero-optimized blades are presented in **Error! Reference source not found.** (a)-(d). After the shock, flow separates as a esult of shock boundary layer interaction. This separation can be clearly seen in **Error! Reference source not found.** (a)-(d). The separation is characterized by the streamlines going towards the separation line whereas flow reattachment is identified by flow going away from that line. Compared to the baseline Rotor 67 blade, all aero-optimized blades have significantly smaller separation zone on the outer half of the blade span.
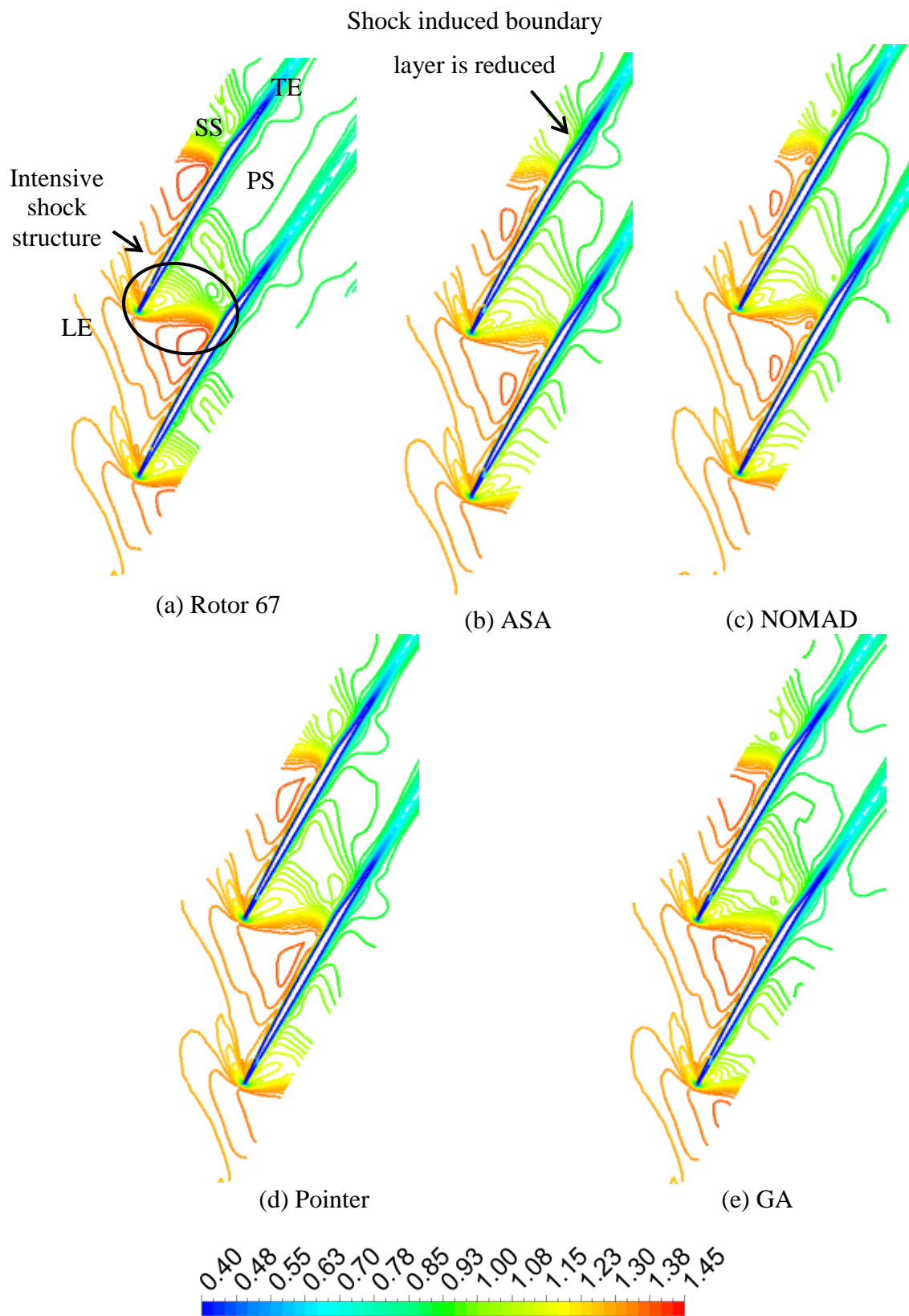
Figure 5-10: Mach contour comparison at 85% span (at design point)

(a) Rotor 67

(b) ASA

(c) NOMAD

(d) Pointer

(e) GA
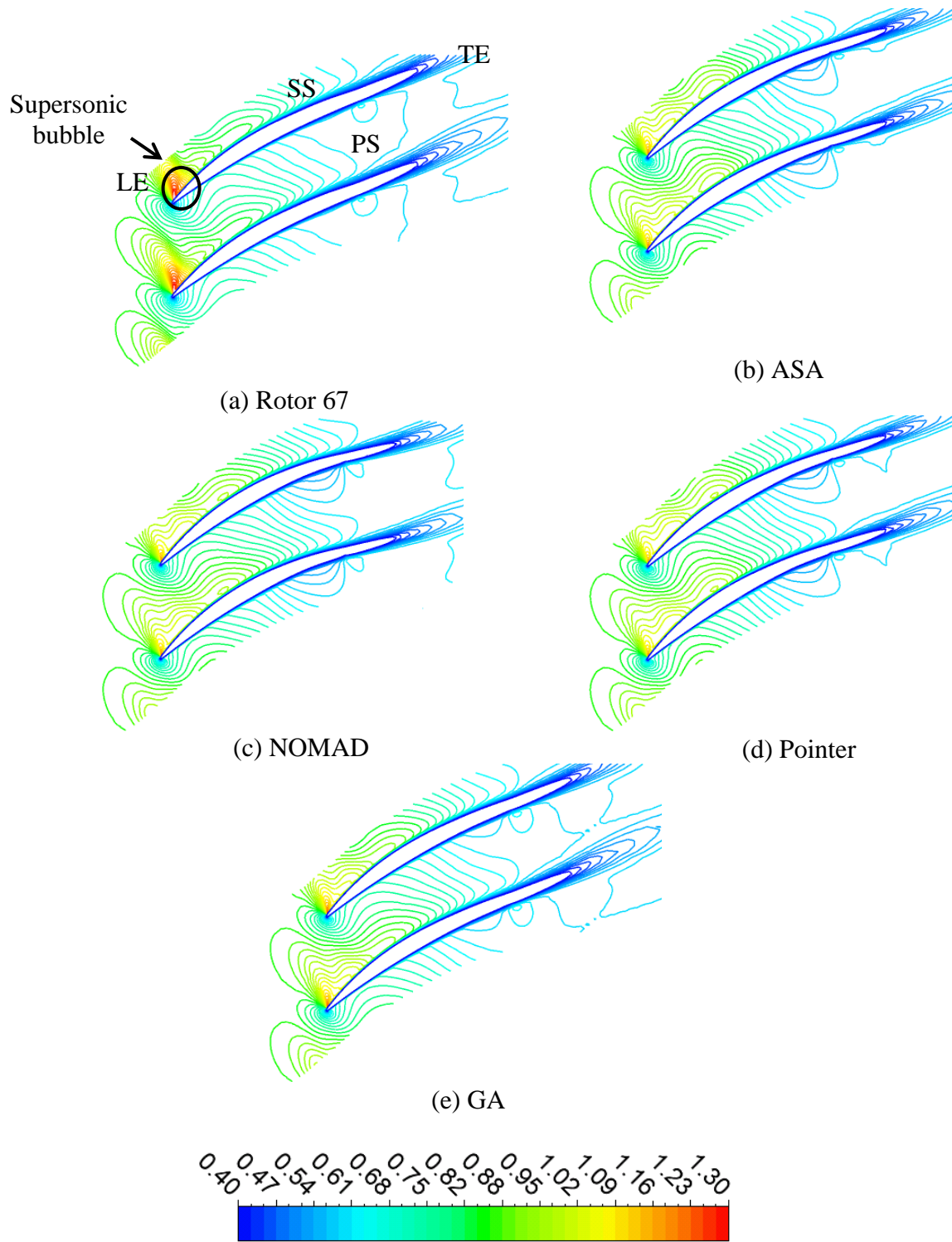
Figure 5-11: Mach contour comparison at 25% span (at design point)

Tip

85% span

LE

TE

25% span

Hub

(a) Rotor 67

(b) ASA

(c) NOMAD

(d) Pointer

(e) GA

45000 52500 60000 67500 75000 82500 90000 97500 105000 112500 120000 127500 135000

[Pa]
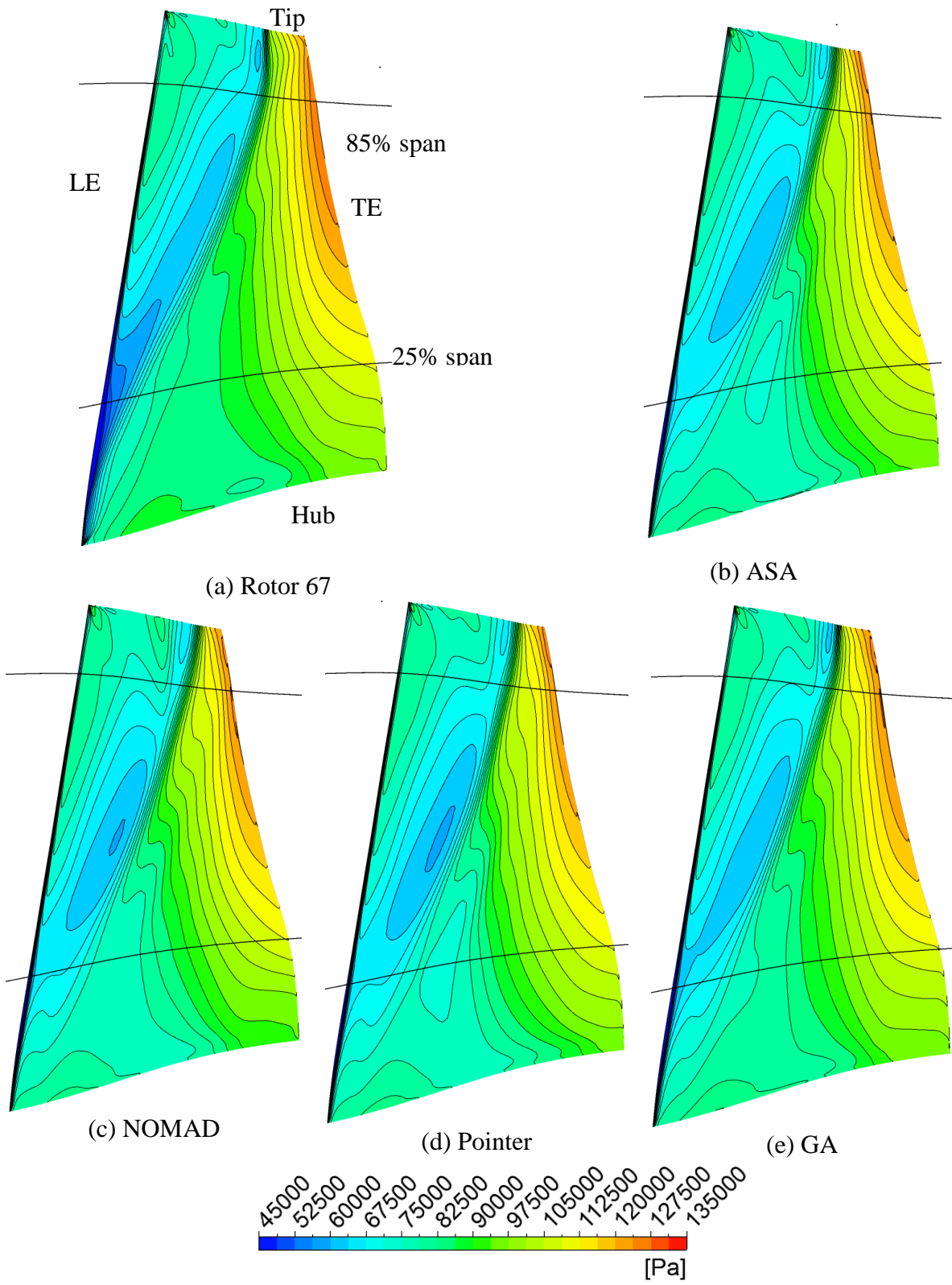
Figure 5-12 Pressure contour comparison at suction side (at design point)

(a) Rotor 67

(b) ASA

(c) NOMAD

(d) Pointer

(e) GA

Figure 5-13: Streamlines close to suction side (at design point)

5.2 Multidisciplinary design optimization (MDO) results

The MDO approach was applied to the multidisciplinary redesign of the NASA Rotor 67 with the aim of achieving maximization of the efficiency with constraints on mass flow rate, total pressure ratio, von-Mises maximum stress and dynamic frequencies (see Section 4.1). The optimization shared the same parameterization as the previous aerodynamic optimization design case and considered 20 geometrical design variables which include β -angles, β -curvature, stacking (θ), thickness (Tb) at mid chord and trailing edge whereas maximum thickness chordwise position along span (ps) are kept the same as Rotor 67. Thickness (Tb) is now added as a design variable as it has a primary role to obtain acceptable steady state stress levels and vibration characteristics. The design space is presented in Table 5-3.

Table 5-3: List of design variables to optimize Rotor 67

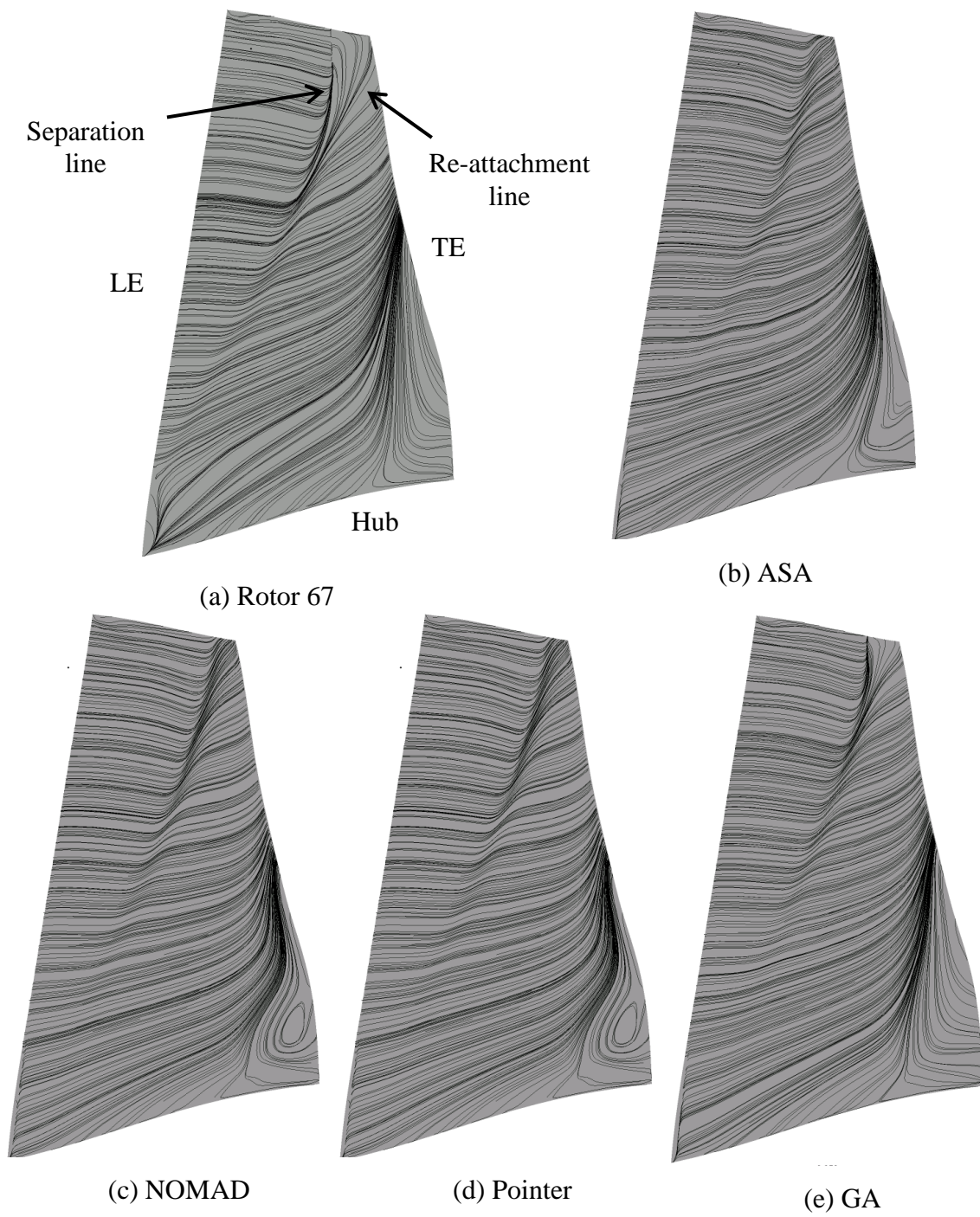| Variables	ΔBounds	Variables	ΔBounds
β at LE hub	[-3° to 3°]	$d\beta/ds$: β curvature at TE hub	[-0.05 to 0.05]
β at LE Tip	[-3° to 3°]	$d\beta/ds$: β curvature at TE tip	[-0.05 to 0.05]
β at TE hub	[-3° to 3°]	Thickness at midchord. T_b	[-0.15 to 0.3] (cm)
β at TE Tip	[-3° to 3°]	Midchord Span	[0 to 1] (%)
β at midchord hub	[-3° to 3°]	Thickness at TE, T_b	[-0.02 to 0.03] (cm)
β at midchord Tip	[-3° to 3°]	TE Span	[0 to 1] (%)
$d\beta/ds:$ 1st beta curvature at mid-chord hub	[-0.05 to 0.05]	dT_b/ds at TE	[-0.1 to 0.3]
$d\beta/ds:$ 1st β -curvature at mid-chord tip	[-0.05 to 0.05]	dT_b/ds Span	[0 to 1] (%)
$d\beta/ds:$ 2nd β curvature at mid-chord hub	[-0.05 to 0.05]	Stacking angle, θ	[-1.7° to 1.7°]
$d\beta/ds$: 2nd β curvature at mid-chord tip	[-0.05 to 0.05]	Stacking Span	[0 to 1] (%)

The three MDO formulations optimization results are presented in Table 5-4: Multidisciplinary feasibility (MDF) (first column), Filtering Approach (second column) and ATC (third column) in comparison with Rotor 67 baseline design (fourth column). Adaptive Simulated Annealing (ASA) and Pointer optimization techniques have been used in Isight commercial optimization software and best of both optimization algorithm results are presented here. All optimized designs are analyzed on a 1-million node grid.

Table 5-4: Comparison between NASA Rotor 67 and the MDO framework optimized designs

(1-million node grid)

MDO formulations Results		MDF	Filtering Approach	ATC	Rotor 67
Aerodynamics	Mass flow rate (kg/s)	1.533 (+0.18%)	1.536 (+0.38%)	1.536 (+0.38)	1.5301
	Pressure Ratio	1.631 (+0.31%)	1.634 (+0.49%)	1.633 (+0.43%)	1.626
	Efficiency ($\Delta\eta$)	91.24 % (+0.19 pts)	91.71 % (+0.66 pts)	91.75% (+0.70 pts)	91.05%
Dynamic frequency mode (Hz)	First, F1	589 (1.7)	595 (7)	590 (2)	559 (-29)
	Second, F2	1207 (31)	1201 (25)	1188 (12)	1299 (-90)
	Third, F3	1851 (83)	1773(8)	1774 (9)	1964 (-29)
Maximum von-Mises Stress, σ_{max} (MPa)		360	458	374	561
Process Time hours (days)		180 (7.5)	132 (5.5)	-	-
Maximum constraint violation (Eq.14)		-	-	0.04	-

For ATC formulation, all the inner loops disciplines optimized objective functions and constraints are listed in Table D-1 (a-d) (Appendix-D). It includes the pressure ratio, mass flow rate and maximum von-Mises stress percentage difference with Rotor 67. It also provides the dynamic frequency constraint values. The dynamic frequency constraints and maximum von-Mises stress need to be greater than zero to get the feasibility, whereas pressure ratio percentage difference need to be $\pm$ 0.5% to attain the feasibility. Here, Table 5-4 lists the aero-optimized blade obtained on 7th outer loop. Note that the SND objective function (f_{SND}) is multiplied by 100 to increase the weight.

Figure 5-14 presents the geometry changes between NASA Rotor 67 (solid sections) and the MDO formulations optimized blades (dotted sections). It clearly shows that thickness near tip section to mid-chord and trailing edge is changing with respect to Rotor 67 which is due to dynamic constraints feasibility (for details see Section 3.4.5). The spanwise maximum thickness distribution in comparison with Rotor 67 is provided in Figure D-4 (Appendix-D). It is also observed that all optimized blade sections have a negative lean (sections moved towards the rotor rotational axis) near hub to mid span. All optimized blades have the similar profile except MDF optimized blade which is slightly more cambered near the hub trailing edge.

The efficiency improvement (feasible and infeasible runs) history plot for MDF and filtering approach is presented in Figure 5-15. Note that the filtering approach has attempted 212 complete runs (including aerodynamic, stress and dynamic analyses) among 785 evaluations whereas MDF has completed 400 evaluations for all three discipline analyses. Efficiency improvement history plot shows that filtering approach required fewer evaluations to obtain a first feasible design. This figure also shows that the initial design problem was infeasible for dynamic constraints. However after three outer loops the dynamic constraints reached close to feasibility while improving the aerodynamic efficiency.

The efficiency history plot for ATC formulation is presented in Figure 5-16. It shows that for the first outer loop efficiency was not increased as it was started with the initial solution from SND-optimized solution and trying to get closer to the original Rotor 67 thickness. Moreover, weights were the same for all consistency constraints. After first run, the weight is updated according to the difference from target values. The efficiency started increasing from 2nd outer loop, which is larger on 7th outer loop as compared to rest.

Figure 5-17 and Figure 5-18 present the convergence history plot for seven outer loops of aerodynamics and SND objective functions for ATC-MDO formulation. Both history plots show that the discipline level optimizations have converged before completing the evaluations as the inner loop stopping criteria was satisfied early.
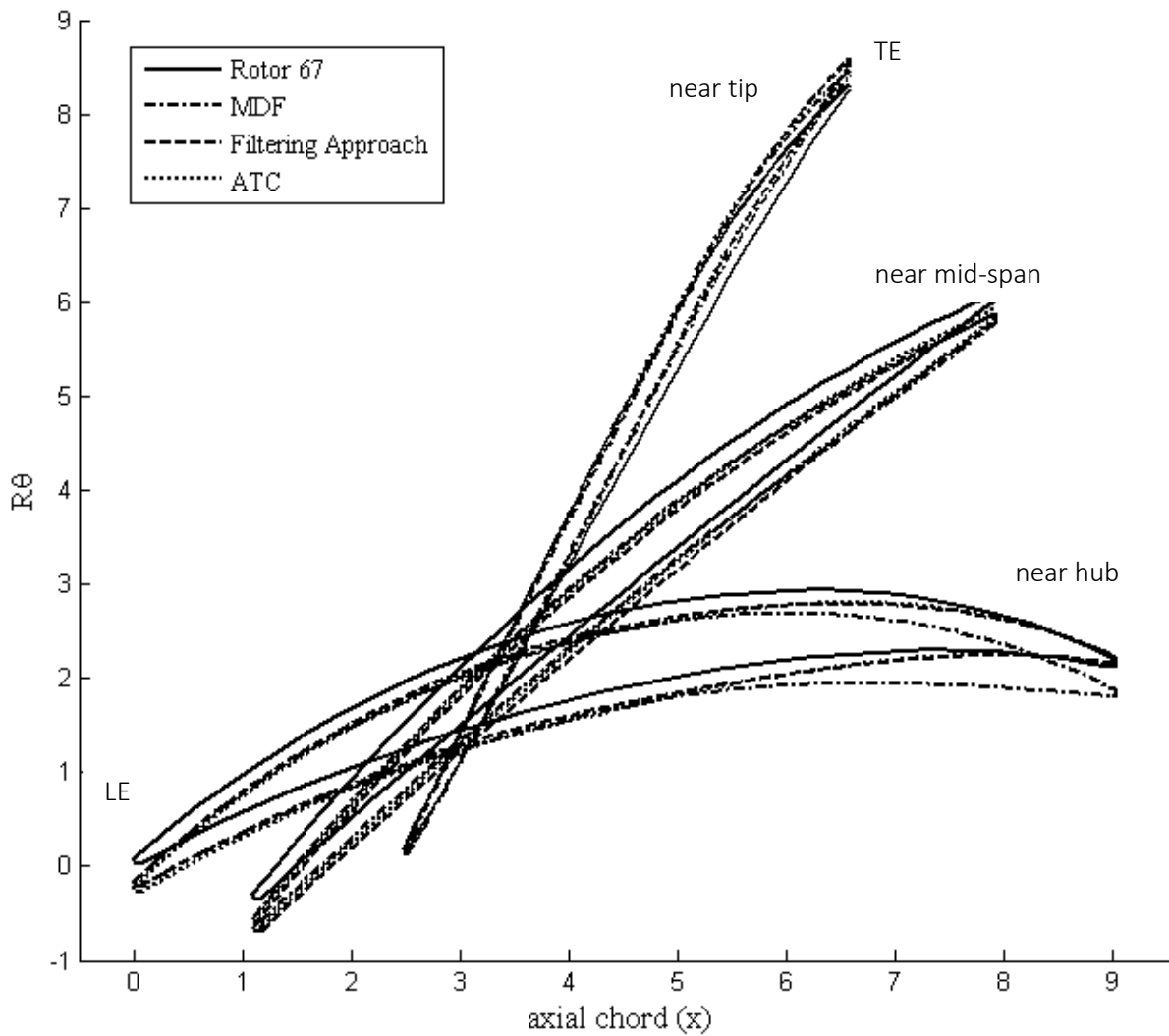
Figure 5-14: Comparison of Optimized Rotor 67 geometry sections obtained by MDO formulation and Original Rotor 67
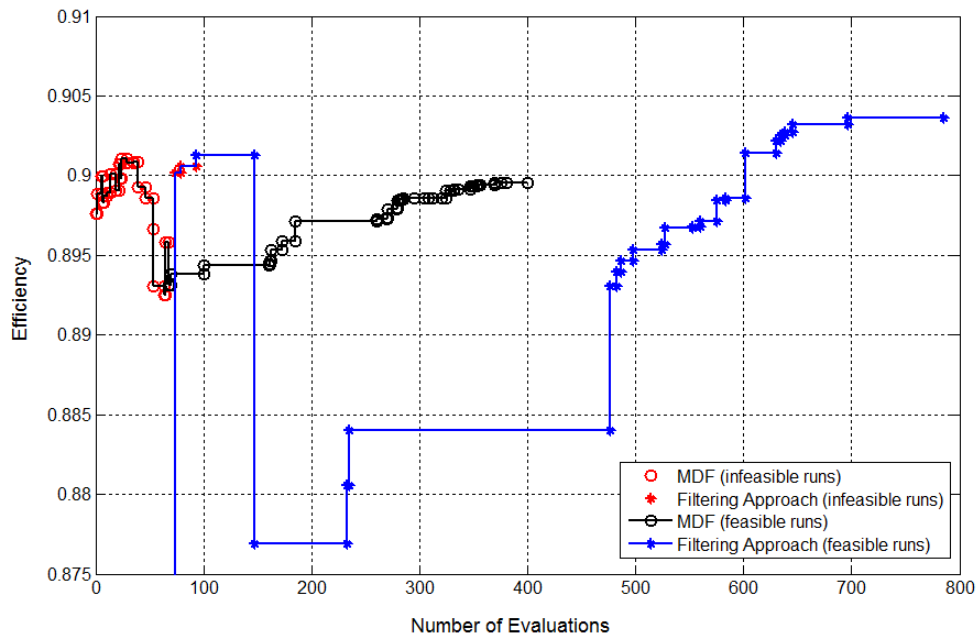
Figure 5-15: Efficiency history plot for MDF and filtering approach MDO formulations
(150, 000-node grid)
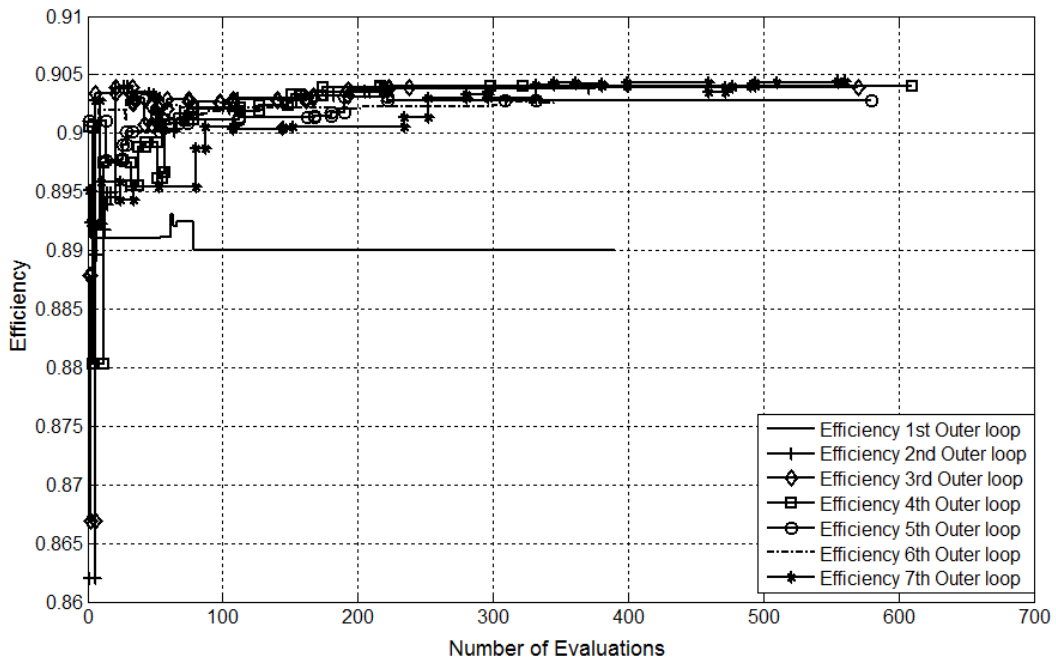
Figure 5-16: Efficiency history plot for ATC MDO formulation (150, 000-node grid)
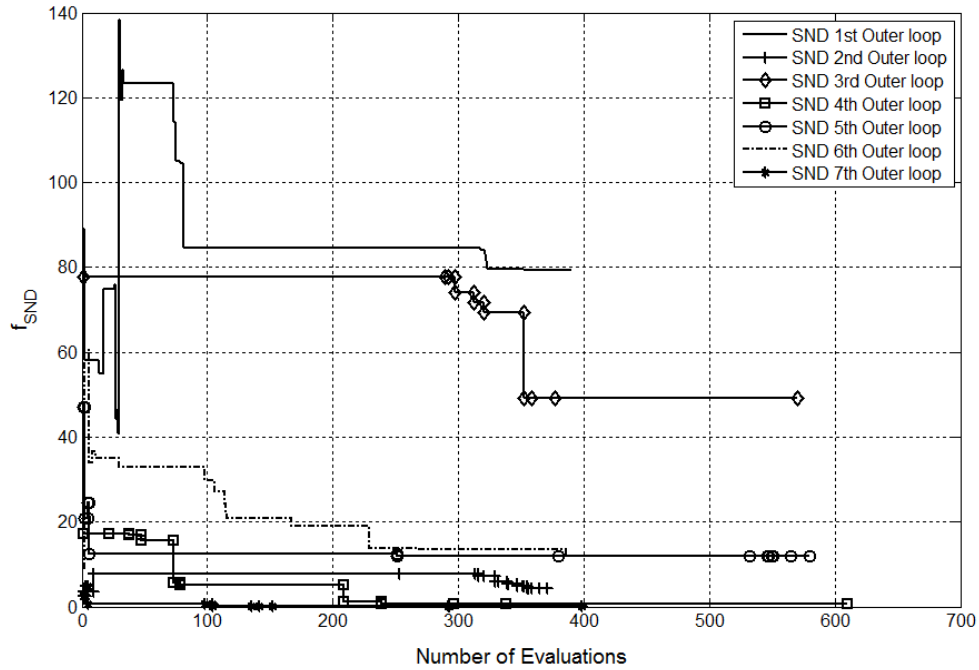
Figure 5-17: The convergence history plot of improved structure and dynamic (SND) objective function for inner loop optimizations
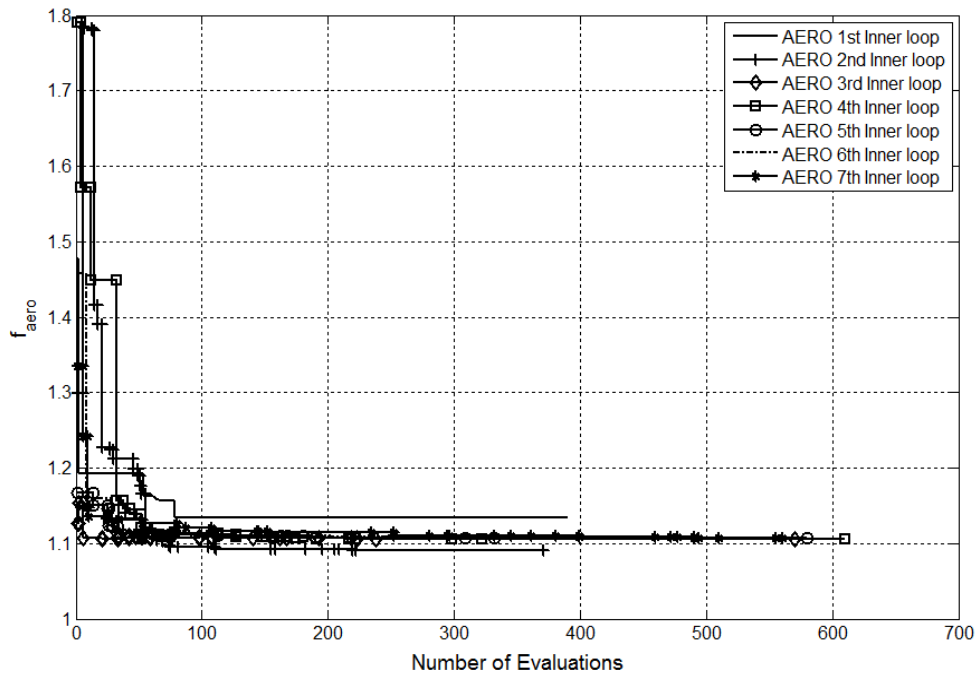
Figure 5-18: The convergence history plot of improved aerodynamic objective function for inner loop optimizations

Figure 5-19 depicts the convergence history plot for outer loops stopping criteria (Eq. (13)). It indicates that all the consistency constraints are not fully satisfied after seven outer loop iterations. The SND disciplines consistency constraints are difficult to achieve; conversely the aerodynamic consistency constraints are close to satisfaction. More outer loops are required to achieve a higher level of discipline consistency. Please note that more outer loops could have been performed with the same evaluations budget if less severe inner loop stopping criterions were considered.
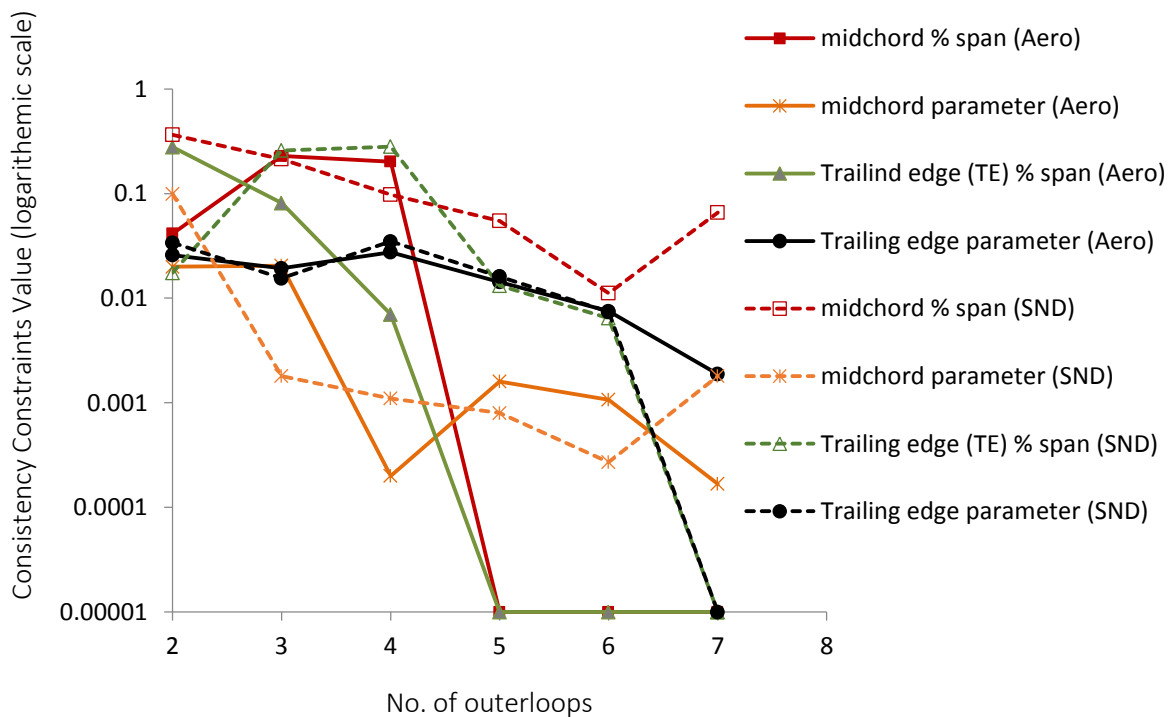
Figure 5-19: The convergence history plot of outer loops stopping function (Eq. 13)

Moreover, it is observed that the dynamic constraint feasibility and efficiency have improved with the addition in outer loops and dynamic constraints are close to feasibility at the end of 4th aero sub-optimization outer loop, see Table D-1 (Appendix-D). In addition, designer can select any design as per the requirements and priority at any stage of optimization. ATC increases the design options for designer.

5.2.1 Flow characteristics of reference and optimum blades

Figure 5-20 illustrates the fan performance characteristic curves for Rotor 67 and optimized designs obtained from MDF, filtering approach and ATC MDO formulations. The ATC optimized design has overall slightly higher efficiencies as compare to MDF and filtering approach optimized blades and Rotor 67.
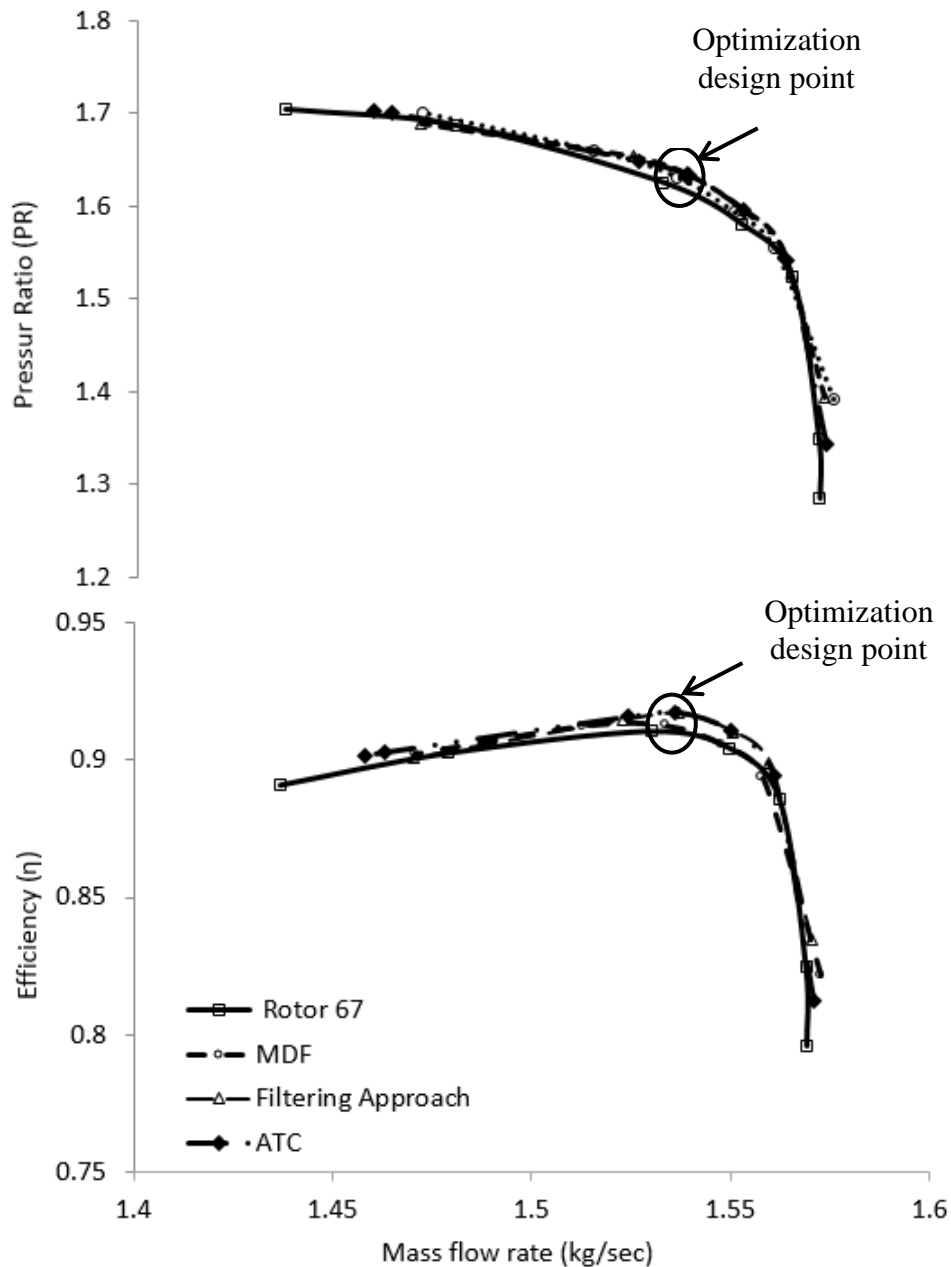
Figure 5-20: Efficiency and pressure ratio versus mass flow rate

The isentropic efficiency and the total pressure ratio of the optimized blades are improved at the design point and vary at off-design points. However, the choke mass flow of all optimized blades is similar to the baseline design. The results show that the multidisciplinary optimized blades off-design performance has suffered. As mentioned earlier in literature review, off-design performance of transonic compressor blades is very important for transonic fan blade design as engine operates at multiple design conditions. Note that multi-point optimization was conducted in another part of this project by other team members.

Figure 5-21 compares the relative isentropic Mach number distributions at 85% spanwise positions. The ATC-optimized blade Mach number plot has a slightly smoother loading at the pressure side whereas at suction side, both filtering approach and ATC blades Mach distribution is less steep near to 60% chord as compared to Rotor 67. This effects the shock strength reduction, and pushed it a little upstream. In Figure 5-22, at 25% spanwise positions all three optimized blade have similar Mach number distributions. The isentropic Mach number of the optimized designs decreases very smoothly along the suction surface from the leading edge to the trailing edge and shows a lower loading around the leading edge. In addition, MDF optimized blade is slightly less loaded from 77 % chord to trailing edge.

To understand further the differences in the flow field, the Mach number contour on 85% span and 25% span is compared between Rotor 67, MDF, filtering approach and ATC optimized blades in Figure 5-23 (a)-(d) and Figure 5-24 (a)-(d). At 85% span, contours show that the baseline design has a higher Mach number in front of the shock wave compared to MDO-optimized designs, especially near the suction surface of the blade. Also, the bow shock impingement on the suction side has become more oblique. Moreover, a strong reduction in supersonic bubble is observed in all optimized blades near the leading edge at 25% span. This is similar to the aero-optimized blade designs. A little less separation zone in ATC and filtering approach optimized blades is observed near trailing edge suction side.

Figure 5-25 shows the pressure contour comparison between Rotor 67, filtering approach and ATC blades on suction side. It shows that a strong passage shock is occurred normal to the casing of Rotor 67. Furthermore, the shock inclines forward below 90% span in Rotor 67 flow field whereas the incline starts earlier for Filtering approach and ATC optimized blades flow field almost 93% and 95% span respectively. It was also found that both optimized blades at the

central part of blade span have lost passage shock intensity and become weak. The reduction in the shock strength accounts for the main efficiency gain. These observations are consistent with the isentropic Mach number distribution in Figure 5-21.
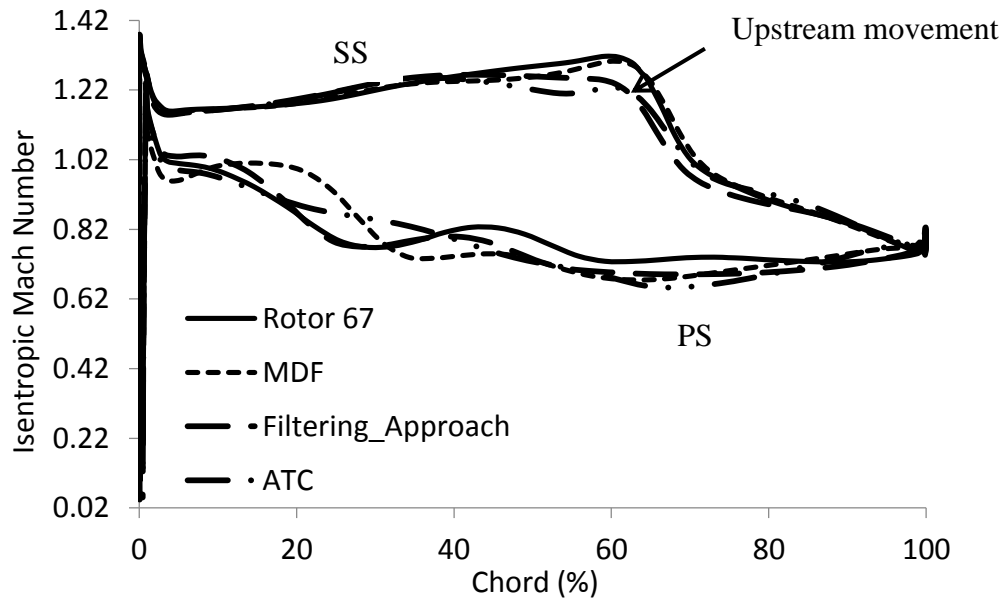
Figure 5-21: Mach number contour comparison at 85% Rotor 67 and optimized blades
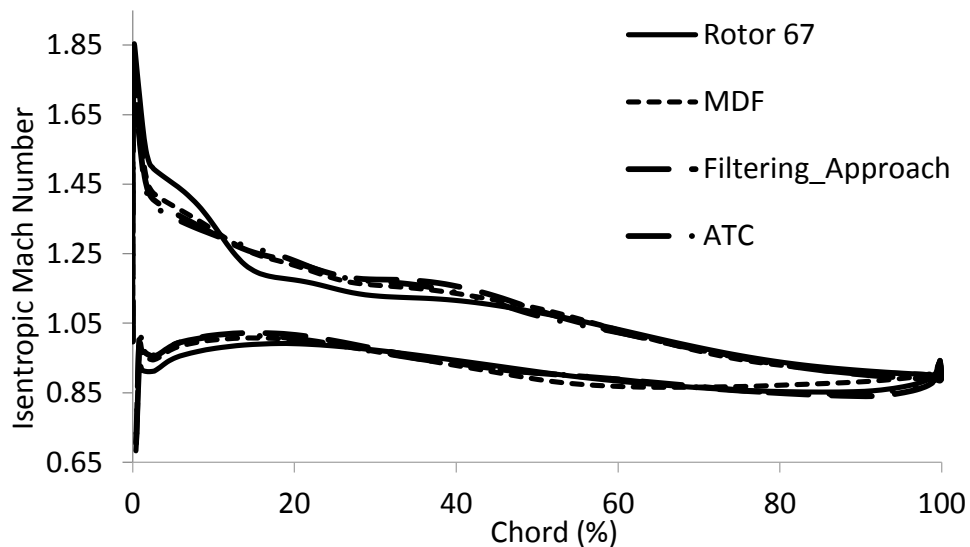
Figure 5-22: Mach number contour comparison at 25% span among Rotor 67 and optimized blades

(a) Rotor 67

(b) MDF

(c) Filtering Approach

(d) ATC
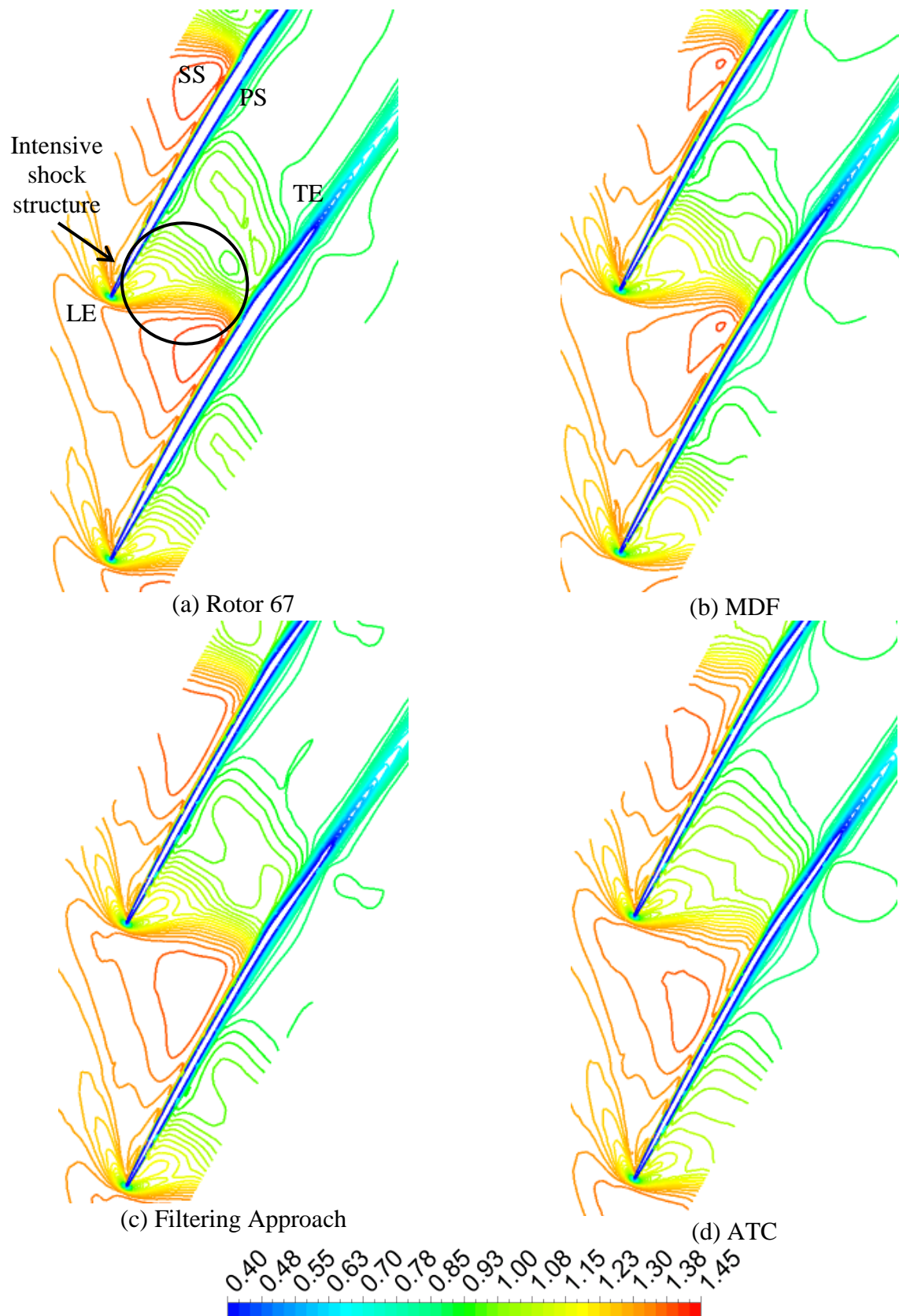
Figure 5-23: Mach number contour comparison at 85% span (at design point)

(a) Rotor 67

(b) MDF

(c) Filtering Approach
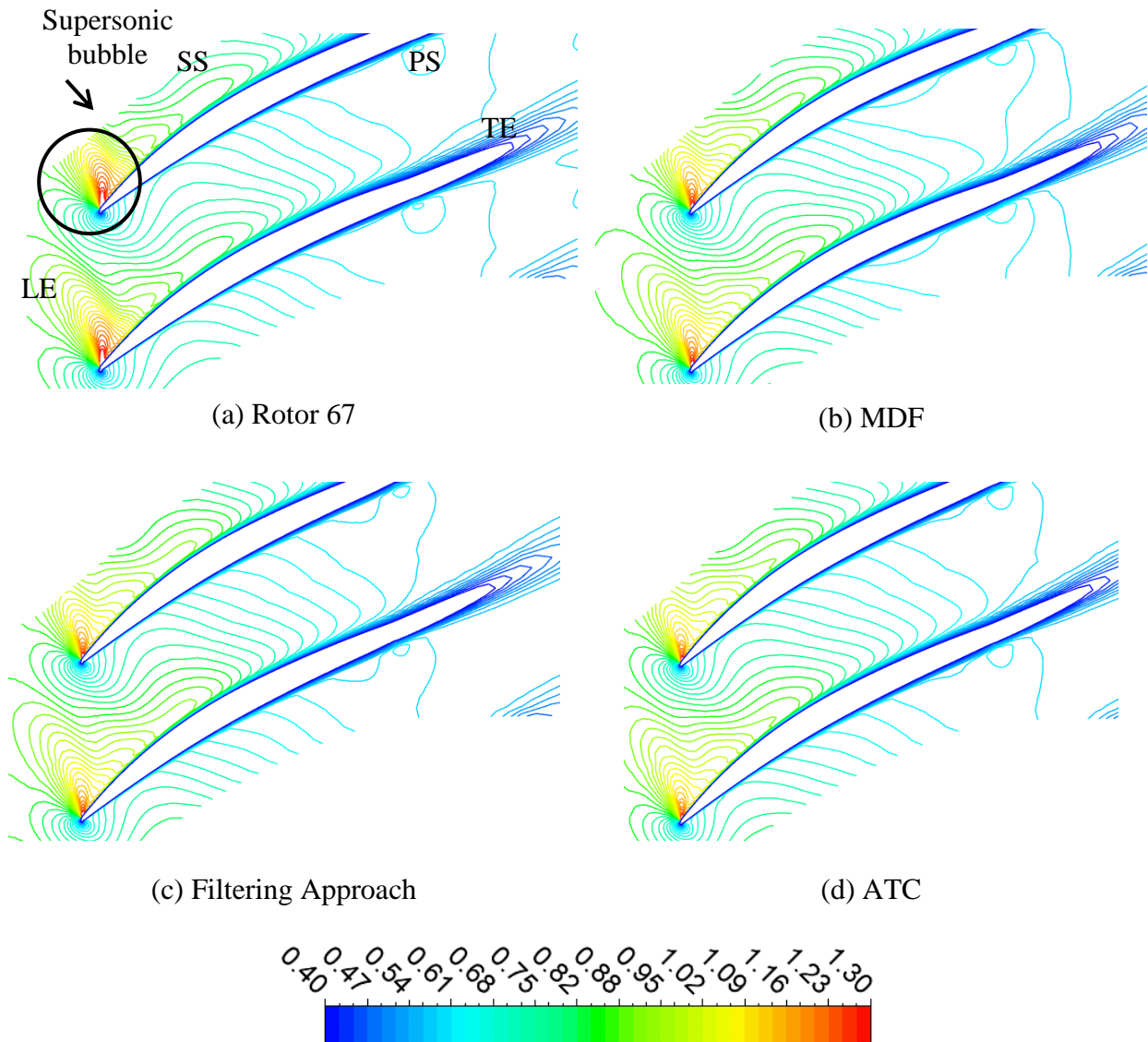
(d) ATC

Figure 5-24: Mach number contour comparison at 25% span (at design point)

Figure 5-26 shows the streamlines of wall shear on the suction side of the Rotor 67, filtering approach and ATC optimized blades. As mentioned earlier, the separation is characterized with the streamlines going towards the separation line whereas flow reattachment is identified by the flow going away from that line. Compared to Rotor 67 blade, the separation region on the outer span is noticeably reduced in both optimized blades. The spanwise distribution of the circumferentially averaged stagnation pressure ratio, stagnation temperature ratio and spanwise flow angle distribution at rotor exit is presented in Figure D-1 to Figure D-3 (Appendix-D).

(a) Rotor 67

(b) Filtering Approach

(c) ATC
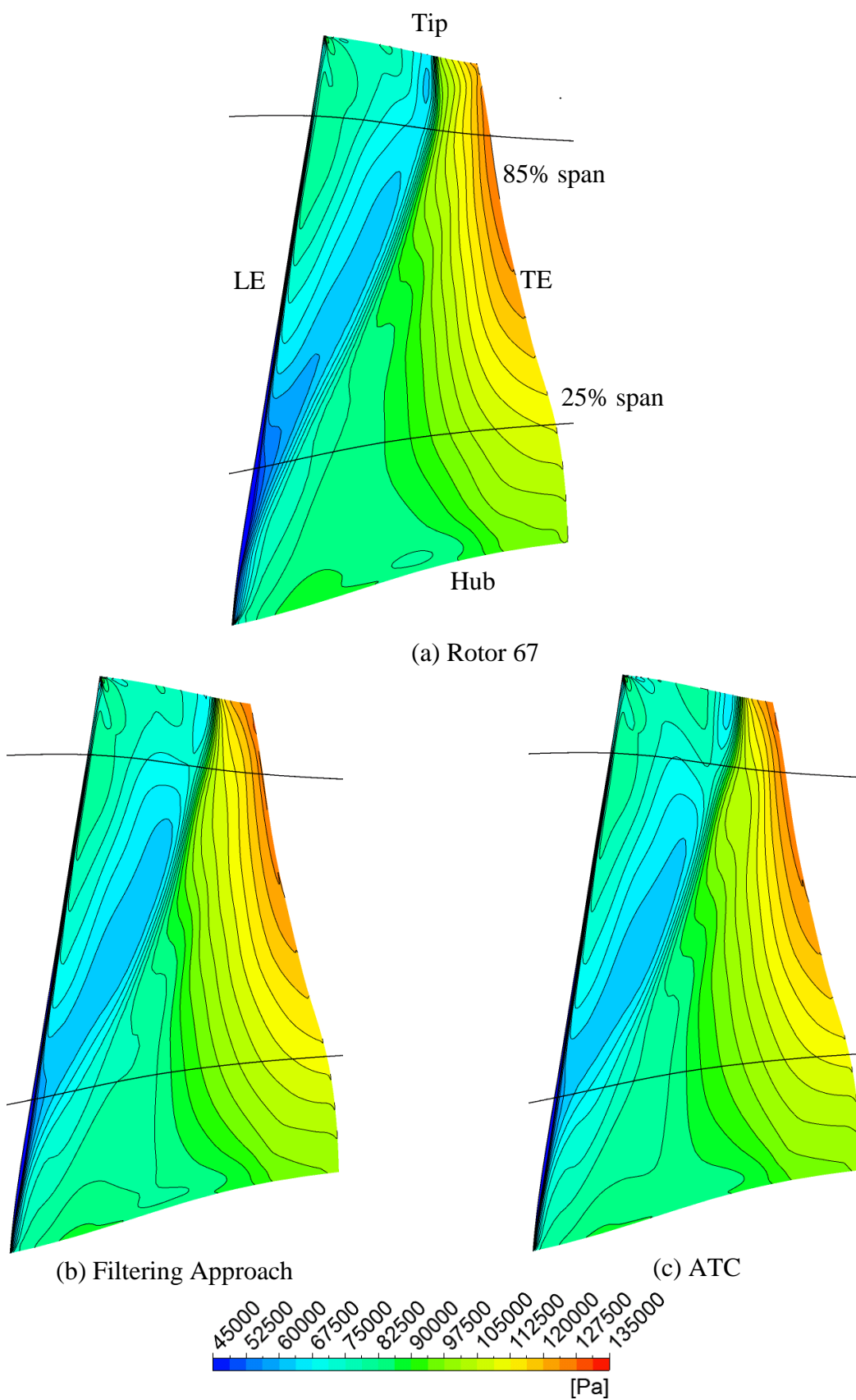
Figure 5-25: Pressure contour comparison at suction side (at design point)

(a) Rotor 67

(b) Filtering Approach

(c) ATC
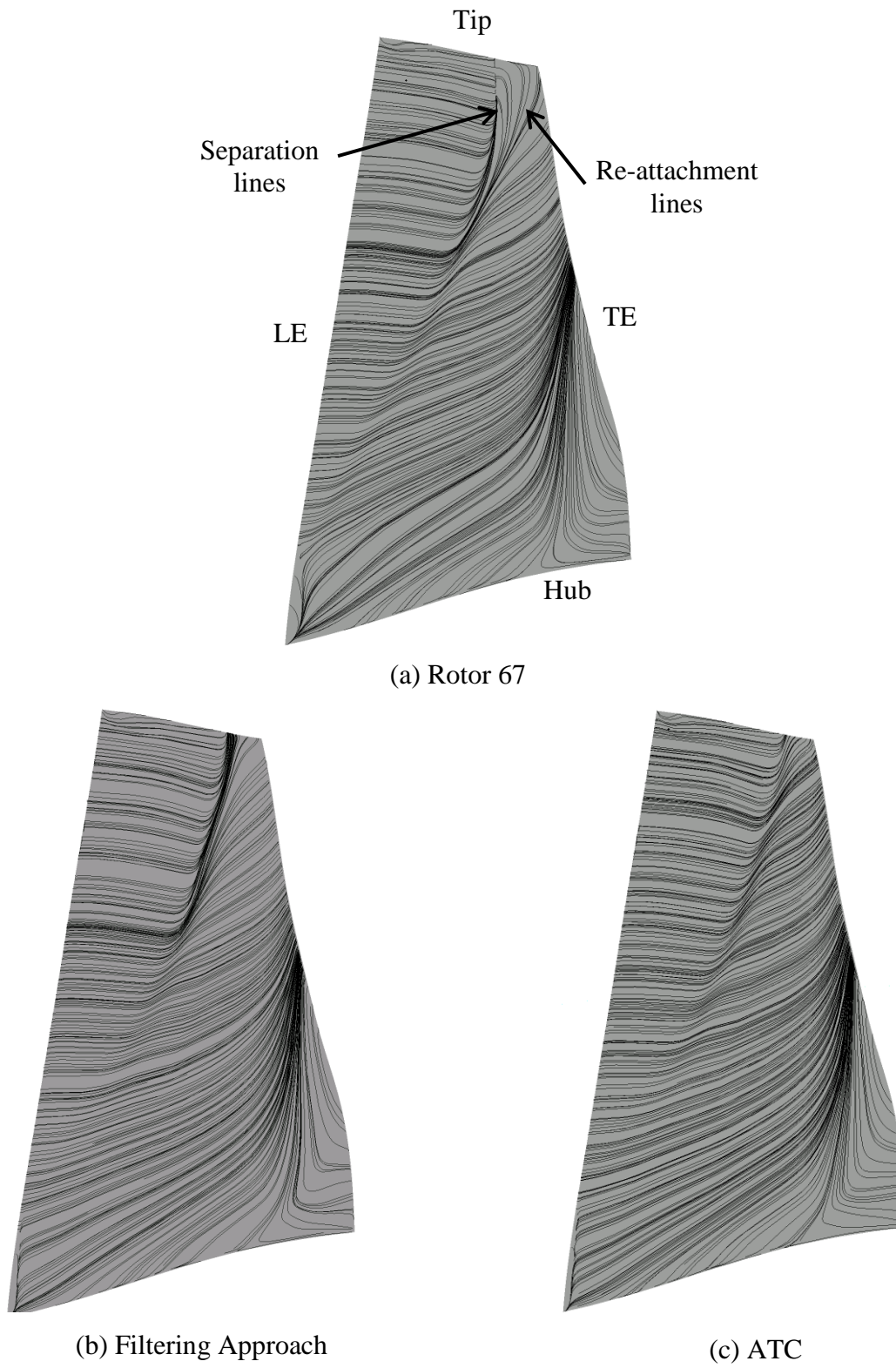
Figure 5-26: Streamlines close to suction side (at design point)

5.2.2 Vibration characteristics of reference and optimum blades

The comparison of the Campbell diagram of Rotor 67 and MDO optimized blades are given in Figure 5-27. The bold black lines represent that the initial three frequency modes for Rotor 67 arise in engine running range (see red circles on purple dotted lines). It shows that MDO optimized designs avoided the intersection between the excitation frequencies and the modal frequencies within the operation rotation speed from 90% to 110% of the blade design speed (100% RPM). Consequently, all the potential resonance points, in the original Rotor 67 (red round points), are eliminated. Thus, the MDO optimized blades, do not run in any resonance risk (see dotted and bold green lines in Figure 5-27) and have the sufficient safety margin between the blade frequencies and the excitation frequencies. It is observed that as 1st dynamic frequency mode of Rotor 67 is close to upper rotational speed limit (i.e. 110% rpm) thus optimizer pushed it up whereas 3rd and 2nd dynamic frequency modes of Rotor 67 are close to lower rotational speed (i.e. 90% rpm) so both optimized frequency modes are pushed down.
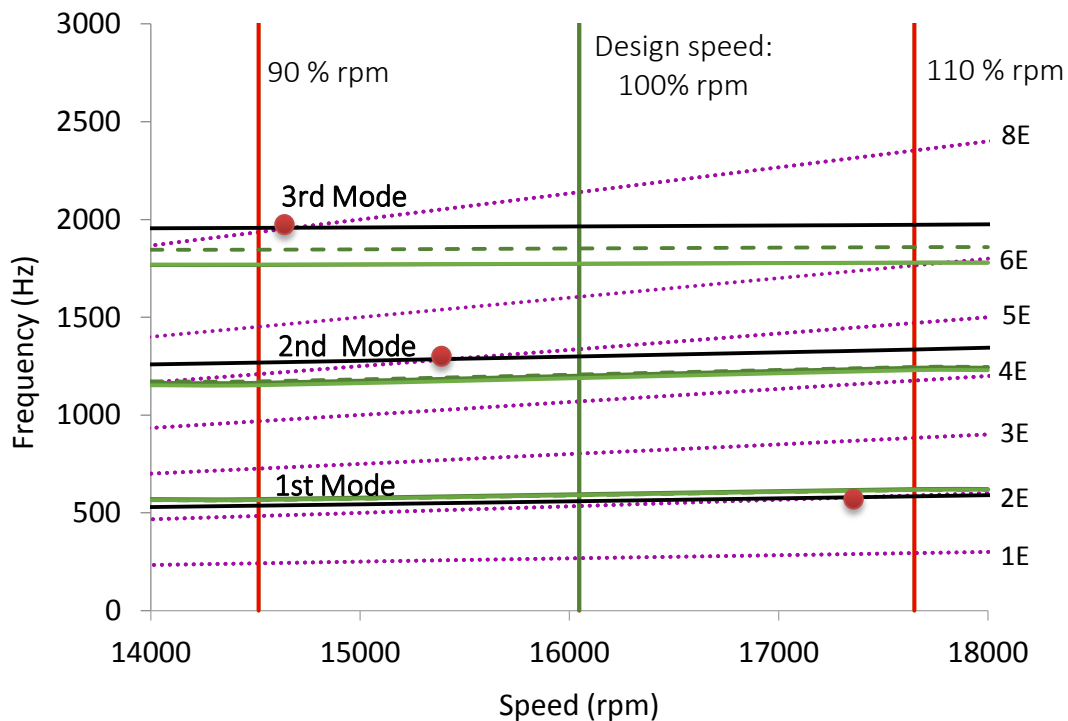
Figure 5-27: Campbell Diagram

5.2.3 Structural characteristics of reference and optimum blades

To understand the von-Mises stress distribution of the optimized blades, a comparison of the stress contours on pressure side for Rotor 67 and optimized blades are presented in Figure 5-28. The maximum von-Mises stresses of optimized designs do not excess the allowable maximum stress.

The comparison shows that the maximum stress is still placed at blade root pressure side. Negative stacking moves the blade sections towards the axis of rotation (lean towards the pressure side), which basically changes the center for mass. Negative lean decreases the maximum stress compared to the original geometry due to the blade camber and thickness distribution.

(a) Rotor 67

σ_{max}: 561 MPa
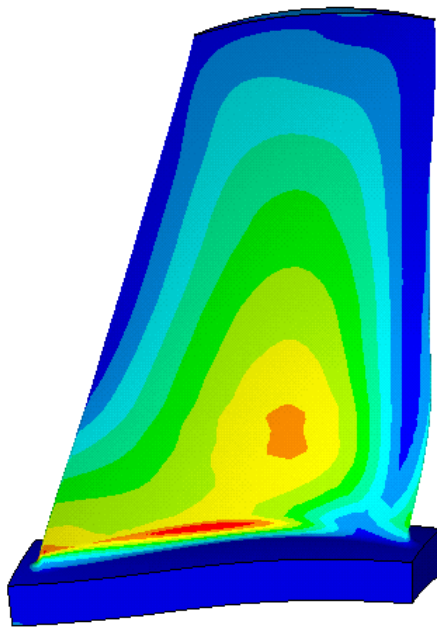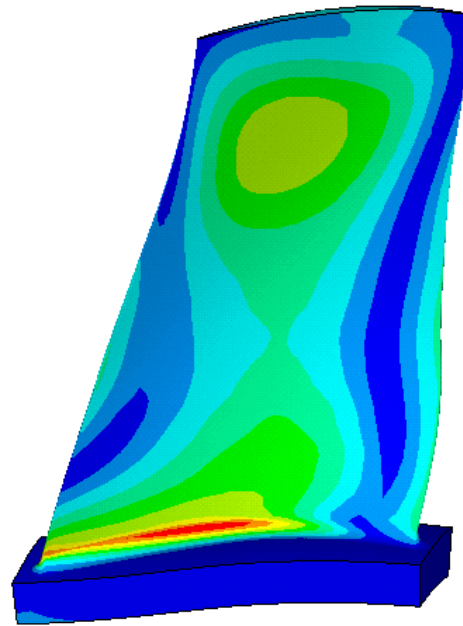
(b) MDF

σ_{max}: 360 MPa

(c) Filtering Approach

σ_{max}: 458 MPa
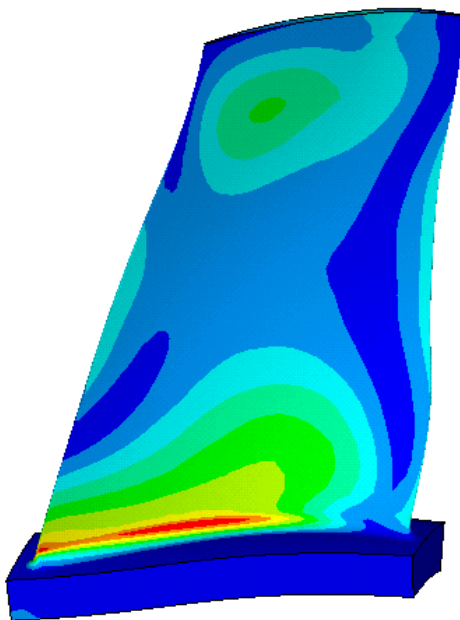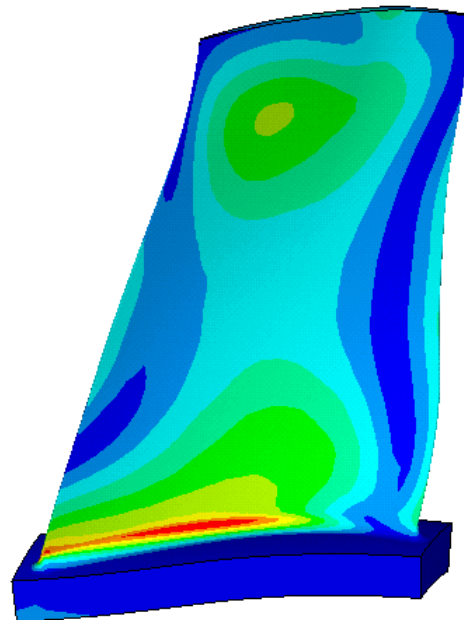
(d) ATC

σ_{max}: 374 MPa

Figure 5-28: Blade von-Mises stress contour at pressure side

5.3   A post optimization trade-off analysis

The purpose of this section is to further analyze the aerodynamics and multidisciplinary design optimization results.

This simple approach is adopted from Ref. [156] and it does not require any additional function evaluations. It can be done by utilizing the cache history of the optimization and might provide a better insight of the design problem in low computational budget. Audet, Dennis et al. [156] proposed this simple method to study the single objective optimization results and trade-off of the optimization problem objective versus the constraints including the bounds in the variables. The output is represented by the two-dimensional plots of objective function versus each constraint. The plot will possibly contain the feasible and infeasible solutions for observed constraint and only feasible solutions for all other constraints. This study might indicate which constraints should be relaxed to improve objective function without any supplementary function calls.

The bound variables can also be considered as design constraints. For example, the β-angle design variable bound i.e. $-3 \leq \beta \leq 3$ can be replaced by $\beta - 3 \leq 0$ or $-\beta - 3 \leq 0$. It should be noted that the constraint $c_0(x) \leq 0$ (Eq. (1)), is called an active constraint, if $c_0(x^*) = 0$ at optimal solution. Moreover, for an active constraint, the plots contain the trade-offs between the objective function values versus the constraint, but for inactive constraint at the optimal solution by changing the bound does not help to improve the objective function.

For aerodynamic optimization, the objective function (i.e. η_{DP}) is plotted versus β and $d\beta/ds$ design variables for pressure ratio feasible solutions (see Figure 5-29(a)-(d)). The sensitivity of the β-angle (at LE, hub) shows that $\beta-3 \leq 0$ is active at the optimal solution (or design point). The gray trend line for the feasible solutions shows that the objective function (i.e. design point efficiency, η_{DP}) might be increased by increasing the upper bound of β-angle. Moreover, Figure 5-29(d) illustrates that the plotted constraint is inactive at the optimal solution, and it appears that it would be active if it is replaced by *dβ/ds* ≥ -0.028 (i.e. *-dβ/ds* -0.05 ≤-0.078). In addition, Figure 5-29(b)-(c) show that both design variables are inactive at the optimal solution and do not support to further improvement in the objective function by changing the bounds. The rest of the design variables are also inactive at the optimal design and not presented here.

The trade-off study for MDF-MDO is presented in Figure 5-30 (a)-(d). The objective function (i.e. η_{DP}) is plotted versus the initial three dynamic frequency mode constraints for pressure ratio,

maximum stress and remaining frequency constraints feasible solutions. It should be noted that 1st frequency (F_1) feasible and infeasible solutions were plotted when the other constraints were also feasible (i.e. F_2 and F_3, PR, σ_{max} feasible). Similarly, F_2 feasible and infeasible solutions were plotted, when PR, σ_{max}, F_1 and F_3, were feasible and so on. In each plot the infeasible solutions, feasible solutions, an optimal solution (design point) and trend are represented by the gray filled diamond, blank diamond, red square and dark gray line respectively.
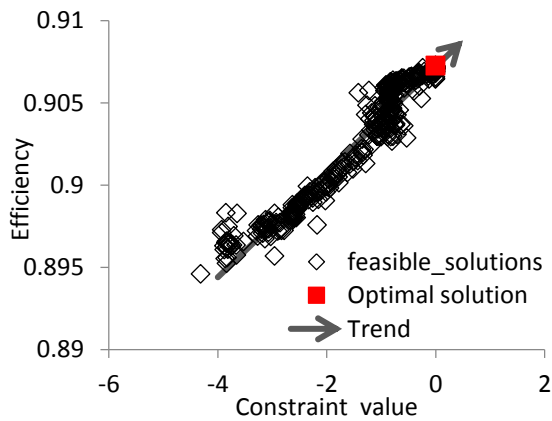
(a) Sensitivity to $\beta-3\leq0$ (LE hub)
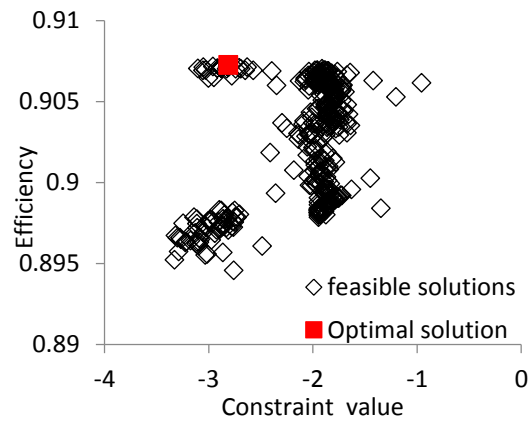
(b) Sensitivity $\beta-3\leq0$ (midchord hub)
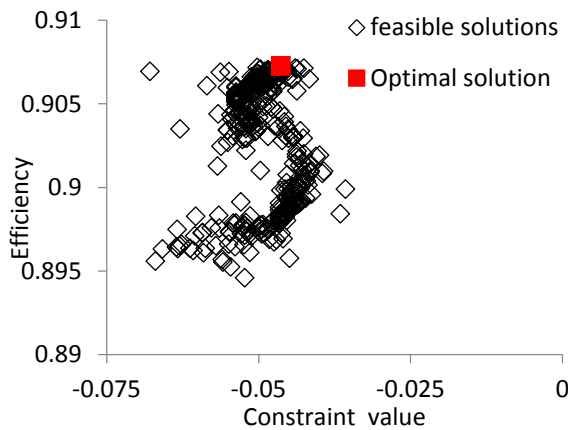
(c) Sensitivity to $-d\beta/ds$ -0.05 ≤0 (midchord tip)
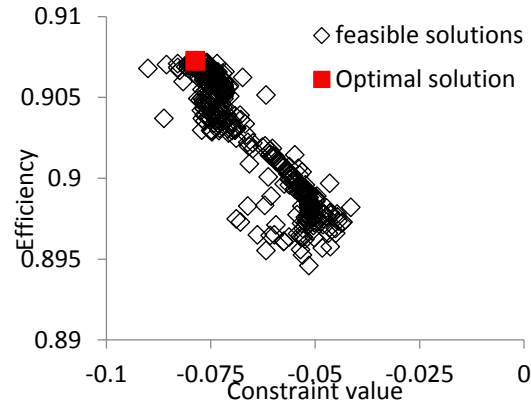
(d) Sensitivity to $-d\beta/ds$ -0.05 ≤0 (TE tip)

Figure 5-29: Simple trade-off study for aerodynamic optimization problem

(a) Sensitivity to 588-$F_1 \leq 0$

(PR, σ_{max}, F_2, F_3 feasible solutions)

(b) Sensitivity to F_2-1209≤ 0

(PR, σ_{max}, F_1, F_3 feasible solutions)

(c) Sensitivity to 1765- $F_3 \leq 0$

(PR, σ_{max}, F_2, F_3 feasible solutions)
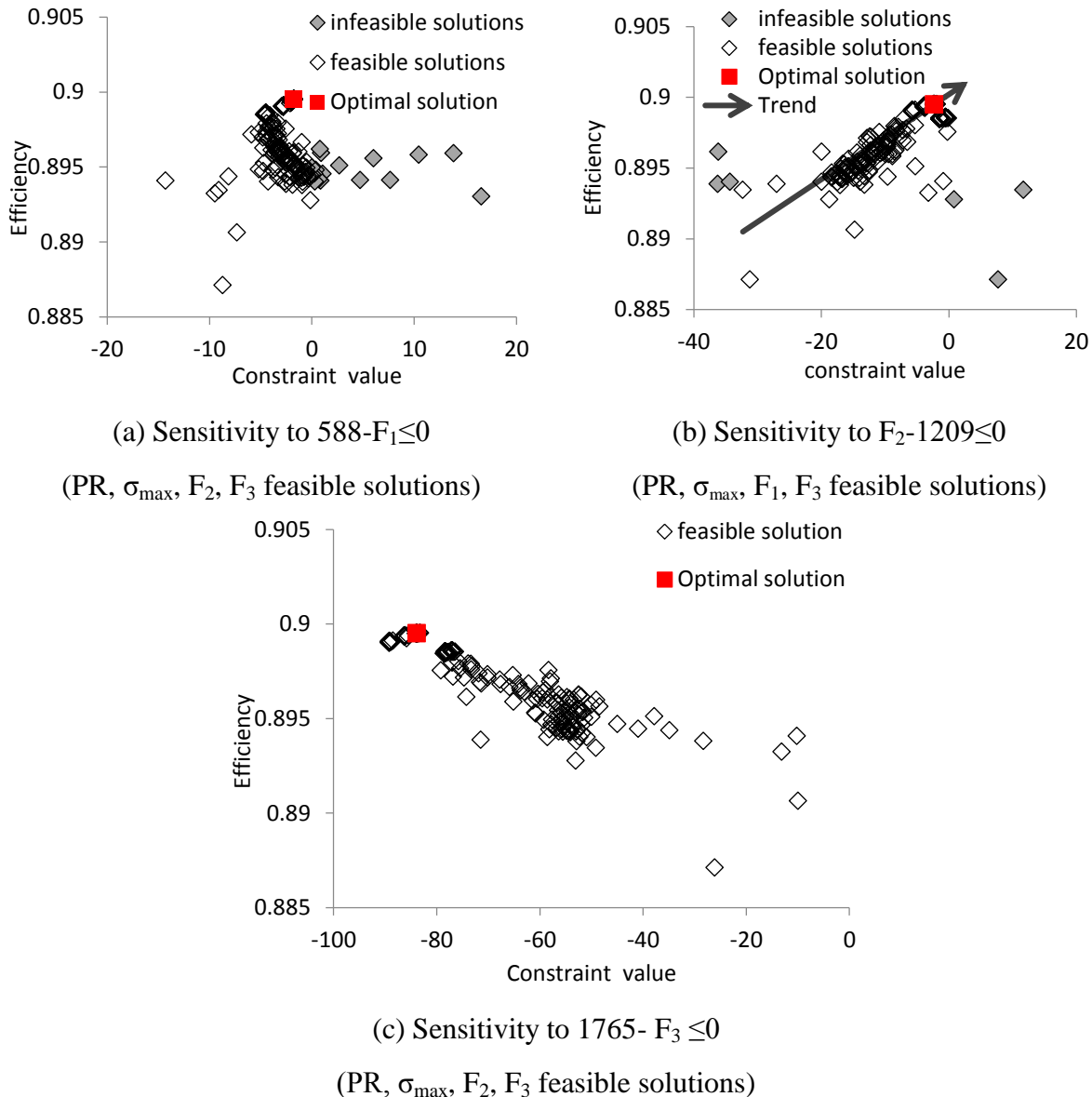
Figure 5-30: Simple trade-off study for MDF-MDO optimization problem

The sensitivity of 2nd dynamic frequency mode (F_2) constraint is shown in Figure 5-30 (b). It can be seen that the objective function is sensitive to F_2 constraint and the optimal solution is placed very close to the upper bound of F_2 constraint. Based on the trend of feasible solutions efficiency toward the F2 constraint upper bound, one can anticipate that the efficiency would be increased if the range of F_2 constraint is relaxed. The literature review findings (see Section 2.2.5.3) also showed that the broad frequency constraint margin makes the optimization problem stiff. In the problem statement (Section 4.2.1), the employed frequency margin is also mentioned wide that is

within 90% to 110% rotational speed no frequency mode arises into engine running range. To give an example, if we consider 92% to 108% speed bound for F_2 frequency mode constraint then the upper bound becomes 1230 Hz frequency rather than 1209 Hz and lower bound modifies from 1170 Hz to 1155 Hz. This modification could lead to 0.7 points improvement in η_{DP}. Moreover, the all other frequency constraints plot show that the objective function is not sensitive to their ranges (see Figure 5-30(a) and Figure 5-30(c)).

In general, this simple inexpensive study provides information on the trade-off the objective function with the constraints, which could help the designers to further investigate the design problem by utilizing the cache history of optimization result.

CONCLUSION AND FUTURE WORK

This study presented an automated three–dimensional aerodynamics and multidisciplinary design optimization processes for a transonic fan blade with the integration of fan blade parameterization, high-fidelity flow and mechanical analyses. The adopted three-dimensional fan blade parameterization was developed and validated by Lupien [67], which has significantly reduced the number of parameters required to generate and modify transonic fan blades in automated optimization process. The performance of high-fidelity CFD and finite element (FE) structural analyses are also verified with the experimental results. A shared CAD modal is developed in CATIA to perform the structural and dynamic analyses. A prototype of MDO based CAD-CFD-FEA automated integrated system is developed and the performance of the new system is tested by the modification of a transonic fan blade. A widely used transonic fan blade NASA Rotor 67 has been selected to compare various approaches. It should be noted that, the Rotor 67 is a complex rotor and it was already optimized by the NASA laboratory. Hence, Rotor 67 is a tough optimization problem and only minor improvement in efficiency is expected.

The transonic fan blade design problem was stated in detail. The handling of the coupling design variables and the sensitivity of the geometrical design variables on the objective function and design constraints were also provided in detail in order to

Aerodynamics optimization was performed as an initial step for transonic fan blade design optimization process to ensure the feasibility of design process. It also helped to find a suitable optimization algorithm and explore the design space. The aerodynamic design optimization was performed to enhance the design point efficiency while maintaining the pressure ratio and mass flow rate. In this work, aerodynamic optimization was able to improve the Rotor 67 efficiency by +0.99 (points) by changing only 18 design parameters within 500 design evaluations (or 150 hours). A number of optimization techniques available in commercial software Isight were employed. A comparison of Mach contours near blade tip for all optimized blade and baseline blade shows that shock strength is reduced and shock regime moves downstream which further helps to reduce the shock induced separation near the trailing edge. The adaptation of maximum thickness location can be associated with the change in shock position at the suction side of the blade near the trailing edge. Furthermore, the aero-optimized blade design results show that the

aero-optimized designs were unable to satisfy the mechanical requirements for maximum stress and vibration frequency.

Therefore, three MDO-formulations including two single-level formulations, MDF and filtering approach, are designed, implemented and compared. The MDO formulation contains the aerodynamic optimization objective and constraints in addition with stress and dynamic disciplines constraints. These are limiting the maximum stress within Rotor 67 and ensure that initial three-frequency, do not arise in the engine running range. MDF-MDO approach is able to attain the feasible design and slightly improve the Rotor 67 efficiency (+0.19 points) by varying 20 design parameters within 400 complete design evaluations (or 180 hours) including aerodynamic, stress and dynamic analyses. The proposed filtering approach MDO formulation is capable to increase the Rotor 67 efficiency by +0.66 (points) with 212 complete evaluations (including aerodynamic, stress and dynamic analyses) and 785 structure and dynamic analyses evaluations (or 132 hours) while satisfying the aerodynamic, stress and dynamic constraints. Moreover, the results show that the initial design is infeasible for dynamic constraint and the optimizer took several evaluations to get the initial feasibility which costs a lot in terms of computation. Additionally, the feasibility of all dynamic constraints is difficult to obtain due to the wide range of operating rotational speeds, which makes the optimizer's job harder to get to a feasible solution. This is also validated by performing the trade–off study to further investigate the MDF-MDO optimization. The sensitivity of the objective function to the bounds of the constraints showed that the objective function can be improved by relaxing the upper bound for 2nd frequency mode.

A multi-level ATC formulation is then presented. In ATC-MDO formulation, the transonic fan design optimization problem is decomposed into two subproblems: 1. Aerodynamic optimization 2. Structure and Dynamic (SND) optimization. The Structure and Dynamic disciplines are combined as Dynamic analysis is taking pre-stressed model from Structure. In this fan design problem the only shared variables between the two subproblems are thickness/geometrical design variables. No coupling variable has been considered. Both subproblems also have local geometrical design variables. The interactions between the subproblems with respect to the shared design variables are managed by penalty functions. The goal of a subproblem is not only to minimize the discipline objective and the deviation of geometrical design variables from targets but also to achieve feasibility with respect to the subproblem constraints. The Augmented

Lagrangian Coordination (ALC) penalty function has been used to update the penalty weights. A total of seven sub-optimizations were performed for both subproblems. It is observed that ATC requires more computational time as compared to MDF and filtering approach. However, ATC explored wider design space and provided a considerably better solution as compare to MDF and slightly better as compare to filtering approach. The computational time may be reduced by running both sub-optimizations in parallel.

The results show that all MDO implemented formulations can result in increased aerodynamic performance while respecting all the structural and vibration constraints. However, the efficiency of the optimization process is strongly affected by the formulation. For example, it can be seen that both single-level formulations are relatively easy to implement and be able to satisfy constraints with slightly raise the efficiency whereas the implementation of multi-level ATC was little challenging and time-consuming to improve slightly better efficiency than single-level formulations. However, ATC was implemented in the current work with lots of simplifications and its performance could be improved by altering the selection of shared variables and formulation.

The following areas are identified as a potential continuation of this work:

- The current research work has demonstrated MDO for fan blade at design point condition only. However, as mentioned earlier, a compressor has to work for different operating conditions which make the process more intricate. Thus, MDO with multi-point design optimization needs to be performed in order to increase the design freedom and chance to find a better solution for the design problem. But, it also requires longer optimization time due to extension of the design problem by considering more objectives and constraints.

- The optimized blade designs may be built and tested in the lab for further validation of algorithms, MDO process performance and any future improvement.

- This work has introduced the transonic fan blade MDO integrated design process with the combination of aerodynamics, structural and dynamics disciplines. However, in future extension of disciplines and analyses such as bird strike analysis, FOD (Foreign object damage) test, hot-to-cold analysis, fatigue analysis, overall cost estimation, etc., and addition of design parameters such as fillet radius, sweep, blade chord, blade inlet

thickness, tip clearance and variable disk geometry etc., could be considered into current MDO process. This could result in a more comprehensive and complete optimization tool which could be applied to fan blade design in industries.

- This work can provide useful knowledge about design parameters implications on the objectives and constraints, aerodynamics, stress, and dynamics analyses and detail implementation of MDO formulations on a transonic fan blade design. A keen industrial designer can benefit from them and can further improve the performance of MDO process by altering the optimization algorithms and running the design analyses in parallel.

- This effort presents first step in implementing ATC-MDO for transonic fan blade design problem using high-fidelity analysis tools, which is to involve aerodynamics, structure and dynamics. However, ATC formulation performance may change by the adaptation of non-hierarchical ATC formulation and addition of more shared design variables such as position of maximum thickness.

BIBLIOGRAPHY

[1]   J. Denton and L. Xu, "The exploitation of three-dimensional flow in turbomachinery design," Proceedings of the Institution of Mechanical Engineers, Part C: Journal of Mechanical Engineering Science, vol. 213, pp. 125-137, 1998.

[2]   R. Biollo and E. Benini, "Recent advances in transonic axial compressor aerodynamics," Progress in Aerospace Sciences, vol. 56, pp. 1-18, 2013.

[3]   W. Calvert and R. Ginder, "Transonic fan and compressor design," Proceedings of the Institution of Mechanical Engineers, Part C: Journal of Mechanical Engineering Science, vol. 213, pp. 419-436, 1999.

[4]   J. Sobieszczanski-Sobieski and R. T. Haftka, "Multidisciplinary aerospace design optimization: survey of recent developments," Structural optimization, vol. 14, pp. 1-23, 1997.

[5]   Y. Lian and M.-S. Liou, "Aerostructural optimization of a transonic compressor rotor," Journal of propulsion and power, vol. 22, pp. 880-888, 2006.

[6]   E. J. Cramer, J. Dennis, JE, P. D. Frank, R. M. Lewis, and G. R. Shubin, "Problem formulation for multidisciplinary optimization," SIAM Journal on Optimization, vol. 4, pp. 754-776, 1994.

[7]   N. M. Alexandrov and R. M. Lewis, "Analytical and computational aspects of collaborative optimization for multidisciplinary design," AIAA journal, vol. 40, pp. 301-309, 2002.

[8]   I. Kroo, "MDO for large-scale design," Multidisciplinary design optimization: state-of-the-art. SIAM, Philadelphia, pp. 22-44, 1997.

[9]   R. J. Balling and J. Sobieszczanski-Sobieski, "Optimization of coupled systems-A critical overview of approaches," AIAA journal, vol. 34, pp. 6-17, 1996.

[10]   R. D. Braun, "Collaborative optimization: an architecture for large-scale distributed design," 1996.

[11]   R. Sellar, S. Batill, and J. Renaud, "Response surface based, concurrent subspace optimization for multidisciplinary system design," AIAA paper, vol. 714, p. 1996, 1996.

[12]   J. Sobieszczanski-Sobieski, "Optimization by decomposition: a step from hierarchic to non-hierarchic systems," NASA STI/Recon Technical Report N, vol. 89, p. 25149, 1989.

[13]   J. Sobieszczanski-Sobieski, M. S. Emiley, J. S. Agte, and R. R. Sandusky, Advancement of bi-level integrated system synthesis (bliss): National Aeronautics and Space Administration, Langley Research Center, 2000.

[14]   H. M. Kim, T. Jiang, N. F. Michelena, and P. Y. Papalambros, "Target cascading in optimal system design," Journal of mechanical design, vol. 125, pp. 474-480, 2003.

[15]   S. Tosserams, L. Etman, and J. Rooda, "Augmented Lagrangian coordination for distributed optimal design in MDO," International journal for numerical methods in engineering, vol. 73, pp. 1885-1910, 2008.

[16]   J. R. Martins and A. B. Lambe, "Multidisciplinary design optimization: A survey of architectures," AIAA journal, vol. 51, pp. 2049-2075, 2013.

[17]   R. T. Haftka, "Simultaneous analysis and design," AIAA journal, vol. 23, pp. 1099-1103, 1985.

[18]   N. M. Alexandrov and R. M. Lewis, Comparative properties of collaborative optimization and other approaches to MDO: Citeseer, 1999.

[19]   S. Chen, F. Zhang, and M. Khalid, "Evaluation of three decomposition MDO algorithms," in Proceedings of 23rd international congress of aerospace sciences, Toronto, Canada, 2002.

[20]   K. Hulme and C. Bloebaum, "A comparison of solution strategies for simulation-based multidisciplinary design optimization," in Proceedings Seventh AIAA/NASA/ISSMO Symposium on Multidisciplinary Analysis and Optimization, 1998, pp. 2143-2153.

[21]   S. Kodiyalam, Evaluation of methods for multidisciplinary design optimization (MDO), Phase I: National Aeronautics and Space Administration, Langley Research Center, 1998.

[22]   S. Kodiyalam and C. Yuan, "Evaluation of Methods for Multidisciplinary Design Optimization (MDO), Part II," NASA contractor report, NASA/CR-2000-210313, 2000.

[23]   R. E. Perez, H. H. Liu, and K. Behdinan, "Evaluation of multidisciplinary optimization approaches for aircraft conceptual design," in AIAA/ISSMO Multidisciplinary Analysis and Optimization Conference, Albany, NY, 2004.

[24] A. De Wit and F. van Keulen, "Numerical comparison of multi-level optimization techniques," in Proceedings of the 3rd AIAA multidisciplinary design optimization specialist conference, Honolulu, HI, 2007.

[25] J. J. Alonso and M. R. Colonno, "Multidisciplinary optimization with applications to sonic-boom minimization," Annual Review of Fluid Mechanics, vol. 44, pp. 505-526, 2012.

[26] R. P. Henderson, J. Martins, and R. E. Perez, "Aircraft conceptual design for optimal environmental performance," Aeronautical Journal, vol. 116, p. 1, 2012.

[27] V. M. Manning, Large-scale design of supersonic aircraft via collaborative optimization, 1999.

[28] R. Ganguli, "A survey of recent developments in rotorcraft design optimization," Journal of Aircraft, vol. 41, pp. 493-510, 2004.

[29] B. Glaz, P. P. Friedmann, and L. Liu, "Helicopter Vibration Reduction throughout the Entire Flight Envelope Using Surrogate-Based Optimization," Journal of the American Helicopter Society, vol. 54, pp. 12007-12007, 2009.

[30] J. L. Walsh, K. C. Young, J. I. Pritchard, H. M. Adelman, and W. R. Mantay, Integrated aerodynamic/dynamic/structural optimization of helicopter rotor blades using multilevel decomposition vol. 3465: National Aeronautics and Space Administration, Langley Research Center, 1995.

[31] G. Kenway and J. Martins, "Aerostructural shape optimization of wind turbine blades considering site-specific winds," in Proc. of 12th AIAA/ISSMO Multidisciplinary Analysis and Optimization Conference, 2008.

[32] R. Braun, A. Moore, and I. Kroo, "Use of the collaborative optimization architecture for launch vehicle design," in Proceedings of the 6th AIAA/NASA/ISSMO Symposium on Multidisciplinary Analysis and Optimization, 1996.

[33] G. Cai, J. Fang, Y. Zheng, X. Tong, J. Chen, and J. Wang, "Optimization of system parameters for liquid rocket engines with gas-generator cycles," Journal of Propulsion and Power, vol. 26, pp. 113-119, 2010.

[34]   Y. Takekoshi, T. Kawamura, H. Yamaguchi, M. Maeda, N. Ishii, K. Kimura, T. Taketani, and A. Fujii, "Study on the design of propeller blade sections using the optimization algorithm," Journal of marine science and technology, vol. 10, pp. 70-81, 2005.

[35]   J. Allison, D. Walsh, M. Kokkolaras, P. Y. Papalambros, and M. Cartmell, "Analytical target cascading in aircraft design," in 44th AIAA aerospace sciences meeting and exhibit, 2006, pp. 9-12.

[36]   C. B. Callahan and F. K. Straub, "Design optimization of rotor blades for improved performance and vibration," Journal of the American Helicopter Society, vol. 38, pp. 62-70, 1993.

[37]   A. Chattopadhyay, T. R. McCarthy, and N. Pagaldipti, "Multilevel decomposition procedure for efficient design optimization of helicopter rotor blades," AIAA journal, vol. 33, pp. 223-230, 1995.

[38]   J. Lee and P. Hajela, "Parallel genetic algorithm implementation in multidisciplinary rotor blade design," Journal of Aircraft, vol. 33, pp. 962-969, 1996.

[39]   C. Tribes, J.-F. Dubé, and J.-Y. Trépanier, "Decomposition of multidisciplinary optimization problems: formulations and application to a simplified wing design," Engineering Optimization, vol. 37, pp. 775-796, 2005.

[40]   R.-Q. Wang, Z.-G. Jia, J.-j. Yang, D.-Y. Hu, J. Fan, and X.-l. Shen, "Study on disk and blade design based on multi-layer optimization strategy," Journal of Aerospace Power, vol. 27, pp. 1201-1209, 2012.

[41]   J. Allison, M. Kokkolaras, M. Zawislak, and P. Y. Papalambros, "On the use of analytical target cascading and collaborative optimization for complex system design," in 6th world congress on structural and multidisciplinary optimization, 2005, pp. 3091-3100.

[42]   J. Yang, J. Chen, and J. Yan, "Comparison of BLISS 2000 and CO in Turbine Blade MDO for Aircraft Engine," in ASME Turbo Expo 2013: Turbine Technical Conference and Exposition, 2013, pp. V06BT43A016-V06BT43A016.

[43]   A. Oyama, M.-S. Liou, and S. Obayashi, "Transonic axial-flow blade optimization: Evolutionary algorithms/three-dimensional Navier-Stokes solver," Journal of Propulsion and Power, vol. 20, pp. 612-619, 2004.

[44]   A. Oyama, K. Fujii, K. Shimoyama, and M.-S. Liou, "Pareto-optimality-based constraint-handling technique and its application to compressor design," in 17th AIAA CFD Conference, paper AIAA, 2005.

[45]   Y. Lian, A. Oyama, and M.-S. Liou, "Progress in design optimization using evolutionary algorithms for aerodynamic problems," Progress in Aerospace Sciences, vol. 46, pp. 199-223, 2010.

[46]   S. Pierret, R. F. Coelho, and H. Kato, "Multidisciplinary and multiple operating points shape optimization of three-dimensional compressor blades," Structural and multidisciplinary optimization, vol. 33, pp. 61-70, 2007.

[47]   D. Buche, G. Guidati, and P. Stoll, "Automated design optimization of compressor blades for stationary, large-scale turbomachinery," in ASME Turbo Expo 2003, collocated with the 2003 International Joint Power Generation Conference, 2003, pp. 1249-1257.

[48]   E. Benini, "Three-dimensional multi-objective design optimization of a transonic compressor rotor," Journal of Propulsion and Power, vol. 20, pp. 559-565, 2004.

[49]   K. Arens, P. Rentrop, S. Stoll, and U. Wever, "An adjoint approach to optimal design of turbine blades," Applied Numerical Mathematics, vol. 53, pp. 93-105, 2005.

[50]   O. Lotfi, J. Teixeira, P. Ivey, I. Kinghorn, and A. Sheard, "Shape optimisation of axial fan blades using genetic algorithms and a 3D Navier-Stokes solver," in ASME Turbo Expo 2006: Power for Land, Sea, and Air, 2006, pp. 1373-1383.

[51]   N. Chen, H. Zhang, Y. Xu, and W. Huang, "Blade parameterization and aerodynamic design optimization for a 3D transonic compressor rotor," Journal of Thermal Science, vol. 16, pp. 105-114, 2007.

[52]   D. Wang, L. He, Y. Li, and R. Wells, "Adjoint aerodynamic design optimization for blades in multistage turbomachines—part ii: Validation and application," Journal of Turbomachinery, vol. 132, p. 021012, 2010.

[53]   W. W. Copenhaver, C. Hah, A. Wadia, and E. Mayhew, "The effect of tip clearance on a swept transonic compressor rotor," Journal of turbomachinery, vol. 118, pp. 230-239, 1996.

[54]	C. Hah and A. Wennerstrom, "Three-dimensional flowfields inside a transonic compressor with swept blades," Journal of Turbomachinery, vol. 113, pp. 241-250, 1991.

[55]	A. Wadia, P. Szucs, and D. Crall, "Inner workings of aerodynamic sweep," Journal of Turbomachinery, vol. 120, pp. 671-682, 1998.

[56]	A. Wadia and C. Law, "Low Aspect Ratio Transonic Rotors: Part 2—Influence of Location of Maximum Thickness on Transonic Compressor Performance," Journal of turbomachinery, vol. 115, pp. 226-239, 1993.

[57]	A. Medd, T. Dang, and L. Larosiliere, "3D Inverse Design Loading Strategy for Transonic Axial Compressor Blading," in ASME Turbo Expo 2003, collocated with the 2003 International Joint Power Generation Conference, 2003, pp. 489-495.

[58]	N. Cai, J. Xu, and A. Benaissa, "Aerodynamic and aeroacoustic performance of a skewed rotor," in ASME Turbo Expo 2003, collocated with the 2003 International Joint Power Generation Conference, 2003, pp. 497-504.

[59]	W. Yi, H. Huang, and W. Han, "Design optimization of transonic compressor rotor using CFD and genetic algorithm," in ASME Turbo Expo 2006: Power for Land, Sea, and Air, 2006, pp. 1191-1198.

[60]	A. Samad and K.-Y. Kim, "Application of surrogate modeling to design of a compressor blade to optimize stacking and thickness," International Journal of Fluid Machinery and Systems, vol. 2, pp. 1-12, 2009.

[61]	A. Samad and K. Kim, "Shape optimization of an axial compressor blade by multi-objective genetic algorithm," Proceedings of the Institution of Mechanical Engineers, Part A: Journal of Power and Energy, vol. 222, pp. 599-611, 2008.

[62]	C.-M. Jang, A. Samad, and K.-Y. Kim, "Optimal design of swept, leaned and skewed blades in a transonic axial compressor," in ASME Turbo Expo 2006: Power for Land, Sea, and Air, 2006, pp. 1279-1288.

[63]	C.-M. Jang, P. Li, and K.-Y. Kim, "Optimization of blade sweep in a transonic axial compressor rotor," JSME International Journal Series B, vol. 48, pp. 793-801, 2005.

[64]   N. Chen, H. Zhang, Y. Xu, and W. Huang, "A study of 3D aerodynamic design for a transonic compressor blading optimized by the locations of aerofoil maximum thickness and maximum camber," Journal of Thermal Science, vol. 12, pp. 198-203, 2003.

[65]   H.-D. Li, L. He, Y. Li, and R. Wells, "Blading aerodynamics design optimization with mechanical and aeromechanical constraints," in ASME Turbo Expo 2006: Power for Land, Sea, and Air, 2006, pp. 1319-1328.

[66]   E. Benini and R. Biollo, "Aerodynamics of swept and leaned transonic compressor-rotors," Applied energy, vol. 84, pp. 1012-1027, 2007.

[67]   A. Lupien, "A 3D approach for transonic fan blade design," Mater's Thesis, sept. 2011.

[68]   A. Arnone, "Viscous analysis of three-dimensional rotor flow using a multigrid method," Journal of turbomachinery, vol. 116, pp. 435-445, 1994.

[69]   A. Arnone, M.-S. Liou, and L. A. Povinelli, "Multigrid calculation of three-dimensional viscous cascade flows," Journal of propulsion and power, vol. 9, pp. 605-614, 1993.

[70]   Y. Lian and M.-S. Liou, "Multi-objective optimization of transonic compressor blade using evolutionary algorithm," Journal of Propulsion and Power, vol. 21, pp. 979-987, 2005.

[71]   H. Okui, T. Verstraete, R. Van den Braembussche, and Z. Alsalihi, "Three-Dimensional Design and Optimization of a Transonic Rotor in Axial Flow Compressors," Journal of Turbomachinery, vol. 135, p. 031009, 2013.

[72]   A. Oyama, "Constraint-handling in evolutionary aerodynamic design," in Constraint-Handling in Evolutionary Optimization, ed: Springer, 2009, pp. 219-236.

[73]   M. M. Joly, T. Verstraete, and G. Paniagua, "Multidisciplinary design optimization of a compact highly loaded fan," Structural and Multidisciplinary Optimization, vol. 49, pp. 471-483, 2014.

[74]   P. Astrua, S. Piola, A. Silingardi, and F. Bonzani, "Multi-Objective Constrained Aero-Mechanical Optimization Of An Axial Compressor Transonic Blade," in ASME Turbo Expo 2012: Turbine Technical Conference and Exposition, 2012, pp. 241-252.

[75]   X. Deng, F. Guo, Y. Liu, and P. Han, "Aero-Mechanical Optimization Design of a Transonic Fan Blade," in ASME Turbo Expo 2013: Turbine Technical Conference and Exposition, 2013, pp. V06BT43A014-V06BT43A014.

[76]   J.-H. Kim, K.-J. Choi, and K.-Y. Kim, "Aerodynamic analysis and optimization of a transonic axial compressor with casing grooves to improve operating stability," Aerospace Science and Technology, vol. 29, pp. 81-91, 2013.

[77]   S. Lee, D.-H. Lee, K.-H. Kim, T. C. Park, B. J. Lim, and Y.-S. Kang, "Multi-disciplinary design optimization and performance evaluation of a single stage transonic axial compressor," Journal of Mechanical Science and Technology, vol. 27, pp. 3309-3318, 2013.

[78]   C. Luo, L. Song, J. Li, and Z. Feng, "A Study on Multidisciplinary Optimization of an Axial Compressor Blade Based on Evolutionary Algorithms," Journal of Turbomachinery, vol. 134, p. 054501, 2012.

[79]   V. K. Sivashanmugam, M. Arabnia, and W. Ghaly, "Aero-Structural Optimization of an Axial Turbine Stage in Three-Dimensional Flow," in ASME Turbo Expo 2010: Power for Land, Sea, and Air, 2010, pp. 967-980.

[80]   R. Fletcher, Practical methods of optimization: John Wiley & Sons, 2013.

[81]   P. E. Gill, W. Murray, and M. H. Wright, "Practical optimization," 1981.

[82]   S. S. Rao and S. Rao, Engineering optimization: theory and practice: John Wiley & Sons, 2009.

[83]   J. J. More, S. J. Wright, and P. M. Pardalos, Optimization software guide vol. 14: SIAM, 1993.

[84]   K. Deb, Optimization for engineering design: Algorithms and examples: PHI Learning Pvt. Ltd., 2012.

[85]   R. M. Hicks and P. A. Henne, "Wing design by numerical optimization," Journal of Aircraft, vol. 15, pp. 407-412, 1978.

[86]   J. J. Reuther, A. Jameson, J. J. Alonso, M. J. Rimlinger, and D. Saunders, "Constrained multipoint aerodynamic shape optimization using an adjoint formulation and parallel computers, part 1," Journal of Aircraft, vol. 36, pp. 51-60, 1999.

[87]   S.-Y. Lee and K.-Y. Kim, "Design optimization of axial flow compressor blades with three-dimensional Navier-Stokes solver," KSME international journal, vol. 14, pp. 1005-1012, 2000.

[88]   J. Luo, C. Zhou, and F. Liu, "Multipoint Design Optimization of a Transonic Compressor Blade by Using an Adjoint Method," Journal of Turbomachinery, vol. 136, p. 051005, 2014.

[89]   S. p. Burguburu, C. Toussaint, C. Bonhomme, and G. Leroy, "Numerical optimization of turbomachinery bladings," in ASME Turbo Expo 2003, collocated with the 2003 International Joint Power Generation Conference, 2003, pp. 1123-1133.

[90]   D. Thévenin and G. Janiga, "and Computational Fluid Dynamics," 2008.

[91]   M. Joly, T. Verstraete, and G. Paniagua, "Full Design of a Highly Loaded and Compact Contra-Rotating Fan Using Multidisciplinary Evolutionary Optimization," in ASME Turbo Expo 2013: Turbine Technical Conference and Exposition, 2013, pp. V06BT43A009-V06BT43A009.

[92]   U. Siller, C. Voß, and E. Nicke, "Automated multidisciplinary optimization of a transonic axial compressor," in Proceedings of AIAA Aerospace Sciences Meeting, 2009.

[93]   A. Keskin and D. Bestle, "Application of multi-objective optimization to axial compressor preliminary design," Aerospace science and technology, vol. 10, pp. 581-589, 2006.

[94]   C. Voß, M. Aulich, B. Kaplan, and E. Nicke, "Automated multiobjective optimisation in axial compressor blade design," in ASME Turbo Expo 2006: Power for Land, Sea, and Air, 2006, pp. 1289-1297.

[95]   S. Geng, N. Chen, H. Zhang, and W. Huang, "An improvement on the efficiency of a single rotor transonic compressor by reducing the shock wave strength on the blade suction surfaces," Journal of Thermal Science, vol. 21, pp. 127-135, 2012.

[96]   M. C. Duta, S. Shahpar, and M. B. Giles, "Turbomachinery design optimization using automatic differentiated adjoint code," in ASME Turbo Expo 2007: Power for Land, Sea, and Air, 2007, pp. 1435-1444.

[97]   L. He, "Harmonic solution of unsteady flow around blades with separation," AIAA journal, vol. 46, pp. 1299-1307, 2008.

[98]   A. Jameson, "Aerodynamic design via control theory," Journal of scientific computing, vol. 3, pp. 233-260, 1988.

[99]   A. Jameson, "Aerodynamic shape optimization using the adjoint method," Lectures at the Von Karman Institute, Brussels, 2003.

[100]   R. Myers and D. C. Montgomery, "Response surface methods," ed: Allyn-Bacon, Boston, Mass, 1971.

[101]   E. Turban and L. E. Frenzel, Expert systems and applied artificial intelligence: Prentice Hall Professional Technical Reference, 1992.

[102]   J. D. Martin and T. W. Simpson, "On the use of kriging models to approximate deterministic computer models," in ASME 2004 International Design Engineering Technical Conferences and Computers and Information in Engineering Conference, 2004, pp. 481-492.

[103]   M. J. Orr, "Introduction to radial basis function networks," ed: Technical Report, Center for Cognitive Science, University of Edinburgh, 1996.

[104]   T. Goel, R. T. Haftka, W. Shyy, and N. V. Queipo, "Ensemble of surrogates," Structural and Multidisciplinary Optimization, vol. 33, pp. 199-216, 2007.

[105]   Y.-S. Kang, T.-C. Park, S.-S. Yang, S.-I. Lee, and D.-H. Lee, "Multi Disciplinary Design Optimization and Performance Evaluation of a Single-Stage Transonic Axial Compressor," in ASME Turbo Expo 2012: Turbine Technical Conference and Exposition, 2012, pp. 361-369.

[106]   A. Samad, K.-Y. Kim, T. Goel, R. T. Haftka, and W. Shyy, "Multiple surrogate modeling for axial compressor blade shape optimization," Journal of Propulsion and Power, vol. 24, pp. 301-310, 2008.

[107]   H. Watanabe and M. Zangeneh, "Design of the blade geometry of swept transonic fans by 3D inverse design," in ASME Turbo Expo 2003, collocated with the 2003 International Joint Power Generation Conference, 2003, pp. 603-612.

[108]   W. Tiow and M. Zangeneh, "Application of a three-dimensional viscous transonic inverse method to NASA rotor 67," Proceedings of the Institution of Mechanical Engineers, Part A: Journal of Power and Energy, vol. 216, pp. 243-255, 2002.

[109] K.-Y. Lee, Y.-S. Choi, Y.-L. Kim, and J.-H. Yun, "Design of axial fan using inverse design method," Journal of Mechanical Science and Technology, vol. 22, pp. 1883-1888, 2008.

[110] P. Hu, M. Zangeneh, B. Choo, and M. Rahmati, "On design of transonic fan rotors by 3D inverse design method," in ASME Turbo Expo 2006: Power for Land, Sea, and Air, 2006, pp. 447-458.

[111] L. He and P. Shan, "Three-dimensional aerodynamic optimization for axial-flow compressors based on the inverse design and the aerodynamic parameters," Journal of Turbomachinery, vol. 134, p. 031004, 2012.

[112] T. Dang, "A fully three-dimensional inverse method for turbomachinery blading in transonic flows," Journal of turbomachinery, vol. 115, pp. 354-361, 1993.

[113] J. Chung and K. D. Lee, "Shape optimization of transonic compressor blades using quasi-3 D flow physics," ASME TURBO EXPO 2000, Munich, Germany, 2000.

[114] D. Bonaiuti, A. Pitigala, M. Zangeneh, and Y. Li, "Redesign of a transonic compressor rotor by means of a three-dimensional inverse design method: A parametric study," in ASME Turbo Expo 2007: Power for Land, Sea, and Air, 2007, pp. 173-187.

[115] W. Tiow, K. C. Yiu, and M. Zangeneh, "Application of simulated annealing to inverse design of transonic turbomachinery cascades," Proceedings of the Institution of Mechanical Engineers, Part A: Journal of Power and Energy, vol. 216, pp. 59-73, 2002.

[116] C.-S. Ahn and K.-Y. Kim, "Aerodynamic design optimization of an axial flow compressor rotor," in ASME Turbo Expo 2002: Power for Land, Sea, and Air, 2002, pp. 813-819.

[117] M. Aulich and U. Siller, "High-dimensional constrained multiobjective optimization of a fan stage," in ASME 2011 Turbo Expo: Turbine Technical Conference and Exposition, 2011, pp. 1185-1196.

[118] A. Samad and K.-Y. Kim, "Multi-objective optimization of an axial compressor blade," Journal of Mechanical Science and Technology, vol. 22, pp. 999-1007, 2008.

[119] X. Wang, S. Wang, and W. Han, "Multi-Objective Aerodynamic Design Optimization Based on Camber Line and Thickness Distribution for a Transonic Compressor Rotor," in ASME 2008 International Mechanical Engineering Congress and Exposition, 2008, pp. 25-32.

[120] K. Deb, Multi-objective optimization using evolutionary algorithms vol. 16: John Wiley & Sons, 2001.

[121] G. Dhondt, The finite element method for three-dimensional thermomechanical applications: John Wiley & Sons, 2004.

[122] F. Pouzadoux, G. Reydellet, E. Taillefer, and M. Masmoudi, "Introduction of multidisciplinary optimization in compressor blade design," in 12th AIAA/ISSMO Multidisciplinary Analysis and Optimization Conference, AIAA, 2008.

[123] A. J. Strazisar, J. R. Wood, M. D. Hathaway, and K. L. Suder, "Laser anemometer measurements in a transonic axial-flow fan rotor," NASA STI/Recon Technical Report N, vol. 90, p. 11245, 1989.

[124] C. Hah and L. Reid, "A viscous flow study of shock-boundary layer interaction, radial transport, and wake development in a transonic compressor," Journal of turbomachinery, vol. 114, pp. 538-547, 1992.

[125] R. V. Chima, Viscous three-dimensional calculations of transonic fan performance: National Aeronautics and Space Administration, 1991.

[126] I. Jennions and M. Turner, "Three-Dimensional Navier–Stokes Computations of Transonic Fan Flow Using an Explicit Flow Solver and an Implicit κ–ε Solver," Journal of Turbomachinery, vol. 115, pp. 261-272, 1993.

[127] J. Adamczyk, M. Celestina, and E. Greitzer, "The role of tip clearance in high-speed fan stall," Journal of turbomachinery, vol. 115, pp. 28-38, 1993.

[128] T. Arima, A. Tamura, K. Kikuchi, T. Sonoda, and M. Shirotori, "A Numerical Investigation of Transonic Axial Compressor Rotor Flow Using a Low-Reynolds-Number k–ε Turbulence Model," Journal of Turbomachinery, vol. 121, pp. 44-58, 1999.

[129] P. MILLER, "Bladecad: an interactive geometric design tool for turbomachinery blades," 1996.

[130] U. Idahosa, V. Golubev, and V. Balabanov, "Application of distributed automated MDO environment to aero/acoustic shape optimization of a fan blade," in 11th AIAA/CEAS aeroacoustics conference (26th aeroacoustics conference), 2005, pp. 1-14.

[131] J. A. Samareh, "A survey of shape parameterization techniques," in NASA Conference Publication, 1999, pp. 333-344.

[132] ANSYS, "Innovative Turbulence Modelling: SST model in ANSYS CFX," ANSYS Inc, 2006.

[133] D. E. Van Zante, A. J. Strazisar, J. R. Wood, M. D. Hathaway, and T. H. Okiishi, "Recommendations for achieving accurate numerical simulation of tip clearance flows in transonic compressor rotors," Journal of turbomachinery, vol. 122, pp. 733-742, 2000.

[134] L. M. Amoo, "On the design and structural analysis of jet engine fan blade structures," Progress in Aerospace Sciences, vol. 60, pp. 1-11, 2013.

[135] H. Doi and J. J. Alonso, "Fluid/structure coupled aeroelastic computations for transonic flows in turbomachinery," in ASME Turbo Expo 2002: Power for Land, Sea, and Air, 2002, pp. 787-794.

[136] M. Hassan, "Vibratory Analysis of Turbomachinery Blades," Rensselaer Polytechnic Institute, 2008.

[137] M. Imregun, "AEROELASTICITY IN AXIAL FLOW TURBOMACHINES," Lecture series, vol. 5, 1999.

[138] M. Arabnia and W. Ghaly, "A strategy for multi-point shape optimization of turbine stages in three-dimensional flow," in ASME Turbo Expo 2009: Power for Land, Sea, and Air, 2009, pp. 489-502.

[139] N. A. Cumpsty, Compressor aerodynamics: Longman Scientific & Technical, 1989.

[140] K. L. Suder, W. Roberts, R. Chima, and A. Strazisar, "The effect of adding roughness and thickness to a transonic axial compressor rotor," Journal of turbomachinery, vol. 117, pp. 491-505, 1995.

[141] H. M. Kim, "Target Cascading in Optimal System Design," University of Michigan,, 2001.

[142] M. S. Bazaraa, H. D. Sherali, and C. M. Shetty, Nonlinear programming: theory and algorithms: John Wiley & Sons, 2013.

[143] D. Bertsekas, "Nonlinear Programming 2nd edn (Belmont, MA: Athena Scientific)," 1999.

[144] S. Tosserams, L. Etman, P. Papalambros, and J. Rooda, "An augmented Lagrangian relaxation for analytical target cascading using the alternating direction method of multipliers," Structural and Multidisciplinary Optimization, vol. 31, pp. 176-189, 2006.

[145] S. Tosserams, M. Kokkolaras, L. Etman, and J. Rooda, "A nonhierarchical formulation of analytical target cascading," Journal of Mechanical Design, vol. 132, p. 051002, 2010.

[146] S. Le Digabel and C. Tribes, NOMAD User Guide: Version 3.5: Groupe d'études et de recherche en analyse des décisions, 2011.

[147] L. M. Rios and N. V. Sahinidis, "Derivative-free optimization: A review of algorithms and comparison of software implementations," Journal of Global Optimization, vol. 56, pp. 1247-1293, 2013.

[148] N. Metropolis, A. W. Rosenbluth, M. N. Rosenbluth, A. H. Teller, and E. Teller, "Equation of state calculations by fast computing machines," The journal of chemical physics, vol. 21, pp. 1087-1092, 1953.

[149] S. Kirkpatrick, "Optimization by simulated annealing: Quantitative studies," Journal of statistical physics, vol. 34, pp. 975-986, 1984.

[150] L. Ingber, "Simulated annealing: Practice versus theory," Mathematical and computer modelling, vol. 18, pp. 29-57, 1993.

[151] A. Van der Velden and P. Koch, "Isight design optimization methodologies," ASM Handbook, vol. 22, 2010.

[152] A. Van der Velden and D. Kokan, "The synaps pointer optimization engine," in ASME 2002 International Design Engineering Technical Conferences and Computers and Information in Engineering Conference, 2002, pp. 159-165.

[153] K. Schittkowski, "NLPQL: A FORTRAN subroutine solving constrained nonlinear programming problems," Annals of operations research, vol. 5, pp. 485-500, 1986.

[154] M. Miki, T. Hiroyasu, M. Kaneko, and K. Hatanaka, "A parallel genetic algorithm with distributed environment scheme," in Systems, Man, and Cybernetics, 1999. IEEE SMC'99 Conference Proceedings. 1999 IEEE International Conference on, 1999, pp. 695-700.

[155] C. Audet and J. E. Dennis Jr, "Mesh adaptive direct search algorithms for constrained optimization," SIAM Journal on optimization, vol. 17, pp. 188-217, 2006.

[156] C. Audet, J. E. Dennis, and S. Le Digabel, Sensitivity to constraints in blackbox optimization: Groupe d'études et de recherche en analyse des décisions, 2010.

[157] M. Joly, T. Verstraete, and G. Paniagua, "Full Design of a Highly Loaded Fan by Multi-Objective Optimization of Through-Flow and High-Fidelity Aero-Mechanical Performances," in ASME Turbo Expo 2012: Turbine Technical Conference and Exposition, 2012, pp. 2293-2301.

[158] S. Tosserams, "Analytical target cascading: convergence improvement by sub-problem post-optimality sensitivities," MS thesis, Eindhoven University of Technology, Eindhoven, The Netherlands, 2004.

APPENDIX A – **Literature Review**

Table A-1: Overview of MDO Formulations

	Formulations	Features
Multidisciplinary Design Analysis and Optimization [6-25]	**All-at-Once (AAO)**	• The complete design is control by a single-level optimizer. • Most basic MDO formulation which has wide industry acceptance, but is restricted to small design problems.
	Multidisciplinary Feasible (MDF)	• Conventional formulation • Computationally expensive, as a complete MDA must perform at each iteration step in the optimization.
	Individual Discipline Feasible (IDF)	• A formulation which avoids a complete MDA (Multidisciplinary Analysis) optimization. • The local disciplines can be feasible but the complete system may not be feasible until optimization converges.
	Collaborative Optimization (CO)	• Bi-level MDO formulation. • Designers have control on every discipline • Parallel execution can be performed by removing iteration loops
	Concurrent Sub-Space Optimization (CSSO)	• For large scale MDO design problems • Designers have control over the local disciplines design.
	Analytical Target Cascading (ATC)	• A multi-level formulation. • Achieve system wide convergence • Designed for problems that are component/objective aligned rather than discipline.

Table A-2: Overview of literature review

References	Validation test case	Design variables	Objective and constraints	Optimization algorithm and analysis tools
Kang, Park et al. [105]	Single stage transonic axial compressor	12-geometrical design variables among 60 selected from sensitivity analysis	Maximize efficiency and safety margin; constraints: pressure ratio and mass flow rate	-
Lian and Liou [5]	NASA Rotor 67	32 design variables	Multi-objective: Maximize pressure ratio and minimize the weight; Constraints: mass flow rate and maximum stress safety factor	Total 1024 Latin Hypercube (LHD) design points, GA Tools: TRAF3D, ANSYS
Siller, Voß et al. [92]	A transonic axial compressor stage	119-design parameters	Multi objective optimization two aerodynamic objective maximize working line efficiency and average stall margin; Constraints: total 4 including, 1 for swirl angle; 2 for mass flow rate maximum 1 for maximum stress	Kriging and ANN Evolutionary algorithm Tools: TRACE, Calculix
Li, He et al. [65]	NASA Rotor 67	Sweep, Lean and compound lean variables	Maximize Efficiency Constraints: geometric position, stress, dynamic; aerodynamic	No information available Tools: Unsteady flow analysis solver, ANSYS
Joly, Verstraete et al. [157]	Transonic compressor Rotor	B-Spline parameterization based on lean, sweep, thickness control points	Multi-objective aeromechanical optimization: maximize the efficiency, with maximum stress constraint	Evolutionary algorithm Tools: TRAF3D, Calculix

Table A-3: Overview of literature review

References	Validation test case	Design variables	Objective and constraints	Optimization algorithm and analysis tools
Luo, Song et al. [78]	NASA Rotor 37	B-Spline parameterization; 19-design variable	Multi-objective aerostructral optimization: maximize efficiency and minimize the maximum stress; constraints: mass flow rate, pressure ratio and dynamic	Evolutionary algorithm Tools: 3D Navier-Stokes equation based solver, ANSYS
Deng, Guo et al. [75]	Transonic fan blade	33-design variables	Aeromechanical multi-objective optimization: Maximize efficiency and the slope of adiabatic efficiency at 95% of cruise mass flow and the design speed. Total 9 constraints for stress and dynamic frequency modes	Evolutionary algorithm Tools: ANSYS CFX, ANSYS Mechanical
Pierret, Coelho et al. [46]	NASA Rotor 67	Blade parameterized 35-design variables	Maximize Efficiency Constraints: pressure ratio, mass flow rate, maximum stress, dynamic frequency modes	Approximation model and Genetic algorithm (GA) Tools:TRAF3D, SAMCEF
Astrua, Piola et al. [74]	Transonic compressor blade	60-design variables	Multipoint multi-objective aeromechanical Optimization algorithm Reduce the rotor loss at stall, choke margin and constraint: structural safety margin	ANN and random walk Tools: TRAF3D, Calculix

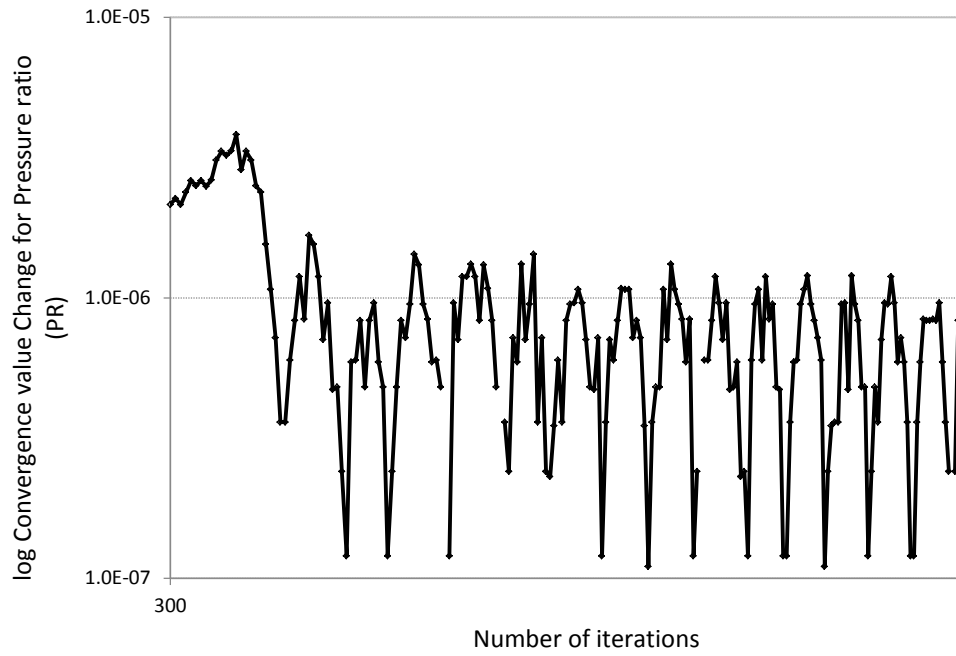# APPENDIX B – Parameterization and Analysis Methodologies

Figure B-1: Plot the pressure ratio (PR) change from iteration to iteration on a log scale, i.e. log (PR [n] – PR [n-1]) for 150,000-node grid
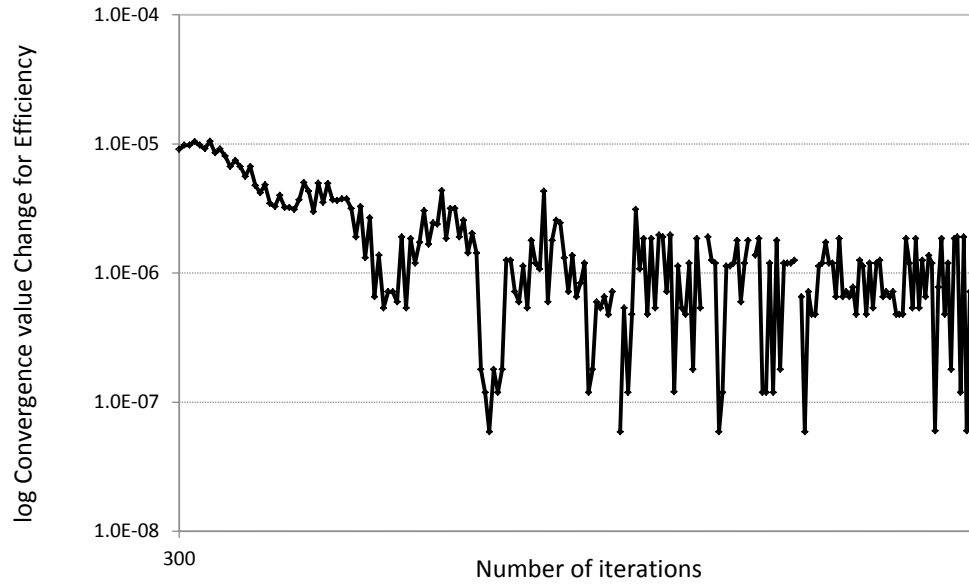
Figure B-2: Plot the efficiency change from iteration to iteration on a log scale, i.e. log (mdot[n] – mdot [n-1]) for 150,000-node grid
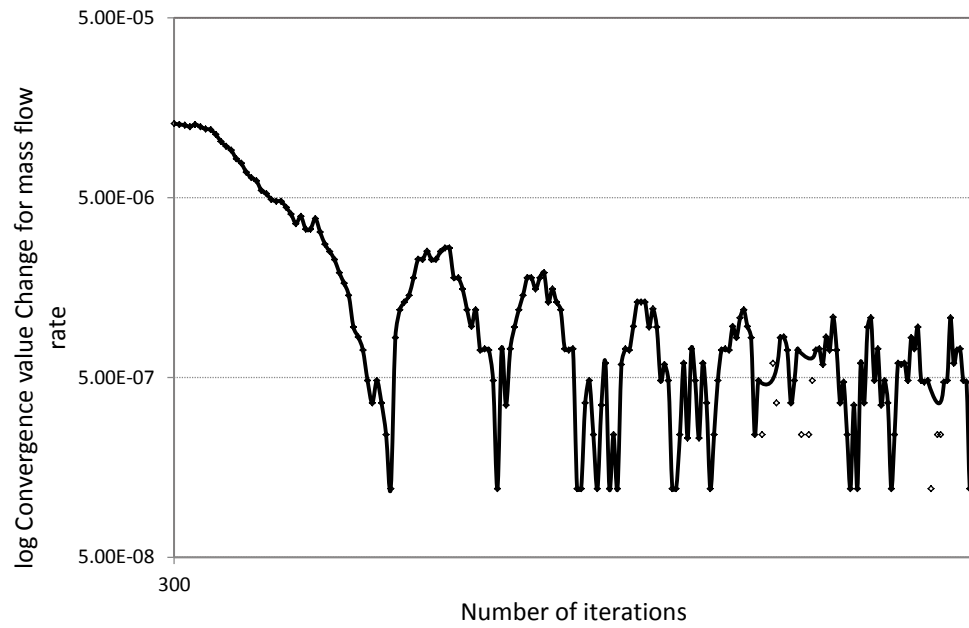

Figure B-3: Plot the mass flow rate change from iteration to iteration on a log scale, ie. Log (Eff [n] – Eff [n-1]) for 150,000-node grid

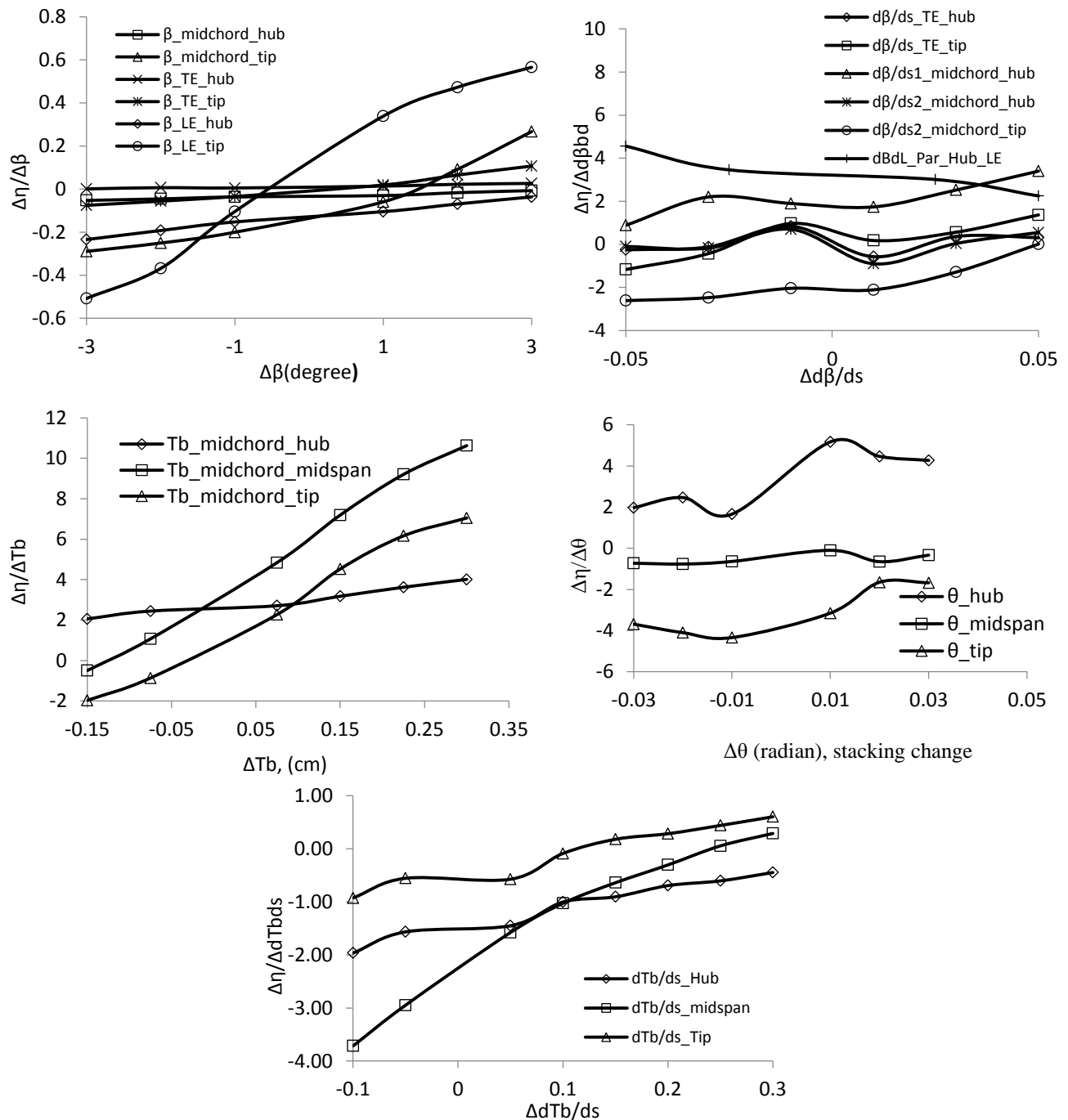# APPENDIX C – MDO of a Transonic Fan Blade

Figure C-1: The sensitivity of the design point efficiency to the geometrical design variables
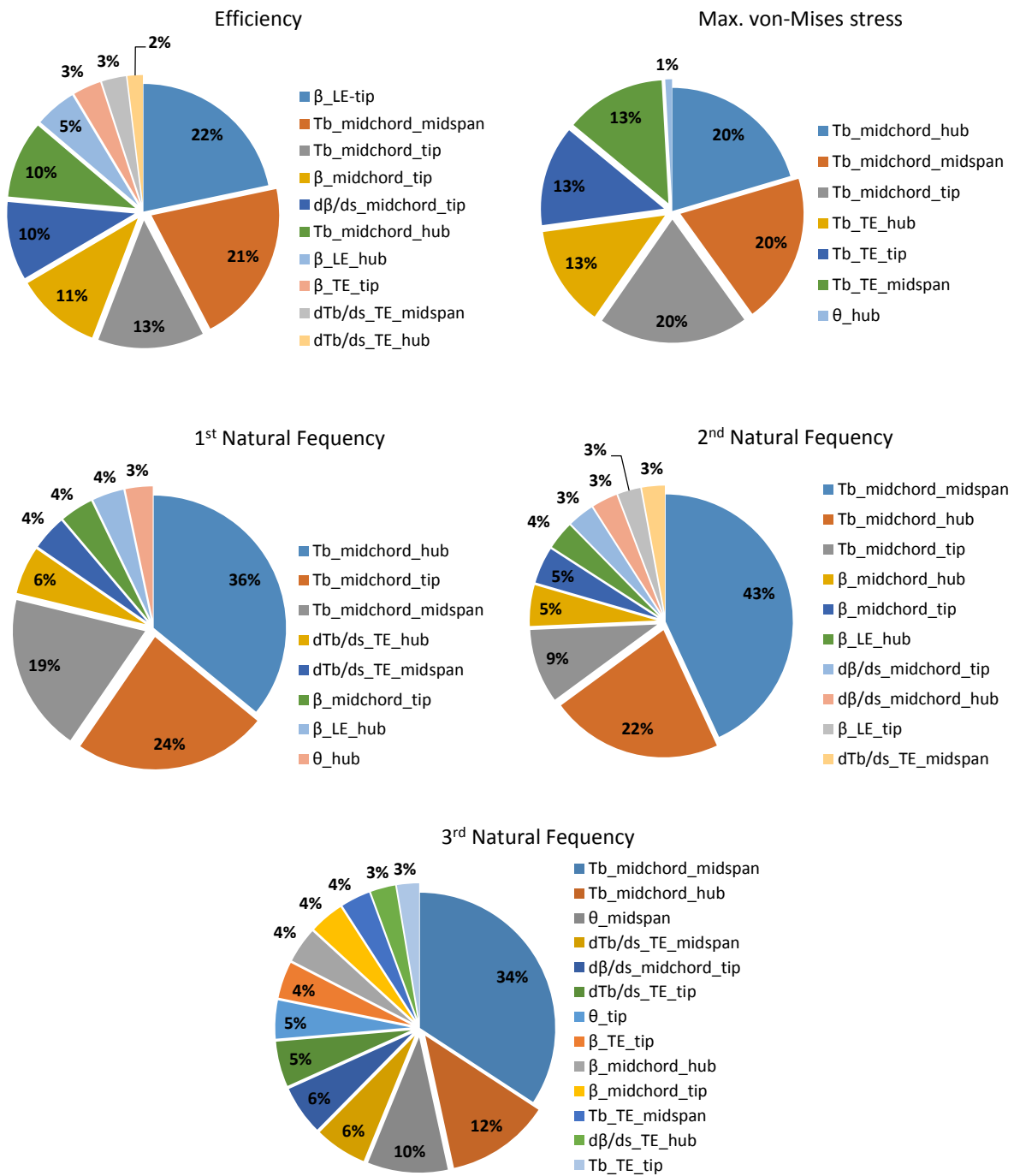
Figure C-2: The sensitivity of the design point efficiency, maximum stress, 1st , 2nd and 3rd natural frequencies to the geometrical design variables

C.1 ATC analytical problem

This problem is a reduced version of geometric optimization problem taken from Tosserams [158]. This is presented here to provide a simplified ATC framework for an analytical problem. However the solution of this problem is not presented here.

This problem contains 7 variables (z_i; $i=1,2,..,7$), a single objective function (f), two equality (h_i;$i=1,2$) and two inequality constraints (g_i;$i=1,2$).

$$minimize \qquad f = z_1^2 + z_2^2$$

$$with\ rexpect\ to \qquad z_1, \dots z_7$$

$$subject\ to \qquad g_1 = z_3^{-2} + z_1^2 + z_5^2 \le 0$$

$$g_2 = z_5^2 + z_6^{-2} + z_7^2 \le 0$$

$$h_1 = z_1^2 - z_3^2 - z_4^{-2} - z_5^2 = 0$$

$$h_2 = z_2^2 - z_5^2 - z_6^2 - z_7^2 = 0$$

$$z_1, \dots z_7 \ge 0$$

The problem is divided into two sublevel problems and one system/top level problem. A possible partitioning of this two-level problem is depicted in Figure C-3.

where; $x_{11=}[z_3\ ,z_4], x_{12=}[z_6\ ,z_7], a_{11=}h_1\ , a_{12=}h_2,\ g_{11=}[g_1],\ g_{12=}[g_2]$
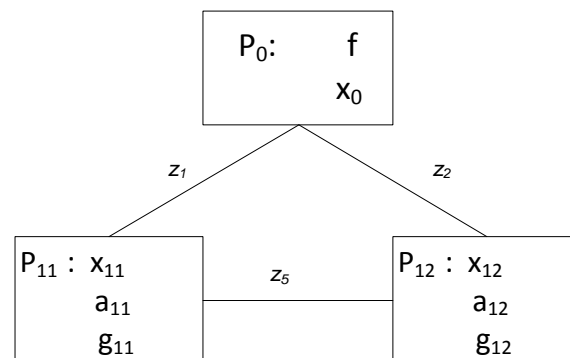

Figure C-3: Partitioning for geometrical optimization problem

The functional dependence table (FDT) form is presented in Table C-1. Where, the function of row depends on the variables of column. $R= [z_1, z_2]$ declares the response variables of top level problem (P_0) which become target for both sublevel problems (P_{11} & P_{12}). Thus top-level linked through P_{11} with variable z_1 and P_{12} with z_2. Both sub-level problems are linked through $y= [z_5]$, called linking variable target. Here, z_3 and z_4 are local variable for problem P_{11}, whereas z_6 and z_7 are local variables for problem P_{12}. *i.e.* $x= [z_3, z_4, z_6, z_7]$. The response from problems P_{11} and P_{12} are formed from h_1 and h_2 respectively.

Table C-1: Functional Dependence Table (FDT) for geometrical optimization

		R		**y**	**x**			
		z_1	z_2	z_5	z_3	z_4	z_6	z_7
P_0	**f**	■	■					
P_{11}	**h_1**	■		■	■	■		
	g_1			■	■	■		
P_{12}	**h_2**		■	■			■	■
	g_2			■			■	■

Top level Problem (P_0):

$minimize$ $\qquad f_0(\bar{x}_0) = z_1^2 + z_2^2 + \|w_{11}^R \circ (R_{01} - r_{11})\|_2^2 + \|w_{12}^R \circ (R_{02} - r_{12})\|_2^2 +$
$\|w_{11}^Y \circ (Y_{11} - y_{11})\|_2^2 + \|w_{12}^Y \circ (Y_{12} - y_{12})\|_2^2$

$with\ rexpect\ to$ $\qquad \bar{x}_0$

$subject\ to$ $\qquad h_0(\bar{x}_0) = 0$

where;

$y_{01} = y_{02} = [z_5]$, $R_{01} = [z_1]$, $R_{02} = [z_2]$, $\bar{x}_0 = [R_{01}, Y_{01}, R_{02}, Y_{02}]$

$f_0(\bar{x}_0) = z_1^2 + z_2^2$

$h_0(\bar{x}_0) = y_{01} - y_{02}$

Problem P_{11}:

minimize $\qquad \|w_{11}^R \circ (R_{01} - r_{11})\|_2^2 + \|w_{11}^Y \circ (Y_{01} - y_{01})\|_2^2$

with rexpect to $\qquad \bar{x}_{11}$

subject to $\qquad h_{11}(\bar{x}_{11}) = 0$

$\qquad\qquad\qquad g_{11}(\bar{x}_{11}) \leq 0$

where;

$y_{11} = [z_5]$, $r_{11} = [z_1]$, $\bar{x}_{11} = [x_{11}, r_{11}, y_{11}]$, $x_{11} = [z_3, z_4]$

$g_{11}(\bar{x}_{11}) = z_3^{-2} + z_4^2 - z_5^2$

$a_{11}(\bar{x}_{11}) = \sqrt{z_3^2 + z_4^{-2} + z_5^2}$

$h_{11}(\bar{x}_{11}) = [r_{11} - a_{11}(\bar{x}_{11})]$

Problem P_{12}:

minimize $\qquad \|w_{12}^R \circ (R_{02} - r_{12})\|_2^2 + \|w_{12}^Y \circ (Y_{02} - y_{02})\|_2^2$

with rexpect to $\qquad \bar{x}_{12}$

subject to $\qquad h_{12}(\bar{x}_{12}) = 0$

$\qquad\qquad\qquad g_{12}(\bar{x}_{12}) \leq 0$

where;

$y_{12} = [z_5]$, $r_{12} = [z_2]$, $\bar{x}_{12} = [x_{12}, r_{12}, y_{12}]$, $x_{12} = [z_6, z_7]$

$g_{12}(\bar{x}_{12}) = z_3^{-2} + z_4^2 - z_5^2$

$a_{12}(\bar{x}_{12}) = \sqrt{z_5^2 + z_6^2 + z_7^2}$

$h_{12}(\bar{x}_{12}) = [r_{12} - a_{12}(\bar{x}_{12})]$

APPENDIX D – **Results and Discussion**

Table D-1: Discipline objective functions and constraints results at the beginning and end of the discipline level optimizations (a) 1st and 2nd outer loops (b) 3rd and 4th outer loops (c) 5th and 6th outer loops (d) 7th outer loops (cont.)

Objective function and constraints values		1st outer loop		2nd outer loop	
		Beginning of optimization	End of optimization	Beginning of optimization	End of optimization
Structure Dynamic (SND) optimized design	Efficiency, η (%)	89.76	89.71	-	88.98
	Pressure ratio percentage difference, ΔPR (%)	-	0.92	-	0.43
	Mass flow rate percentage difference, Δm_{dot} (%)	-	0.72	-	0.52
	Maximum stress percentage difference, $\Delta \sigma_{max}$ (%)	-	36	27	23
	Dynamic constraints, ΔF_j	(-28,-90,-29)	(0.62,24,110)	(-5,0.39,118)	(0.3,13,153)
Aerodynamic optimized design	Efficiency, η (%)	89.63	89.00	88.96	90.38
	Pressure ratio percentage difference, ΔPR (%)	-0.43	-0.37	0.80	-0.37
	Mass flow rate percentage difference, Δm_{dot} (%)	-0.39	-0.46	0.79	-0.26
	Maximum stress percentage difference, $\Delta \sigma_{max}$ (%)	-	21	-	25
	Dynamic constraints, ΔF_j	-	(-27,-52,-35)	-	(-13,-38,32)

(a)

Table D-1: Discipline objective functions and constraints results at the beginning and end of the discipline level optimizations (b) 3rd and 4th outer loops (cont.)

Objective function and constraints values		3rd outer loop		4th outer loop	
		Beginning of optimization	End of optimization	Beginning of optimization	End of optimization
Structure Dynamic (SND) optimized design	Efficiency, η (%)	-	90.19	-	90.0007
	Pressure ratio percentage difference, ΔPR (%)	-	0.12	-	0.25
	Mass flow rate percentage difference, Δm_{dot} (%)	-	0.066	-	0.20
	Maximum stress percentage difference, $\Delta\sigma_{max}$ (%)	27	5.4	5.5	9.5
	Dynamic constraints, $\varDelta F_j$	(16,-43,55)	(5,31,14)	(-6,6,60)	(1.15,14,12)
Aerodynamic optimized design	Efficiency, η (%)	90.33	90.39	90.19	90.40
	Pressure ratio percentage difference, ΔPR (%)	-0.37	0	0.43	0.49
	Mass flow rate percentage difference, Δm_{dot} (%)	-0.26	0.06	0.40	0.46
	Maximum stress percentage difference, $\Delta\sigma_{max}$ (%)	-	6	-	13
	Dynamic constraints, $\varDelta F_j$	-	(-30,-14,23)	-	(8,-8,41)

(b)

Table D-1: Discipline objective functions and constraints results at the beginning and end of the discipline level optimizations (c) 5th and 6th outer loops (cont.)

Objective function and constraints values		5th outer loop		6th outer loop	
		Beginning of optimization	End of optimization	Beginning of optimization	End of optimization
Structure Dynamic (SND) optimized design	Efficiency, η (%)	-	90.28	-	90.28
	Pressure ratio percentage difference, ΔPR (%)	-	0	-	0.86
	Mass flow rate percentage difference, Δm_{dot} (%)	-	0.066	-	0.72
	Maximum stress percentage difference, $\Delta \sigma_{max}$ (%)	14	24	23	17
	Dynamic constraints, ΔF_j	(4,29,9)	(7,32,47)	(12,-11,38)	(2,31,22)
Aerodynamic optimized design	Efficiency, η (%)	90.19	90.27	90.31	90.28
	Pressure ratio percentage difference, ΔPR (%)	-0.12	0.31	1.623	0
	Mass flow rate percentage difference, Δm_{dot} (%)	-0.06	0.26	1.525	0
	Maximum stress percentage difference, $\Delta \sigma$ (%)	-	21	-	15
	Dynamic constraints, ΔF_j	-	(24,-56,121)	-	(7,29,81)

(c)

Table D-1: Discipline objective functions and constraints results at the beginning and end of the discipline level optimizations (d) 7th outer loops (cont.)

Objective function and constraints values		7th outer loop	
		Beginning of optimization	End of optimization
Structure Dynamic (SND) optimized design	Efficiency, η (%)	-	0.9029
	Pressure ratio percentage difference, ΔPR (%)	-	0.12
	Mass flow rate percentage difference, Δm_{dot} (%)	-	0.13
	Maximum stress percentage difference, Δσ (%)	16	31
	Dynamic constraints, ΔF_j	(-5, -4, 8)	(2, 3, 8)
Aerodynamic optimized design	Efficiency, η (%)	90.28	0.9044
	Pressure ratio percentage difference, ΔPR (%)	0	0.31
	Mass flow rate percentage difference, Δm_{dot} (%)	0	0.26
	Maximum stress percentage difference, $\Delta\sigma_{max}$ (%)	-	33
	Dynamic constraints, ΔF_j	-	(2, 12, 9)

(d)

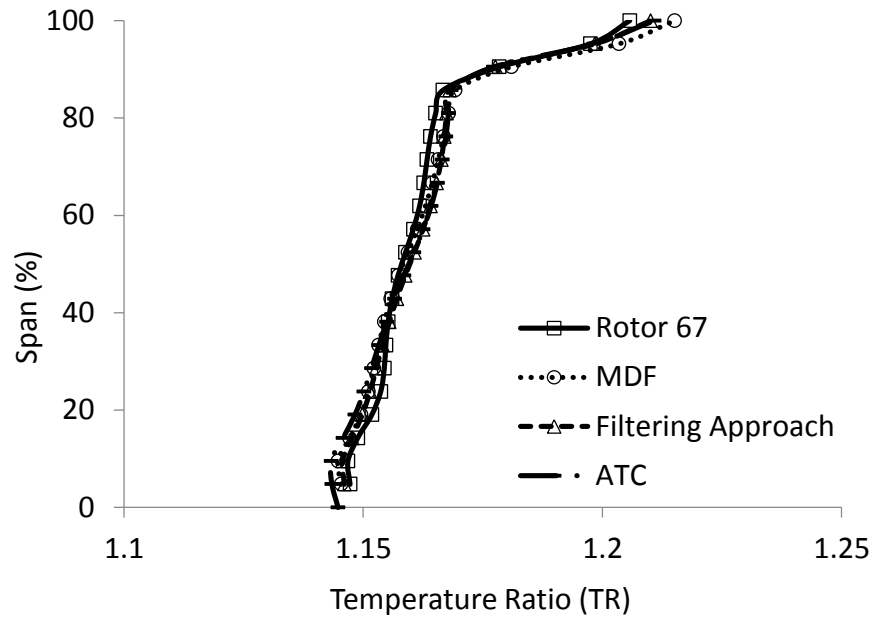Selected aero-ATC design for final comparison

Figure D-1: Spanwise distributions of the temperature ratio for the Rotor 67 and the optimized
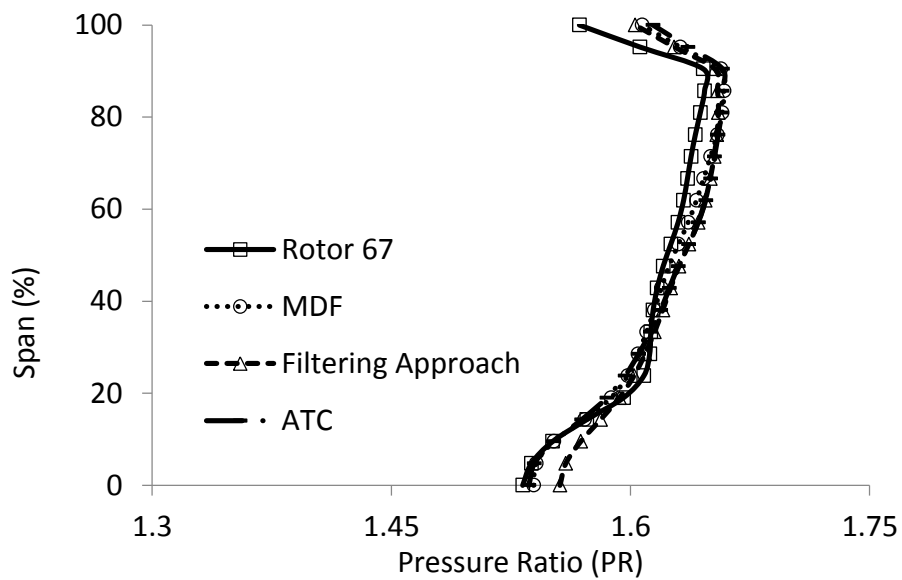
blades

Figure D-2: Spanwise distributions of the pressure ratio for the Rotor 67 and the optimized
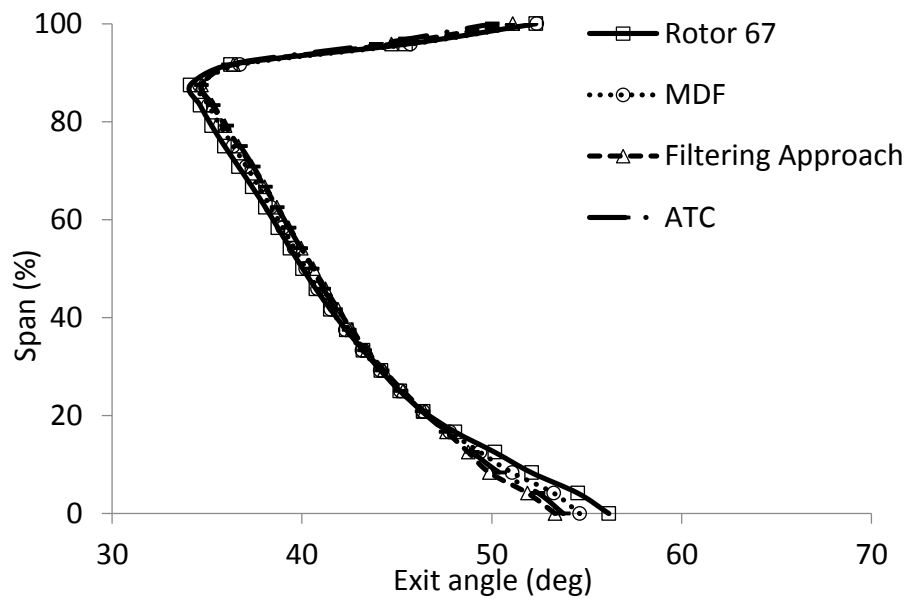
blades

Figure D-3: Spanwise distributions of the exit flow angle for the Rotor 67 and the optimized blades (downstream the of blade)
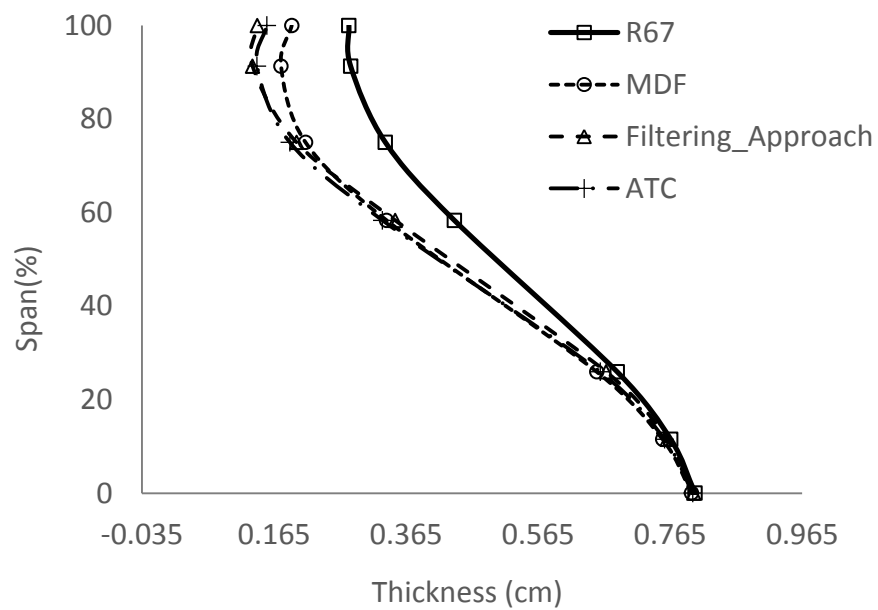

Figure D-4: Spanwise distributions of the maximum thickness for the Rotor 67 and the optimized blades